THESIS REPORT

Ph.D.

SYSTEMS RESEARCH CENTER

Supported by the National Science Foundation Engineering Research Center Program (NSFD CD 8803012), the University of Maryland, Harvard University, and Industry

Dynamic Analysis and Synthesis of Geared Robotic Mechanisms

by D.-Z. Chen

Advisor: L.-W. Tsai

Ph.D. 91-6

ABSTRACT

Title of Dissertation: DYNAMIC ANALYSIS AND SYNTHESIS OF GEARED ROBOTIC MECHANISMS

Dar-Zen Chen, Doctor of Philosophy, 1991

Dissertation directed by: Lung-Wen Tsai, Professor
Mechanical Engineering Department
and
Systems Research Center

The objective of this research is to develop a systematic approach for the dynamic analysis of geared robotic mechanisms and to establish systematic and rational methodologies for the determination of gearing configuration and gear ratios.

First, a systematic methodology is developed for the dynamic analysis of geared robotic mechanisms. The formulation of dynamic equations is based on the concept of an equivalent open-loop chain. It is shown that reaction force analysis of such mechanisms can be efficiently carried out by a *forward* evaluation along its transmission lines followed by a *backward* evaluation along the equivalent open-loop chain.

Then, two methodologies are developed for the determination of gearing configuration and gear ratios. The first methodology considers the design from both kinematics and dynamics points of view. It is

shown that, through proper choice of gear ratios, certain gear-coupled manipulators can be designed to possess kinematic isotropy and maximum acceleration capacity (KIMAC) conditions at a given reference point while individual-joint drive manipulators can not be designed to possess such conditions. The train values of those gear-coupled manipulators can be thought of as a product of two-stage gear reductions. The second-stage gear reduction is used to define the kinematic isotropic condition while the first-stage gear reduction is used to optimize the acceleration capacity. The second methodology considers the design from just the dynamics point of view. It is shown that, to achieve a maximum acceleration capacity (MAC), the mass inertia matrix of the input links reflected at the joint-space should be equal to that of the major links. It is also shown that the maximum acceleration capacity is independent of the gearing configuration.

The methodologies developed in this research provide an efficient and systematic approach for the dynamic analysis and synthesis of geared robotic mechanisms.

DYNAMIC ANALYSIS AND SYNTHESIS OF GEARED ROBOTIC MECHANISMS

by

Dar-Zen Chen

Dissertation submitted to the Faculty of the Graduate School
of the University of Maryland in partial fulfillment
of the requirements for the degree of
Doctor of Philosophy

1991

Advisory Committee:

Professor Lung-Wen Tsai, Chairman/Advisor
Professor Edward Magrab
Professor Jackson C.S. Yang
Associate Professor Shapour Azarm
Associate Professor Mark A. Shayman

ACKNOWLEDGEMENT

The author wishes to express his sincere appreciation to his dissertation advisor, Dr. Lung-Wen Tsai. Without his encouragement, support and guidance, this work would not be possible. Much appreciation is also due to Dr. Roger J. Chen for his encouragement and discussions during the early stage of development of this dissertation.

The author gratefully acknowledges the advice and support provided by the members of his advisory committee, Drs. Edward Magrab, Jackson Yang, Shapour Azarm and Mark Shayman.

This research was supported in part by the U.S. Department of Energy, Grant DEF05-88ER13977, and in part by the NSF Engineering Research Centers Programs, NSDF CDR8803012. Such support does not constitute an endorsement by the supporting agencies of the views expressed in this dissertation.

Finally, the author extends his deepest appreciation to his wife and parents for their love, and encouragement.

TABLE OF CONTENTS

LIST OF TABLES

LIST OF FIGURES

NOMENCLATURE

Φ	displacement vector associated with actuator-space,
Θ	displacement vector associated with joint-space,
X	displacement vector associated with end-effector-space,
ξ	generalized force vector associated with actuator-space,
τ:	generalized force vector associated with joint-space,
F	generalized force vector associated with end-effector-space,
J	Jacobian matrix,
A	structure matrix,
K_v	generalized velocity ratio,
KCN	Kinematic condition number,
K_d	generalized effective inertia,
DCN	dynamic condition number,
$\theta_{i,j}$	the relative angular displacement of link i with respect to link j
q_{i-1}	the joint angle $\theta_{i,i-1}$,
$\dot{q}_{i-1}$	the rate of change of the joint angle q_{i-1},
S_i	$\sin(q_{i-1})$,
C_i	$\cos(q_{i-1})$,
N_i	teeth number of link i,
$r_{i,j}$	$= N_i/N_j$, the gear ratio at gear pair (i, j),
ω_i	the angular velocity of link i,
$\dot{\omega}_i$	the angular acceleration of link i,
v_i	the linear velocity of the origin of i-th coordinate system, O_i,
v_{si}	the linear velocity of the mass center of link i,

$\dot{v}_{si}$ the linear acceleration of mass center of link i.

s_i the position vector of mass center of link i with respect to its own coordinate system,

p_i^* the position vector from origin of (i-1)-th coordinate system to that of i-th coordinate system,

M_m inertia matrix associated with the equivalent open-loop chain expressed in joint-space,

M_r inertia matrix associated with input links due to their relative motion, expressed in joint-space,

M_g inertia matrix associated with intermediate carried links due to their relative motion, expressed in joint-space,

M_c inertia matrix associated with the carried links due to their relative motion, expressed in joint-space, $M_c = M_r + M_g$,

F_k^* inertia force associated with link k,

T_k^* inertia torque associated with link k,

O_{jk} mass center of link k,

$d_{j,k}$ position vector of carried link j from O_{jc} to the location of revolute joint [j, k],

d_{ja} position vector of carried link j from O_{jc} to the contact point of gear pair [j, j-1],

d_{jb} position vector of carried link j from O_{jc} to the contact point of gear pair [j+1, j],

$d_{k,\,k-1}$ position vector of major link k from O_{jk} to the location of revolute joint [k, k-1],

$d_{k,i}$ position vector of major link k from O_{jk} to the contact point of gear pair [k, i],

$\gamma_{j,j-1}$ gear force exerted on link j by link j-1,

$f_{j,k}$ force exerted on link j by link k in the revolute joint [j, k],

$t_{j,k}$: moment exerted on link j by link k in the revolute joint [j, k].

CHAPTER 1

Introduction

1.1 Subject Background

The need to establish design criteria and design methologies for robotic manipulators by taking both kinematics and dynamics into consideration has been recognized as a major research subject recently. Almost all manipulators in use today have very simple geometric structures, which can be analyzed by simple computational procedures but which do not provide the functional capacity of more general devices. The design of a general robotic manipulator is an expensive, time-consuming and challenging task, because of the large number of system design parameters involved.

The kinematic structure of serially-jointed manipulators has an open-loop configuration. Intuitively, an actuator can be mounted on each joint axis to drive the manipulator directly. However, this simple idea, called direct-drive, is not feasible using today's motor technology. This is because a direct-drive manipulator needs motors that can generate a very large torque at reasonably low speed. Usually, such motors are heavy, and use of it will significantly increase the system inertia and reduce the dynamic performances of the manipulator. Thus, most industrial manipulators are driven through gears, chains, linkages, cables or other power transmission mechanisms. In doing so, motors can be mounted remotely from the joints to reduce system inertia and to achieve torque amplification. Manipulators using gears for power transmission are essentially geared robotic mechanisms.

Robot kinematics deals with the analytical study on the geometry of motion of a manipulator with respect to a fixed reference coordinate system without regard to the forces and moments that cause the motion. Thus, kinematics deals with the analytical description of spatial displacement of a robot as a function of time and, in particular, the relations between the input-space and the position and orientation of the end-effector. The kinematic analysis of geared robotic mechanisms has been studied by a few researchers (Freudenstein et al., 1985; Litvin and Zhang, 1986; and Tsai, 1988). Of these, Tsai (1988) developed a systematic approach to the kinematic analysis of geared mechanisms using the fundamental circuit theory and coaxiality conditions.

Robot dynamics, on the other hand, deals with mathematical formulation of the equations of motion including the applied and inertia forces. Such equations of motion are useful for computer simulation of robot motions, design of control law, sizing of the actuators and supporting bearing, and the evaluation of the kinematic structure of a manipulator. However, conventional dynamic models developed for the analysis have been restricted to the open-loop chains. The inertia of drive system are usually not considered and the coupling effect due to gearing has not been investigated previously. Hence, it is important to develop methodologies for the analysis and synthesis of geared robotic mechanisms including the effects of rotor inertias and mechanical coupling.

1.2 Survey of Pertinent Literature

A review of some historical developments and relevant literature in the areas of manipulator dynamics, performance indices and design criteria is given in this section.

1.2.1 Development of Manipulator Dynamics

The importance of dynamics of robot manipulators stems from its use in simulation, analysis, control and design for the next generation robotic systems intended for high speed and precision operations. The need for an efficient mathematical formulation of manipulator dynamics has been recognized and the development of such a formulation has rapidly progressed in the past decade.

The dynamic model of a manipulator can be derived from well-known laws of mechanics such as Newtonian mechanics and Lagrangian mechanics. This leads to the development of dynamic equations of motion for various open-loop manipulators in terms of their geometric and inertia parameters. Various approaches, such as the Lagrange-Euler formulation (Uicker, 1965), Recursive-Lagrange formulation (Hollerbach, 1980), Newton-Euler formulation (Luh, et al., 1980), and Generalized D'alembert formulation (Lee, et al., 1983) have been developed. The structure of these equations may differ from one another as they are derived for different reasons and purposes. Some are derived to achieve fast computation in evaluating the joint torques for servoing a manipulator, others are derived to facilitate control system analysis and synthesis, and still others are derived to facilitate computer simulation of robot motion.

Uicker (1965) proposed a method for the derivation of equations of motion for spatial mechanisms using 4 by 4 transformation matrices and the Lagrange equations. The method was applied to open-loop manipulators by Kahn (1969), but it required excessive computation time and was recognized as impractical for real time control applications. Bejczy (1974) considered a simpler approach for computing actuator torques by neglecting the velocity-related terms, but the results could be inaccurate in many cases. In a parallel effort to reduce computation time, Whitney (1969) and Raibert (1977) considered the possibility of using lookup tables. A dramatic cut in the time required for calculations may be attained. However, the amount of storage necessary for control of a general spatial manipulator is extremely large. Furthermore, additional problems in storage and access of information may occur.

The inefficiency of Uicker/Khan formulation has led researchers to look for alternative formulations. In the effort to make real time dynamic computation feasible, recursive algorithms have been developed using both Newton-Euler (Walker and Orin, 1982; Luh, et al., 1980) and Lagrange formulations (Hollerbach, 1980). Silver (1982) has shown that, with a proper choice, the Lagrangian formulation is indeed equivalent to the Newton-Euler formulation. In these methods, the velocity and acceleration of each link are evaluated sequentially starting with the base link. Then, beginning at the free end and working toward the fixed base, the forces or torques acting on each joint are successively determined. These recursive methods are computationally efficient for evaluating actuator torques for a prescribed arm motion state. However, their use for design is limited to trail-and-error analysis, because the geometric properties of manipulators are hidden in their recurrence relation.

As for reaction forces and moments analysis of open-loop manipulators, which is especially important for the sizing of bearings in high speed manipulators, Newton-Euler approach provides an efficient and systematic recursive procedure while Lagrangian approach reveals no information on it.

Although many manipulators are driven by motors through the use of reasonably high speed gear reduction devices, most of the commonly used models do not include any detail of the drive system and are, in reality, only applicable to direct-drive manipulators. The effect of actuator rotors on system dynamics was investigated by Chen (1989). A systematic methodology for the kinematic analysis of bevel epicyclic gear trains was developed by Tsai (1988). These serve as the foundation for a systematic procedure for the formulation of equations of motion developed in this research.

1.2.2 Development of Performance Indices and Design Criteria

The design of manipulators generally calls for a sequence of analysis leading toward a solution which meets economical and technical requirements. Contemporary methods of computer aided design are of great assistance for engineers in performance evaluation, by carrying out lengthy computations to determine and visualize the main relations between design parameters and performance requirements.

Most of the robots currently in use were designed using the invertibility, i.e., requiring the inverse kinematic solution be solvable in closed form as a constraint. Some researchers (Kohli and Spanos, 1985; Gupta, 1986; Kumar and Patel, 1986) considered the manipulator workspace as a design criterion. Others (Vijaykumar et al., 1986; Yoshikawa, 1985a and 1985b) investigated the dexterity or manipulability for design optimization.

Recent development in numerical algorithms (Tsai and Morgan, 1985; Angeles, 1985), capable of inverting serial manipulators of arbitrary architecture, allows designers to relax the constraint of invertibility and thus open the avenue for new design criteria. Several researchers used the condition number of the Jacobian matrix as an index for measuring the quality of a manipulator (Salisbury and Craig, 1982; Angeles and Rojas, 1987). Yoshikawa (1985) proposed the idea of manipulability measure, defined as the distance between current position of an end-effector and its singular point. Asada and Cro Granito (1985) used the condition number and average velocity ratio to establish the optimality criteria. Gosselin and Angeles (1988) defined a global condition index to measure the global behavior of a manipulator. Chiu (1988) found that the manipulability must be obtained at the expense of accuracy, and defined a task-dependent performance measure. All these kinematic and static methods of evaluation are based on the Jacobian matrix. Since these performance measures are based on the transformation between the joint-space and end-effector-space, they are only useful for the evaluation or design of direct-drive manipulators. However, they are not very helpful in evaluating non-direct drive manipulators such as geared robotic mechanisms which use gear trains for power transmission.

As for the dynamic performance measure, Asada (1983) proposed a generalized inertia ellipsoid to represent the dynamic characteristics of a manipulator geometrically. By varying the link lengths and mass distribution, he showed that the generalized moment of inertia can be made uniform in all directions and the nonlinear force can be eliminated. Yoshikawa (1985b) defined the relation between input joint torques and the end-effector acceleration as the dynamic manipulability index. Yang and Tseng (1986) proposed a method for simplifying and linearlizing the manipulator dynamics by eliminating nonlinear terms in the system's kinetic and potential energy equations through the redistribution of link inertia properties. Since these methods are all based on redistribution of inertia properties, the design can be time-consuming and sometimes even impractical. Nevertheless, these methods do not take the inertia effects of drive system into consideration and are perhaps only useful for the design of direct-drive manipulators. In this dissertation, the inertia effects of drive system will be included as a design parameter, and methodologies will be developed for the optimal design of geared robotic mechanisms.

1.3 Scope of the Study

The objective of this research is to develop systematic methodologies for dynamic analysis and dynamic synthesis of geared robotic mechanisms. The results should lead to a more accurate modeling of system dynamics and a rational procedure for the selection of gearing configuration and gear ratios in designing such complex mechanical systems.

The content of this dissertation can be categorized into two major parts: dynamic analysis and dynamic synthesis. In dynamic analysis, two subtopics are discussed: (i) the formulation of equations of motion (chapter two), and (ii) the reaction force analysis for a general class of geared robotic mechanisms (chapter three). In dynamic synthesis, two subtopics are explored: (i) the establishment of performance indices (chapter four), and (ii) the selection and determination of gearing configuration and gear ratios (chapters five and six).

The main idea for the formulation of dynamic equations is based on the separation of major links from the carried links. In chapter two, canonic graph and equivalent open-loop chain are defined from which the major links and carried links in a geared robotic manipulator can be identified. The contributions to the generalized inertia forces are then divided into two parts. The first part is due to the motion of the major links and the second part is due to the relative motion of the carried links with respect to the major links. The generalized active forces are expressed in terms of actuator torques. Finally the equations of motion are formulated by equating the generalized active forces to the generalized inertia forces.

In chapter three, an efficient and systematic methodology for the computation of reaction forces is developed for geared robotic mechanisms. It will be shown that the computation sequence can be carried out in two steps. The first step is a link-by-link *forward* evaluation of the reaction forces acting on the carried links in each transmission line, starting from the input link. The second step is a link-by-link *backward* evaluation of the reaction forces acting on the major links of the equivalent open-loop chain, starting from the output link.

In chapter four, performance indices are established for the evaluation of multi-degree-of-freedom (D.O.F.) geared robotic manipulators. These performance indices are based on the concept of velocity ratio and effective inertia derived for the performance evaluation of single-D.O.F. mechanisms.

In chapters five and six, methodologies for the determination of gearing configuration are established. The principle of inertia match is extended from one-D.O.F. systems to multi-D.O.F. systems. The selection of gearing configuration and its characteristics are also discussed. It will be shown that optimal gear ratios of a manipulator can be determined.

Design examples are discussed in chapter seven. A two-D.O.F. planar manipulator is used to illustrated the determination of gear ratios to achieve kinematic isotropy and maximum acceleration capacity conditions. A three-D.O.F. Bendix-type wrist mechanism is used to illustrate the determination of gear ratios to achieve a maximum acceleration capacity condition. Reaction force analysis is performed.

The major contributions of this research are:

1. Development of a systematic methodology for the formulation of equations of motion of geared robotic mechanisms.
2. Development of an efficient and systematic procedure for reaction force analysis in geared robotic mechanisms.
3. Development of performance indices for the evaluation of geared robotic mechanisms.
4. Development of a design methodology for the kinematic and dynamic synthesis of geared robotic mechanisms.
5. Generalization of the principle of inertia match.

CHAPTER 2

Kinematics and Dynamics of Geared Robotic Mechanisms

2.1 Introduction

Since Hooker and Margulies (1965) started to investigate the dynamics of general n-body satellite, there have been numerous articles on the dynamics of multi-body systems. At first, only open tree-structured systems made up of rigid bodies connected by perfect revolute joints were considered. Gradually, systems involving closed loops and flexible bodies connected by joints other than revolute have also been studied not only for space application but also for ground-based application. One of the more recent application areas is robot manipulators. Out of these efforts many general purpose programs capable of modeling certain classes of systems become available; some are government sponsored, such as NBOD2 and DISCOS (Bodley et al., 1978), some are commercially available, such as ADAMS (MDI, 1981), DADS (CADSI, 1988) and SD/FAST (SDI, 1988), and still some others have been developed by corporations for their internal uses. Although existing programs can be applied to many different mechanical systems, they are not suitable for geared mechanisms such as the PUMA wrist mechanism shown schematically in Fig. 2-1. In the PUMA wrist, link 5, 6 and 8 are the input links and link 4 is the end-effector link. The three joint axes, a, b and c intersect at a common point. Link 5 drives link 2 through the spur gear pair (5, 2) as shown in the figure, Link 6 drive link 3 through the spur gear pair (6, 7) followed by the bevel gear pair (7,3), and link 8 drives link 4 through the spur gear pair (8, 9) followed by two bevel gear pair (9, 10) and (10, 11). The end-effector possesses a three D.O.F. spherical motion.

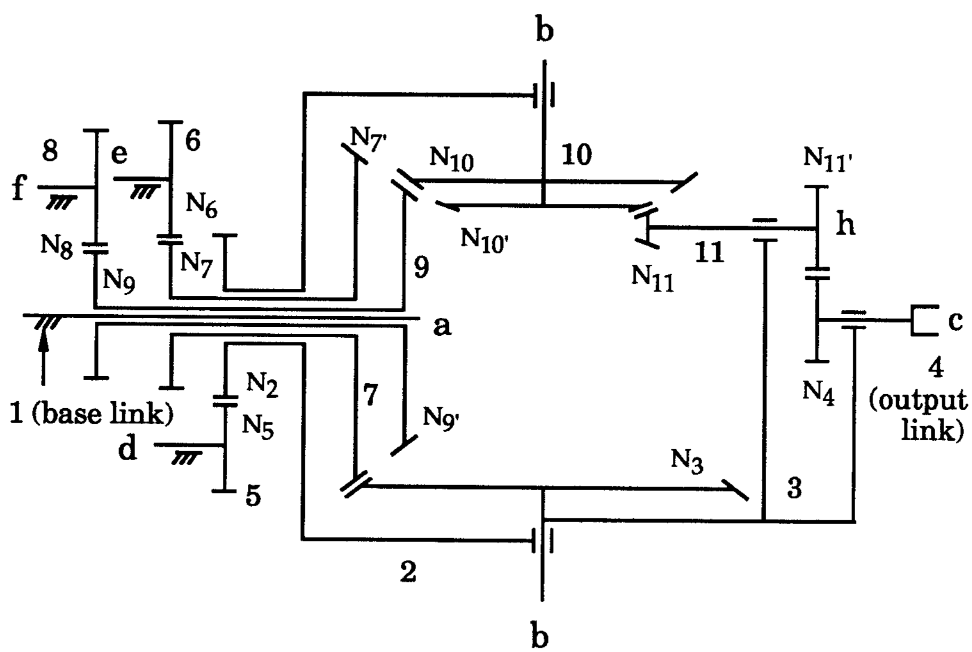

Fig. 2-1: Schematic Drawing of PUMA Wrist Mechanism.

Gears have been used for centuries by humans to transmit mechanical power from one rotation axis to another. They are also used to achieve desired rotation speeds at the output axes. With the advent of robotic manipulators in our work places comes a complicated form of gearing systems that provide motions similar to those of a human. These robots are made to be compact and light weight, and some of them have all their motors mounted away from the joints so that the complete robot manipulators have more favorable mass distributions. The system depicted in Fig. 2-1 is an example of such mechanisms. Motors can be attached to each of links 5, 6 and 8 as the mechanical power source. Through spur and bevel gear trains, the power is transmitted to the output link 4 on which payload can be attached.

Formulating the equations of motion is an important part of robot analysis that will provide necessary information for the design of control laws and mechanical components. Before the process of formulation can begin, idealization of the robot system into a model amenable to analysis has to be performed. Assumptions such as rigid bodies, perfect revolute joints and gear meshing, complete isolation between electrical phenomena and mechanical motions and idealized torque transmission in the gear trains are used in this research.

In order for a designer to better design such an articulated gear mechanism, detailed dynamic analysis of such gear systems need to be accurately and efficiently performed. Extensive literature search does not result in any article addressing this issue directly. However, some recent developments in the kinematics and the dynamics of articulated gear mechanisms provide the necessary bases for achieving such analysis systematically (Tsai, 1988; Chen, 1989).

2.2 Background

The dynamic analysis of a multi-D.O.F. articulated gear mechanism, such as the one shown in Fig. 2-1, can be quite complicated. This is especially true when the dynamic loads on the bearings and on the gear teeth are to be evaluated for engineering design. The complexity arises from the large number of moving links and joints between the links, ten moving links and seventeen joints in this case. Conventional methods for formulating the dynamic equations will be discussed in the following to give an indication of the complexity.

The first method to be discussed is the use of Lagrange's equations and Lagrange multipliers which is employed in some commercially available multi-body dynamic analysis programs such as DADS and ADAMS. In this method, six or more generalized coordinates are used to describe the motion of each rigid body. Constraints due to joints and gear meshings are then introduced to restrict the motion. Each constraint equation requires a Lagrange multiplier in the Lagrange's equations. With six coordinates for each rigid body, there will be totally sixty coordinates and thus sixty Lagrange's equations for the system shown in Fig. 2-1. Since the system has only three degrees of freedom, there should be fifty-seven constraint equations and, thus, fifty-seven

Lagrange's multipliers. Therefore, simulation of this system is accomplished by solving simultaneously the one hundred and seventeen variables, sixty coordinates and fifty-seven multipliers, in one hundred and seventeen differential algebraic equations, sixty Lagrange's equations and fifty-seven constraint equations. This approach demands significant computation efforts. Furthermore, if constraint forces and torques are of interest, additional analyses have to be performed. In addition, inverse dynamic analysis for evaluating the driving torques for a given motion of the system also requires significant amount of computation. Its advantage is the relative ease of implementation for general mechanisms.

Next, an alternative method will be discussed. It can be observed that kinematic analysis of the system can be performed to determine the motions of all the links using only three generalized coordinates. Then the kinetic energy of the system is formulated in terms of these three coordinates and three Lagrange's equations of motion can be derived. Alternatively, Kane's equations or virtual work principle can be applied to derive the same equations. These equations can be numerically solved to yield the coordinates as functions of time. As for the inverse dynamics, the three Lagrange's equations can easily be rearranged for the analysis.

From the narratives above, it can be easily argued that the second method is much more efficient computationally. It, however, requires the analyst to apply skillful and significant amount of analysis on each individual system before the computer can be used to perform the numerical computations. It is the objective of this chapter to present a systematic and efficient approach for the derivation of dynamic equations of a general class of articulated gear mechanisms. The reaction force analysis will be discussed in the following chapter.

2.3 Kinematic Analysis

A systematic procedure for the kinematic analysis of spatial robotic bevel-gear trains was presented by Tsai (1988). This procedure involves the development of canonical graph representation for the system, the identification of equivalent open-loop chain, and the formulation of angular displacement equations.

2.3.1 Canonic Graph and Equivalent Open-Loop Chain

Graph representation is used to organize the analysis. In a graph representation, links are denoted by vertices, turning pairs by thin edges and gear meshings by heavy edges. The thin edges are labeled according to their axes locations in space. When there are three or more links that are connected together via coaxial revolute joints, the joints among these coaxial links can be reconfigured without changing the functionality of the mechanism. Rearranging the revolute joints will also change the graph representation. A *canonic graph* is an uniquely defined representation of a gear train in which there is no repeated axis labels in a thin-edged path starting from the base link (Tsai, 1988). Figure

2-2 shows the graph representation of the PUMA wrist mechanism, and Fig. 2-3 shows its canonic graph representation.

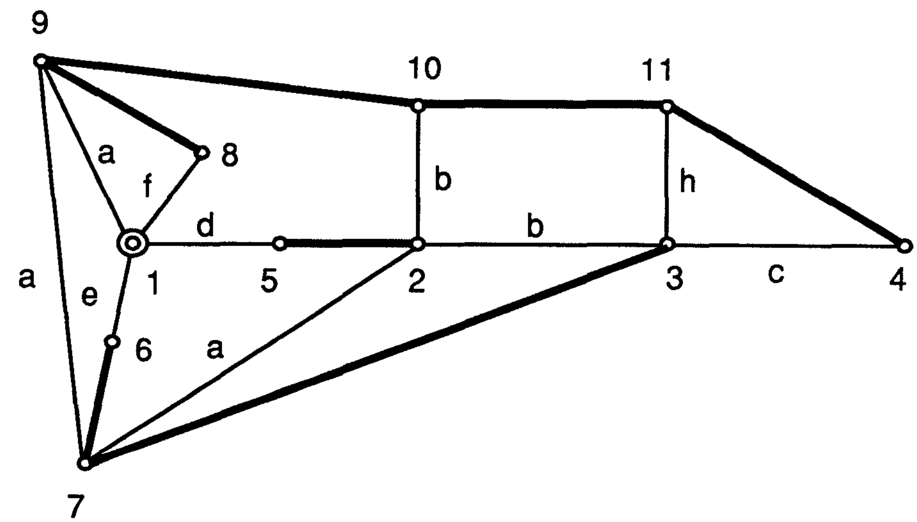

Fig. 2-2: Graph Representation of PUMA wrist Mechanism.

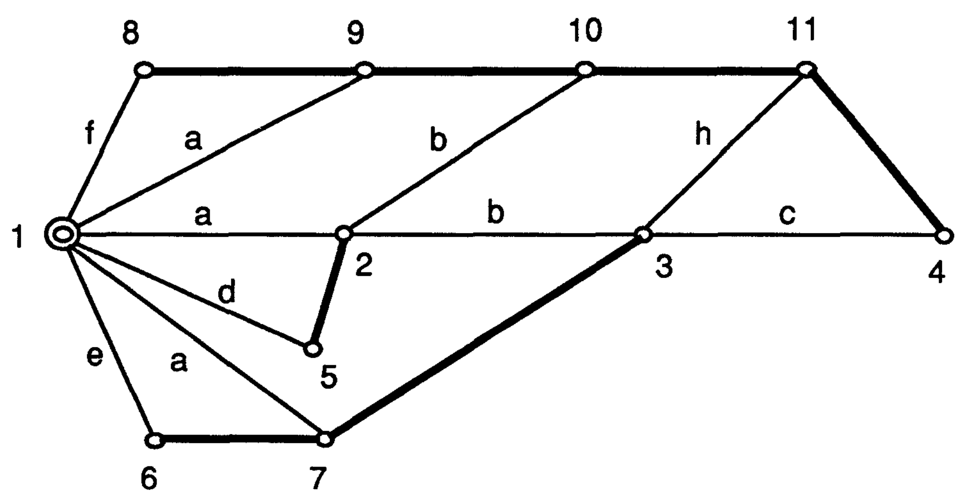

Fig. 2-3: Canonical Graph Representation of PUMA Wrist Mechanism.

The *equivalent open-loop chain* (EOLC) of a system is defined as the linkage made up of those links and joints along the thin-edged path from the base link to the output link in the canonical graph (Tsai, 1988). Figure 2-4 shows the equivalent open-loop chain of the example system.

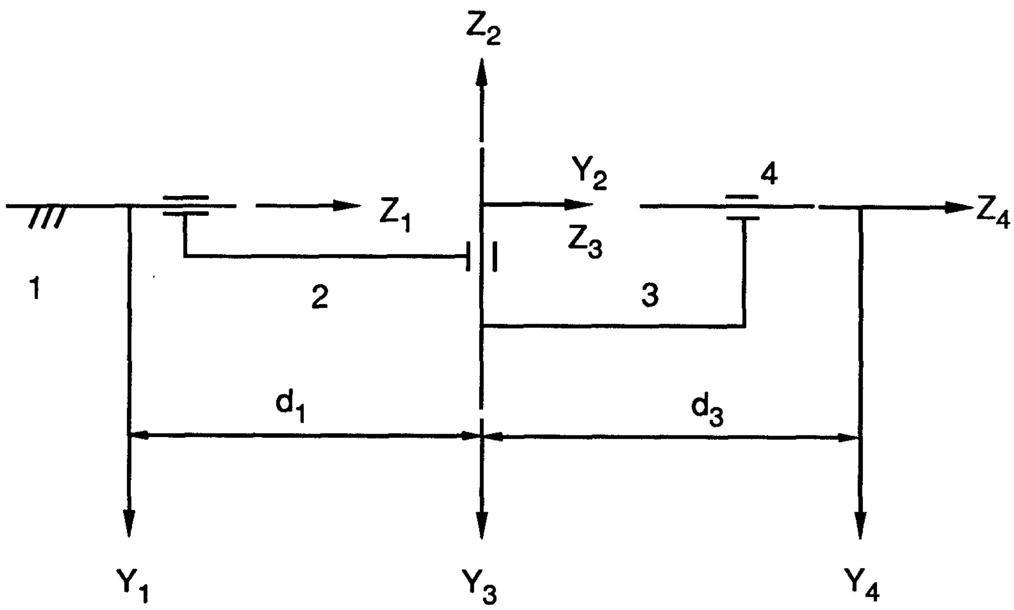

Fig. 2-4: The Equivalent Open-Loop Chain of PUMA Wrist Mechanism.

In order to facilitate the analysis, a coordinate system (X_i, Y_i, Z_i) is attached to each link of the equivalent open-loop chain in accordance with the Hartenberg and Denavit Convention (1955) as shown in Fig. 2-4. Thus the coordinate system (X_1, Y_1, Z_1) is attached to link 1 (the reference frame); (X_2, Y_2, Z_2) is attached to link 2; (X_3, Y_3, Z_3) is attached to link 3; and (X_4, Y_4, Z_4) is attached to link 4 (the end-effector). The origin of the first coordinate system should be located at the intersection of the Z_1-axis and the common normal between Z_1-axis and the last axis of a robot arm. In Fig. 2-4, the origin O_1 and X_1-axis are chosen arbitrarily since we do not know how the wrist is attached to the arm at this time. The Hartenberg and Denavit parameters for the PUMA wrist mechanism are given in Table 2-1, where a_i and α_i denote the offset distance and the twist angle between Z_i and Z_{i+1} axes, and d_i denotes the translational distance along Z_i-axis.

i	a_i	α_i	d_i
1	0	$\pi / 2$	d_1
2	0	$-\pi / 2$	0
3	0	0	d_3

Table 2-1: Hartenberg and Denavit Parameters for the PUMA Wrist Mechanism

Each link in Fig. 2-4 is referred to as a *major link* or *carrier*, and the angle $\theta_{i,j}$ measured from the X_j-axis to X_i-axis about the Z_j-axis is referred to as the *joint angle* in the equivalent open-loop chain. Throughout this dissertation, the word "joint angle" will be used to denote the joint angle in the equivalent open-loop chain. All the links other than the major links are called the *carried links*. In the canonical graph representation, all the carried links are connected directly to one of the major links by a revolute joint. Thus, as shown in Fig. 2-3, links 5, 6, 7, 8 and 9 are carried by major link 1, link 10 is carried by major link 2, and link 11 is carried by major link 3.

2.3.2 Kinematics of the Carriers

Kinematic properties of the major links, including the output link, can be found in terms of the open-loop joint angles by matrix method or vector approach. One of the most efficient and systematic approach in deriving the kinematic information of open-loop manipulators is the use of forward recursive equation presented by Walker and Orin (1982). This set of recursive equations can be applied to the links sequentially. The forward recursive propagates kinematic information such as angular velocity, angular acceleration, linear velocity and linear acceleration from the base reference frame (inertia frame) to the end-effector. This set of equation, with the aid of Fig. 2-5, referenced in its own link coordinate system can be written as follows.

$$^{i}\omega_{i} = {}^{i}R_{i-1}({}^{i-1}\omega_{i-1} + \dot{q}_{i-1}\,{}^{i-1}Z_{i-1}) \tag{2.1}$$

$$^{i}\dot{\omega}_{i} = {}^{i}R_{i-1}({}^{i-1}\dot{\omega}_{i-1} + \ddot{q}_{i-1}\,{}^{i-1}Z_{i-1} + {}^{i-1}\omega_{i-1} \times \dot{q}_{i-1}\,{}^{i-1}Z_{i-1}) \tag{2.2}$$

$$ {}^{i}v_i = {}^{i}\omega_i \times p_i^* + {}^{i}R_{i-1}\,{}^{i-1}v_{i-1} + {}^{i}\omega_i \times ({}^{i}\omega_i \times p_i^*) \tag{2.3} $$

$$ {}^{i}v_{si} = {}^{i}\omega_i \times {}^{i}s_i + {}^{i}v_i \tag{2.4} $$

$$ {}^{i}\dot{v}_i = {}^{i}\dot{\omega}_i \times p_i^* + {}^{i}\dot{v}_i + {}^{i}\omega_i \times ({}^{i}\omega_i \times p_i^*) \tag{2.5} $$

$$ {}^{i}\dot{v}_{si} = {}^{i}\dot{\omega}_i \times {}^{i}s_i + {}^{i}\dot{v}_i + {}^{i}\omega_i \times ({}^{i}\omega_i \times {}^{i}s_i) \tag{2.6} $$

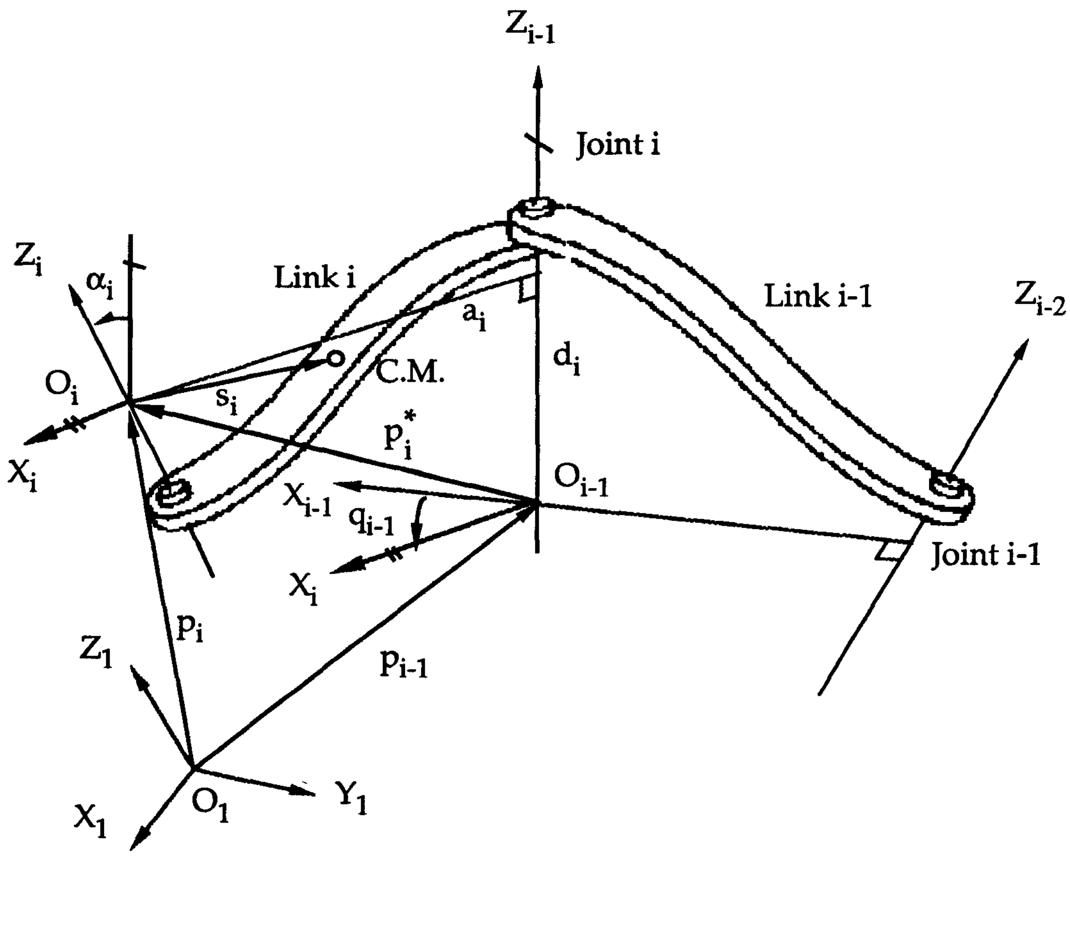

Fig. 2-5: Coordinate Systems of Major Links.

where a leading superscript denotes the coordinate system in which the vector is referred to and if it is omitted, inertia frame is implied, and where ${}^{i}R_{i-1}$ is the rotational matrix which transfers a vector υ from the (i-1)-th to the i-th coordinate system such that

$$ {}^{i}\upsilon = {}^{i}R_{i-1} \cdot {}^{i-1}\upsilon \tag{2.7}$$

where

$$ {}^{i}R_{i-1} = \begin{bmatrix} C_{i-1} & S_{i-1} & 0 \\ -C_{\alpha_i} S_{i-1} & C_{\alpha_i} C_{i-1} & S_{\alpha_i} \\ S_{\alpha_i} S_{i-1} & -S_{\alpha_i} C_{i-1} & C_{\alpha_i} \end{bmatrix} \tag{2.8}$$

and where $S_{\alpha i} = \sin(\alpha_i)$ and $C_{\alpha i} = \cos(\alpha_i)$.

From eq. (2.1), it can be shown that the angular velocity of a major link, say link j, is only a function of the rate of change of the joint angles preceding link j and it can be written as

$$ {}^{j}\omega_j = \sum_{s=1}^{j-1} (U_{js} \dot{q}_s) \tag{2.9}$$

Note that U_{js} is a unit vector defined along the s-th joint axis in the equivalent open-loop chain and expressed in the j-th link coordinate system. Also note that these unit vectors U_{js}, s = 1, 2, ⋯, j-1, are functions of the joint angles q_s, s= 1, 2, ⋯, j-1.

For the example system, angular velocities of the major links can be written as

$$ {}^{2}\omega_{2} = \begin{bmatrix} 0 \\ 1 \\ 0 \end{bmatrix} \dot{q}_{1} \tag{2.10} $$

$$ {}^{3}\omega_{3} = \begin{bmatrix} S_{2} \\ 0 \\ C_{2} \end{bmatrix} \dot{q}_{1} + \begin{bmatrix} 0 \\ -1 \\ 0 \end{bmatrix} \dot{q}_{2} \tag{2.11} $$

and

$$ {}^{4}\omega_{4} = \begin{bmatrix} S_{2}C_{3} \\ -S_{2}S_{3} \\ C_{2} \end{bmatrix} \dot{q}_{1} + \begin{bmatrix} -S_{3} \\ -C_{3} \\ 0 \end{bmatrix} \dot{q}_{2} + \begin{bmatrix} 0 \\ 0 \\ 1 \end{bmatrix} \dot{q}_{3} \tag{2.12} $$

2.3.3 Kinematics of the Carried Links

Coaxial and fundamental circuit equations (Tsai, 1988) can be used to find the angular displacements of all the carried links in terms of the open-loop joint angles. A fundamental circuit consists of a gear pair and its carrier, relative to which the gears can be considered to be performing simple fixed axis rotations. In a fundamental circuit, the rotation of one gear with respect to its carrier is equal to the rotation of the other gear multiplied by their gear ratio. For example, it can be seen from Fig. 2-3, that link 2 is the carrier for the gear pair (9, 10), thus one can write

$$ \theta_{9,2} = r_{10,9'}\, \theta_{10,2} \tag{2.13} $$

where $r_{10,9'} = \pm N_{10}/N_{9'}$ is the gear ratio, positive or negative depending on whether a positive rotation of one gear produces a positive or negative rotation of the other about their predefined axes of rotation.

When two turning pairs share a common joint axis, they are coaxial and simple relationship, called coaxiality condition, exists between relative angular displacements and velocities. For example, from Fig. 2-3, revolute pairs (9,1) and (1,2) are coaxial, and one can write

$$\theta_{9,2} = \theta_{9,1} + \theta_{1,2} = \theta_{9,1} - \theta_{2,1} \tag{2.14}$$

With the fundamental-circuit equations and the appropriate coaxiality conditions, the rotational speed of a carried link i with respect to its carrier j in an n-D.O.F. geared mechanism can be written as a linear summation of the joint rates as shown below:

$$\dot{\theta}_{i,j} = \sum_{s=j}^{n} (b_{is} \dot{q}_s) \tag{2.15}$$

where b_{is}, is the influence coefficient associated with $\dot{q}_s$ and is a function of gear ratios in a transmission line. Furthermore, if the carried link i is an input link on the s-th transmission line, then b_{is}, s = j, j+1, $\cdots$, n, are the elements of the s-th column in the structure matrix A defined by Chang and Tsai (1990), and a collection of these $\dot{\theta}_{i,j}$'s forms the actuator velocity vector $\dot{\Phi}$.

For the example system, the input and output joint velocities can be related by

$$\begin{bmatrix} \dot{\theta}_{5,1} \\ \dot{\theta}_{6,1} \\ \dot{\theta}_{8,1} \end{bmatrix} = A^T \begin{bmatrix} \dot{q}_1 \\ \dot{q}_2 \\ \dot{q}_3 \end{bmatrix} \tag{2.16}$$

where

$$A = \begin{bmatrix} g_{11} & g_{12} & g_{13} \\ 0 & g_{22} & g_{23} \\ 0 & 0 & g_{33} \end{bmatrix} \tag{2.17}$$

and where $(\,)^T$ denotes the transpose of $(\,)$, $g_{11} = r_{2,5}$, $g_{12} = r_{7,6}$, $g_{22} = g_{12}\, r_{3,7'}$, $g_{13} = r_{9,8}$, $g_{23} = g_{13}\, r_{10,9'}$, $g_{33} = g_{23}\, r_{11,10'}\, r_{4,11'}$, $\Phi = [\, \theta_{5,1}, \theta_{6,1}, \theta_{8,1} \,]^T$, and where $\Theta = [\, \theta_{2,1}, \theta_{3,2}, \theta_{4,3} \,]^T = [\, q_1, q_2, q_3 \,]^T$ are considered as the generalized coordinates.

We note that the matrix A shown in eq. (2.17) is called the *structure matrix* which can be derived systematically by inspecting the kinematic structure of a mechanism (Chang and Tsai, 1990).

The angular velocity of links 7, 9, 10, and 11 with respect to their carriers can also be written in a matrix form as

$$\begin{bmatrix} \dot{\theta}_{7,1} \\ \dot{\theta}_{9,1} \\ \dot{\theta}_{10,2} \\ \dot{\theta}_{11,3} \end{bmatrix} = \begin{bmatrix} 1 & r_{3,7} & 0 \\ 1 & r_{10,9'} & r_{10,9'} r_{11,10'} r_{4,11'} \\ 0 & 1 & r_{11,10'} r_{4,11'} \\ 0 & 0 & r_{4,11'} \end{bmatrix} \begin{bmatrix} \dot{q}_1 \\ \dot{q}_2 \\ \dot{q}_3 \end{bmatrix} \tag{2.18}$$

2.4 Equations of Motion

The basic concept for this approach was presented by Chen (1989). The contribution of the carried links to the generalized inertia forces can be divided into two parts. The first part is due to the motion with the carriers and the second part is due to the motion relative to their carriers. It is computationally advantageous to incorporate the first part of the generalized inertia forces with that of the appropriate major links. This can be done by treating the carried links as being rigidly attached to their carriers and then the generalized inertia forces due to the resulted open-loop linkage are formulated. Next, the effects due to relative motion of the carried links with respect to their carriers are derived and added to the generalized inertia forces mentioned above. Finally, generalized active forces are formulated and combined with generalized inertia forces to form the equations of motion.

2.4.1 Generalized Inertia Force Due to Motion of the Major Links: M_m

All the carried links are treated as being fixed in their respective carriers. The combined mass properties such as the combined mass, the combined center of mass location, and the combined moment of inertia for each major link and its carried links are evaluated. Then the mass center velocity and linear acceleration of the major links in the resulted open-loop chain are computed using eqs. (2.4) and (2.6). Several methods such as Lagrangian formulation (Hollerbach, 1980) and Newton-Euler formulation (Lee, et al., 1985; Thomas and Tesar, 1982; Walker and Orin, 1982) can be used to formulate the generalized inertia forces of this open-loop type kinematic chain. It is well acknowledged that, in general, the use of Lagrangian formulation provides more physical insight on the modelled system while the Newton-Euler formulation is more efficient computationally.

The generalized inertia forces, F^*_m, (Kane and Levinson, 1985) for such an open-loop chain system can always be put in the following form.

$$F^*_m = M_m(\Theta)\left[\ddot{\Theta}\right] + C_m(\Theta,\dot{\Theta}) + G_m(\Theta) \tag{2.19}$$

where $M_m(\Theta)$ is a 3 by 3 inertia matrix, $C_m(\Theta, \dot{\Theta})$ is a 3 by 1 matrix specifying the coriolis and centrifugal effects, and $G_m(\Theta)$ is a 3 by 1 matrix specifying the gravitational effects.

For our example, the three-D.O.F. mechanism shown in Fig. 2-4 is the open-loop manipulator whose generalized inertia force will be formulated. The mass and inertia properties of links 5 to 9 should be incorporated in link 1, which is fixed to the ground and thus has no effects. The mass and inertia properties of link 10 should be included in link 2 and those of link 11 in link 3. Let m_4 be the mass of link 4, $m_{2'}$ the combined mass of links 10 and 2, and $m_{3'}$ the combined mass of links 11 and 3, respectively. Let $s_{2'} = [\ 0, p_{2y}, p_{2z}\ ]$, $s_{3'} = [\ 0, p_{3y}, p_{3z}\ ]$ and $s_4 = [\ 0, 0, p_{4z}\ ]$ be the combined centers of mass locations of links 2, 3, and 4 and expressed in their respective link coordinate systems. And let the combined moments of inertia about their respective center-of-mass coordinate systems be

$$mi_{2'} = \begin{bmatrix} I_{2,11} & 0 & 0 \\ 0 & I_{2,22} & I_{2,23} \\ 0 & I_{2,23} & I_{2,33} \end{bmatrix} \tag{2.20}$$

$$mi_{3'} = \begin{bmatrix} I_{3,11} & 0 & 0 \\ 0 & I_{3,22} & I_{3,23} \\ 0 & I_{3,23} & I_{3,33} \end{bmatrix} \tag{2.21}$$

and

$$mi_4 = \begin{bmatrix} I_{4,11} & 0 & 0 \\ 0 & I_{4,22} & 0 \\ 0 & 0 & I_{4,33} \end{bmatrix} \tag{2.22}$$

Then, the generalized inertia forces of this equivalent open-loop chain, with the gravitational effect neglected, can be written as

$$F^*_m = M_m(\Theta)[\ddot{\Theta}] + C_m(\Theta,\dot{\Theta}) \tag{2.23}$$

where

$$M_m = \begin{bmatrix} \varphi_1 + S_2^2(\varphi_2+\varphi_6+\varphi_8) + \varphi_5 + I_{4,33}C_2^2 & C_2\varphi_3 - S_2C_3S_3\varphi_7 & I_{4,33}C_2 \\ C_2\varphi_3 - S_2C_3S_3\varphi_7 & \varphi_4+\varphi_6+\varphi_9 & 0 \\ I_{4,33}C_2 & 0 & I_{4,33} \end{bmatrix} \tag{2.24}$$

and

$$C_m[1,1] = C_2C_3(2\varphi_{10}\dot{q}_1\dot{q}_2 - \varphi_7(S_3\dot{q}_2^2 + 2S_2^2\dot{q}_1\dot{q}_3) - \varphi_{11}S_2\dot{q}_2\dot{q}_3 \tag{2.25}$$

$$C_m[2,1] = -\varphi_{10}C_2S_2\dot{q}_1^2 + 2\varphi_7C_3S_3\dot{q}_2\dot{q}_3 - \varphi_{11}S_2\dot{q}_1\dot{q}_3 \tag{2.26}$$

$$C_m[3,1] = \varphi_{11}S_2\dot{q}_1\dot{q}_2 + C_3S_3\varphi_7(S_2^2\dot{q}_1^2 - \dot{q}_2^2) \tag{2.27}$$

and where

$$\varphi_1 = m_{2'}p_{2z}^2 + I_{2,22} \tag{2.28a}$$

$$\varphi_2 = m_{3'}p_{3z}^2 + I_{3,11} \tag{2.28b}$$

$$\varphi_3 = m_{3'}p_{3y}p_{3z} - I_{3,23} \tag{2.28c}$$

$$\varphi_4 = m_{3'}p_{3z}^2 + I_{3,22} \tag{2.28d}$$

$$\varphi_5 = m_3 . p_{3y}^2 + C_2^2 I_{3,33} \tag{2.28e}$$

$$\varphi_6 = m_4 (d_3 + p_{4z})^2 \tag{2.28f}$$

$$\varphi_7 = (I_{4,11} - I_{4,22}) \tag{2.28g}$$

$$\varphi_8 = (C_3^2 I_{4,11} + S_3^2 I_{4,22}) \tag{2.28h}$$

and

$$\varphi_9 = (S_3^2 I_{4,11} + C_3^2 I_{4,22}) \tag{2.28i}$$

$$\varphi_{10} = \varphi_6 + \varphi_8 - I_{4,33} + \varphi_2 - I_{3,33} \tag{2.28j}$$

$$\varphi_{11} = \varphi_7 (C_3^2 - S_3^2) - I_{4,33} \tag{2.28k}$$

2.4.2 Generalized Inertia Forces Due to Relative Motion of the Carried Links: M_r and M_g

The kinetic energy due to the relative rotation of a carried link, i, with respect to its carrier, link j, can be written as (Chen, 1989)

$$K_{i,j} = \frac{1}{2} I_i \dot{\theta}_{i,j}^2 + I_i \dot{\theta}_{i,j} (\omega_j \cdot \upsilon_i) \tag{2.29}$$

where

$K_{i,j}$ is that part of kinetic energy of a carried link i due to its motion with respect to the carrier, link j,

υ_i is a unit vector along the "positive" axis of rotation of link i with respect to link j,

and

I_i is the moment of inertia of link i about its axis of rotation on the carrier.

Substituting eqs. (2.9) and (2.15) into (2.29), yields

$$K_{i,j}=\frac{1}{2} I_i \left[\sum_{s=j}^{n} (b_{is}\dot{q}_s)\right]^2 + I_i \sum_{s=j}^{n} (b_{is}\dot{q}_s)\left[\sum_{s=1}^{j-1} (U_{js}\dot{q}_s)\cdot {}^j\upsilon_i\right] \tag{2.30}$$

Applying Lagrangian equation to eq. (2.30), yields

for $r \geq j$:

$$F^*_{ir} = I_i b_{ir}\left[\sum_{s=j}^{n} (b_{is}\ddot{q}_s) + \sum_{s=1}^{j-1} (U_{js}\ddot{q}_s)\cdot {}^j\upsilon_i + \sum_{s=1}^{j-1} (\dot{U}_{js}\dot{q}_s)\cdot {}^j\upsilon_i\right], \tag{2.31}$$

and for $r < j$:

$$F^*_{ir} = I_i\left[\sum_{s=j}^{n} (b_{is}\ddot{q}_s)(U_{jr}\cdot {}^j\upsilon_i) + \sum_{s=j}^{n} (b_{is}\dot{q}_s)\cdot(\dot{U}_{jr}\cdot {}^j\upsilon_i) - \sum_{s=j}^{n} (b_{is}\dot{q}_s)\sum_{s=1}^{j-1}\left(\frac{\partial U_{js}}{\partial q_r}\dot{q}_s\right)\cdot {}^j\upsilon_i\right] \tag{2.32}$$

where F^*_{ir} denotes the generalized inertia forces due to the relative motion of a carried link i with respect to its carrier, major link j, and associated with the generalized coordinate q_r. In what followed, we shall divided F^*_{ir} into two groups, one for the input links and the other for the intermediate carried links. Each group can be arranged in a form similar to that shown in eq. (2.23). We shall denote the inertia matrix matrix associated with the input links as M_r and that with the intermediate carried links as M_g, and the sum of the two inertia matrices as M_c.

For the example system, the kinetic energy contribution due to relative motions of carried links 5, 6, 7, 9, 8, 10 and 11 with respect to their carriers need to be evaluated. Substituting the appropriate equations and their derivatives of eq. (2.16) and eqs. (2.9) to (2.12) into eq. (2.30), yields the kinetic energy of the input links as

$$K_{5,1} = I_5 g_{11}^2 \dot{q}_1^2 / 2 \tag{2.33}$$

$$K_{6,1} = I_6 (g_{12}\dot{q}_1 + g_{22}\dot{q}_2)^2 \tag{2.34}$$

and

$$K_{8,1} = I_8 (g_{13}\dot{q}_1 + g_{22}\dot{q}_2 + g_{33}\dot{q}_3)^2 / 2 \tag{2.35}$$

Note that the inertia of an input link includes the inertia of the actuator reflected at the pivot of the input links.

Similarly, the kinetic energy contribution due to the relative motions of intermediate links 7, 9, 10 and 11 can be written as.

$$K_{7,1} = I_7 (\dot{q}_1 + r_{3,7}\dot{q}_2)^2/2 \tag{2.36}$$

$$K_{9,1} = I_9 (\dot{q}_1 + r_{10,9}\cdot\dot{q}_2 + r_{10,9}\cdot r_{11,10}\cdot r_{4,11}\cdot\dot{q}_3)^2/2 \tag{2.37}$$

$$K_{10,2} = I_{10} (\dot{q}_2 + r_{11,10}\cdot r_{4,11}\cdot\dot{q}_3)^2/2 \tag{2.38}$$

$$K_{11,3} = I_{11}\, r_{4,11}\cdot [r_{4,11}\cdot\dot{q}_3^2 / 2 + \cos(q_2)\dot{q}_1\dot{q}_3] \tag{2.39}$$

Here it is assumed that the axis of rotation of link 11 relative to link 3 is parallel to Z_3 axis, which is always perpendicular to Z_2 axis while Z_2 axis remains perpendicular to Z_1 axis.

From eqs. (2.31) and (2.32), the contribution to the generalized inertia forces of input links 5, 6 and 8 can be obtained as

$$F_r^* = M_r\left[\ddot{\Theta}\right] + C_r(\Theta,\dot{\Theta}) \tag{2.40}$$

where

$$M_r = \begin{bmatrix} I_5 g_{11}^2 + I_6 g_{12}^2 + I_8 g_{13}^2 & I_6 g_{12} g_{22} + I_8 g_{13} g_{23} & I_8 g_{13} g_{33} \\ I_6 g_{12} g_{22} + I_8 g_{13} g_{23} & I_6 g_{22}^2 + I_8 g_{23}^2 & I_8 g_{23} g_{33} \\ I_8 g_{13} g_{33} & I_8 g_{23} g_{33} & I_8 g_{33}^2 \end{bmatrix} \tag{2.41}$$

$$C_r(\Theta,\dot{\Theta}) = [\,0 \quad 0 \quad 0\,]^T \tag{2.42}$$

Similarly, the contributions to the generalized inertia forces due to the intermediate carried links 7, 9, 10 and 11 can be obtained as

$$F_g^* = M_g(\Theta)\left[\ddot{\Theta}\right] + C_g(\Theta,\dot{\Theta}) \tag{2.43}$$

where

$$M_g(\Theta) = \begin{bmatrix} M_{g11} & M_{g12} & M_{g13} \\ M_{g12} & M_{g22} & M_{g23} \\ M_{g13} & M_{g23} & M_{g33} \end{bmatrix} \tag{2.44}$$

$$C_g(\Theta,\dot{\Theta}) = \begin{bmatrix} -I_{11} r_{4,11'} S_2 \dot{q}_2 \dot{q}_3 \\ I_{11} r_{4,11'} S_2 \dot{q}_1 \dot{q}_3 \\ -I_{11} r_{4,11'} S_2 \dot{q}_1 \dot{q}_2 \end{bmatrix} \tag{2.45}$$

and where

$$M_{g11} = I_7 + I_9 \tag{2.46a}$$

$$M_{g12} = I_7 r_{3,7} + I_9 r_{10,9'} \tag{2.46b}$$

$$M_{g13} = I_9 r_{10,9'} r_{11,10'} r_{4,11'} + I_{11} r_{4,11'} C_2 \tag{2.46c}$$

$$M_{g22} = I_7 r^2_{3,7'} + I_9 r^2_{10,9'} + I_{10} \tag{2.46d}$$

$$M_{g23} = I_9 r^2_{10,9'} r_{11,10'} r_{4,11'} + I_{10} r_{11,10'} r_{4,11'} \tag{2.46e}$$

$$M_{g33} = I_9 (r_{10,9'} r_{11,10'} r_{4,11'})^2 + I_{10} (r_{11,10'} r_{4,11'})^2 + I_{11}\, r^2_{4,11'} \tag{2.46f}$$

Thus, the additional contributions to generalized inertia forces of the carried links, from eqs. (2,40) and (2.43), can be written as

$$\begin{aligned} F^*_c &= F^*_r + F^*_g \\ &= M_c(\Theta)\left[\ddot{\Theta}\right] + C_c(\Theta,\dot{\Theta}) \end{aligned} \tag{2.47}$$

where

$$M_c(\Theta) = M_r(\Theta) + M_g(\Theta) \tag{2.48}$$

and

$$C_c(\Theta,\dot{\Theta}) = C_r(\Theta,\dot{\Theta}) + C_g(\Theta,\dot{\Theta}) \tag{2.49}$$

Finally, the generalized inertia forces of the system, from eqs. (2.23) and (2.47), can be obtained as

$$\begin{aligned} F^* &= F^*_m + F^*_c \\ &= (M_m(\Theta) + M_c(\Theta))\left[\ddot{\Theta}\right] + (C_m(\Theta,\dot{\Theta}) + C_c(\Theta,\dot{\Theta})) + G_m(\Theta) \end{aligned} \tag{2.50}$$

2.4.3 Generalized Active Forces

The formulation of generalized active forces is rather straightforward. From eq. (2.16), it has been shown that the equation relating resultant joint torques in the equivalent open-loop chain to the input actuator torques is given by (Chang and Tsai, 1990)

$$\tau = A\ \xi \tag{2.51}$$

where τ is the vector of resultant joint torques and ξ is the vector of input actuator torques.

The generalized active forces in the Lagrange's equations of motion, Q, can be written as

$$Q = \frac{\partial \Phi}{\partial q_i} \xi \qquad i = 1,2,\cdots,n \tag{2.52}$$

It has also been shown that the resultant joint torques are, in fact, the generalized active forces, F, if the joint angles are used as the generalized coordinates, i.e.

$$F = \tau \tag{2.53}$$

Hence, the resultant joint torques can be thought of as a set of torques acting on the joint of the equivalent open-loop chain directly.

For the example system, the generalized active forces, from eqs. (2.16) and (2.51), can be written as

$$\begin{bmatrix} \tau_1 \\ \tau_2 \\ \tau_3 \end{bmatrix} = \begin{bmatrix} g_{11} & g_{12} & g_{13} \\ 0 & g_{22} & g_{23} \\ 0 & 0 & g_{33} \end{bmatrix} \begin{bmatrix} \xi_5 \\ \xi_6 \\ \xi_8 \end{bmatrix} \tag{2.54}$$

2.4.4 Dynamic Equations

Thus, by equating generalized inertia forces and generalized active forces, the equations of motion can be obtained as

$$F^* = A\,\xi \tag{2.55}$$

or

$$M\left[\ddot{\Theta}\right] + C(\Theta,\dot{\Theta}) + G_m(\Theta) = A\,\xi \tag{2.56}$$

where

$$M = M_m(\Theta) + M_c(\Theta) \tag{2.57}$$

$$C(\Theta,\dot{\Theta}) = C_m(\Theta,\dot{\Theta}) + C_c(\Theta,\dot{\Theta}) \tag{2.58}$$

2.5 A Two-D.O.F. Planar Manipulator

Fig. 2-6 shows a two-D.O.F. planar manipulator. The corresponding graph and canonic graph representations are shown in Figs. 2-7 and 2-8, respectively.

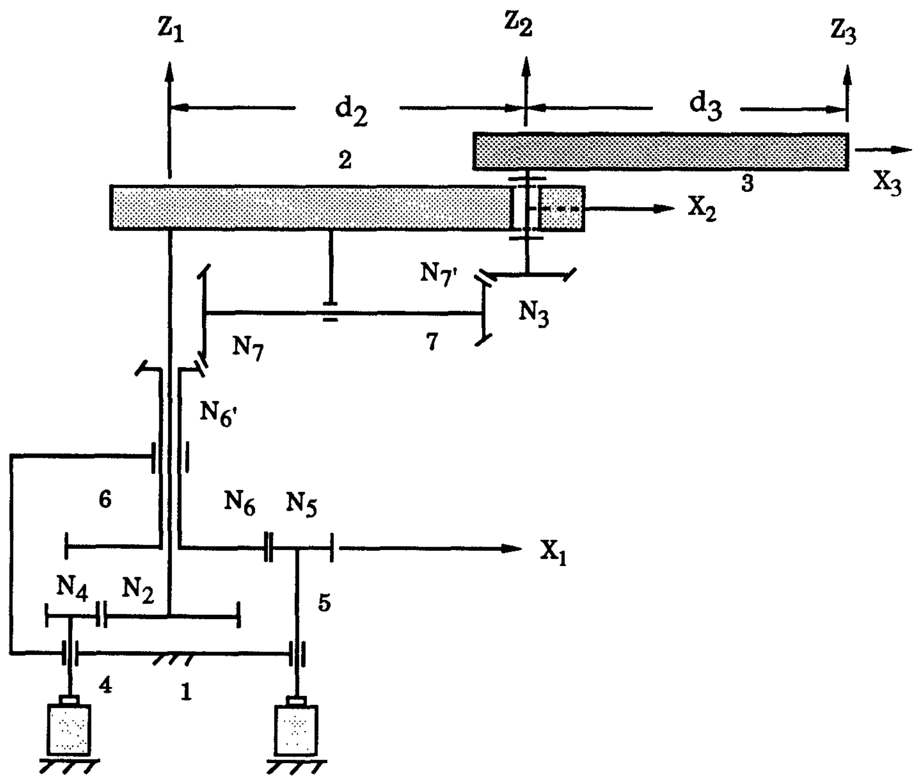

Fig. 2-6: A Two-D.O.F. Planar Gear-Coupled Manipulator.

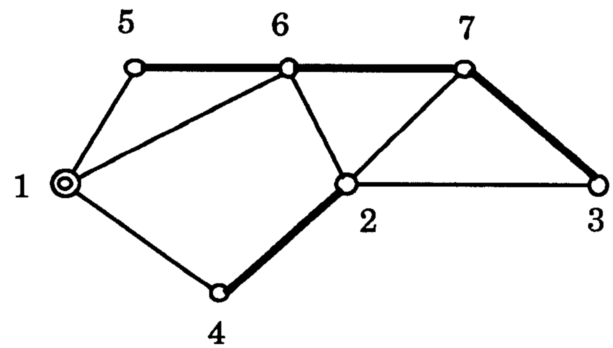

Fig. 2-7: Actual Graph Representation of The Two-D.O.F. Planar Gear-Coupled Manipulator Shown in Fig. 2-6.

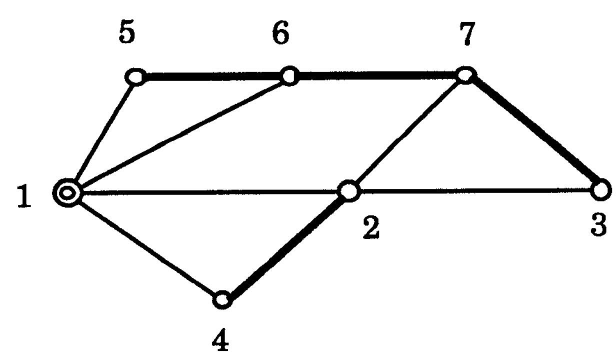

Fig. 2-8: Canonic Graph Representation of The Two-D.O.F. Planar Gear-Coupled Manipulator Shown in Fig. 2-6.

Let $P_2 = [\ p_{2x}, 0\ ]^T$ be the position vector of the combined mass center of links 2 and 7 and expressed in the link 2 coordinate system, $P_3 = [\ p_{3x}, 0$

$]^T$ the position vector for the center of mass of link 3 and expressed in the link 3 coordinate system, m_2 the combined mass of links 2 and 7, m_3 the mass of link 3, I_{2z} the resulted moment of inertia of links 2 and 7 about a line passing through its combined mass center and parallel to the Z_2-axis, I_{3z} the moment of inertia of link 3 about a line passing through its mass center and parallel to the Z_3-axis. Then, it can be shown that the generalized inertia force contribution of the corresponding equivalent open-loop chain can be written as shown in eq. (2.23), where

$$M_m = \begin{bmatrix} m_{m11} & m_{m12} \\ m_{m12} & m_{m22} \end{bmatrix} \tag{2.59}$$

and

$$C_m = \begin{bmatrix} -m_3 d_2 d'_3 S_2 (2\dot{q}_1 \dot{q}_2 + \dot{q}_2^2) \\ m_3 d_2 d'_3 S_2 \dot{q}_1^2 \end{bmatrix} \tag{2.60}$$

where

$$m_{m11} = m_2 d'^2_2 + I_{2z} + m_3 [d'^2_3 + d_2^2 + 2d_2 d'_3 C_2] + I_{3z} \tag{2.61a}$$

$$m_{m12} = m_3 (d'^2_3 + d_2 d'_3 C_2) + I_{3z} \tag{2.61b}$$

$$m_{m22} = m_3 d'^2_3 + I_{3z} \tag{2.61c}$$

$$d'_2 = p_{2x} + d_2 \tag{2.62a}$$

$$d'_3 = p_{3x} + d_3 \tag{2.62b}$$

Note that both P_{2x} and P_{3x} are negative numbers. Let I_i be the axial moment of inertia of gear i, then the generalized inertia forces contribution due to the relative motion of input links with respect to its carrier can be written as shown in eq. (2.40), where

$$M_r = \begin{bmatrix} I_4 g_{11}^2 + I_5 g_{12}^2 & I_5 g_{12} g_{22} \\ I_5 g_{12} g_{22} & I_5 g_{22}^2 \end{bmatrix} \tag{2.63}$$

and

$$C_r = [0 \quad 0]^T \tag{2.64}$$

where $g_{11} = r_{2,4}$, $g_{12} = r_{6,5}$, $g_{22} = g_{12}\, r_{7,6'}\, r_{3,7'}$.

The generalized inertia forces due to relative motion of the other carried links its carrier can be written as shown in eq. (2.43), where

$$M_g = \begin{bmatrix} I_6 & I_6 r_{7,6'} r_{3,7'} \\ I_6 r_{7,6'} r_{3,7'} & I_6 (r_{7,6'} r_{3,7'})^2 + I_7 r_{3,7'}^2 \end{bmatrix} \tag{2.65}$$

and

$$C_g = [0 \quad 0]^T \tag{2.66}$$

Thus, from eqs.(2.59-2.66), the generalized inertia forces can be formed accordingly.

The generalized active forces, from eq. (2.51), can be written as

$$\tau = \begin{bmatrix} g_{11} & g_{12} \\ 0 & g_{22} \end{bmatrix} \xi \tag{2.67}$$

Hence, the equations of motion for the two-D.O.F. planar manipulator can be established accordingly.

2.6 Discussions and Summary

Equation (2.56) can be rearranged into several different forms for different application. For inverse dynamics, i.e. to compute the required input torques to achieve the system with a prescribed motion state, the required input torques can be found directly from

$$\xi = A^{-1}[\, M[\ddot{\Theta}] + C(\Theta,\dot{\Theta}) + G_m(\Theta)\,] \tag{2.68}$$

As for the direct dynamics, i.e., to compute the resulting motion states with given input torques, eq. (2.56) can be rearranged as

$$[\ddot{\Theta}] = M^{-1}[\, A\xi - (C(\Theta,\dot{\Theta}) + G_m(\Theta))\,] \tag{2.69}$$

Equation (2.69) represents the simulation form of equations of motion. With the input actuator torques and initial conditions of the system, it is possible to solve eq. (2.69) for the joint accelerations. These joint accelerations can be numerically integrated to obtain the motion state of the manipulator at the next time step and the new accelerations can be computed. The procedure repeats itself until the desired simulation time is reached.

In conclusion, a systematic methodology for the derivation of dynamic equations for a general class of articulated gear mechanisms has been developed. This approach combines recently published results related to kinematic and dynamic analyses of such gear systems into a uniform framework. Table 2-2 shows a flow chart describing this systematic approach in a clear and concise manner. The procedure can be implemented in a computer program for automated analysis of a general class of articulated gear mechanisms.

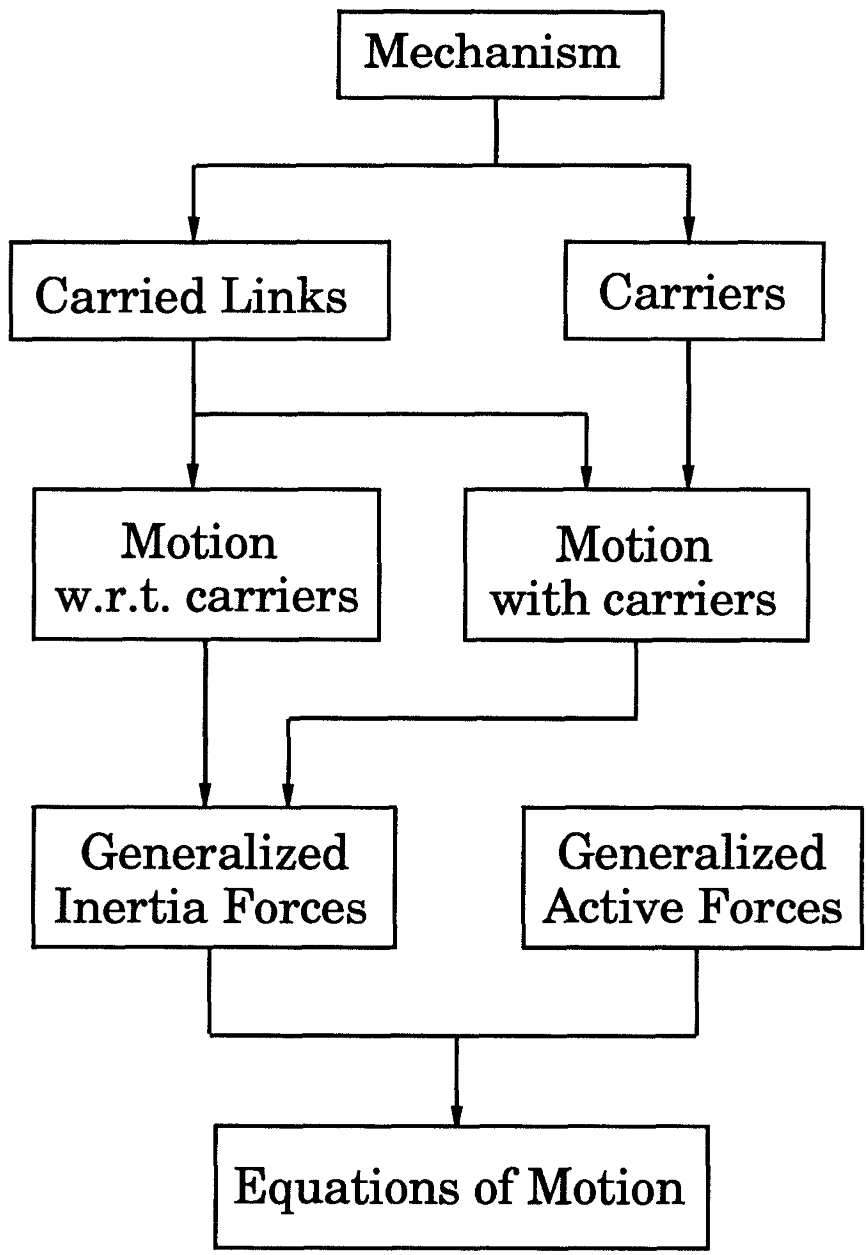

Table 2-2: A Systematic Procedure for Formulation of Dynamic Equations.

CHAPTER 3

Reaction Force Analysis

3.1 Introduction

In order to design a machine or mechanism for reliability, it is necessary to determine the reaction forces and/or torques acting on the individual links. Each component of a machine, however small, should be carefully analyzed for its role in transmitting forces. In chapter two, the forces that cause motion have been considered, but the reaction forces that resulted from the motion of the system have been intentionally avoided. The ability to establish the equations of motion without concerning the reaction forces is a great advantage. If, however, the ultimate objective is the determination of these forces, some additional steps must to be done. These additional steps are the subject of study in this chapter.

Reaction forces are of great importance to a machine designer. They affect the sizes of the machine components. Stress, deflection, bearing loads, wears, and energy consumption are also governed by the magnitudes of reaction forces. Thus, no machine design is considered complete until the reaction forces have been determined and found acceptable for the final design.

There are three standard engineering approaches to the problem of determining reaction forces, each of which is appropriate to a particular type of problem. They are the methods of *Statics, Kinetostatics* and *Dynamics,* and their descriptions follow (Doughty, 1988).

Statics. As the name implies, this approach assume that all components are in equilibrium, and the forces are determined on this basis. This method is valid for a mechanism that is motionless under loads, and is often appropriate for slowly moving (quasistatic) machines. The simplest of the three approaches, this method has been used widely for many years. Unfortunately, if has been applied to many situations where it really was not appropriate.

Kinetostatics. Many mechanisms move without noticeable changes in speeds or with apparently simple speed variation. In either cases, it may be possible to assume an approximate description of the motion, often a relatively simple $\dot{q}$ = constant approximation. The kinetostatics method attempts to account for the effects of motion by assuming that an approximate motion is the true motion, and allowing for the inertial effects thus induced.

Dynamics. When speed variation is clearly present, there is often no adequate, simple, approximate description of the motion. In this case, it is necessary first to determine the motion with given input forces/torques, for direct dynamic problem, or to compute the input forces/torques with a prescribed motion, for inverse dynamic problem, by solving the equations of motion. Then use the results to determine the reaction forces. For most systems, the dynamic analysis is the most difficult and time-consuming of the three approaches. However, it is the most accurate and reliable method.

In this chapter, the reaction force analysis due to dynamic effect will be discussed in detail. Rigid links and frictionless joints are assumed. For simplicity, the problem can be stated as follows:

Assuming the motion state and the input torques are known from the analysis described in chapter two, the problem is to find:
1. reaction forces exerted on all gear meshes, and
2. reaction loads exerted on the revolute joints.

3.2 Evaluation Strategy

The force/moment balance equations of a free-body are the Newton's and the Euler's equations, and they consist of six independent equations. Theoretically it is possible to list all the equations for all the links and then solve for all the unknown constraint forces and torques at the same time. However, this is very computationally intensive and inefficient for complex mechanical systems such as the PUMA and the Bendix wrists shown schematically in Fig. 2-1 and 3-1, respectively. If there are six or fewer unknown constraint forces and torques in the balance equations for a single link, then these forces and torques can be solved independent of those equations for other links. With these forces and torques solved, those for an adjacent link may become solvable also. It is often the case that all the constraint forces and torques acting on input or output link, can be solved with the use of its own free-body force balance equations. Once they are solved, the constraint forces and torques acting on their adjacent links will become solvable. This procedure can continue throughout the system until all the reaction forces are found. For each link, there are only six linear algebraic equations to be solved simultaneously. Hence, the procedure will be more computationally efficient, and this is the strategy used in the development that follows.

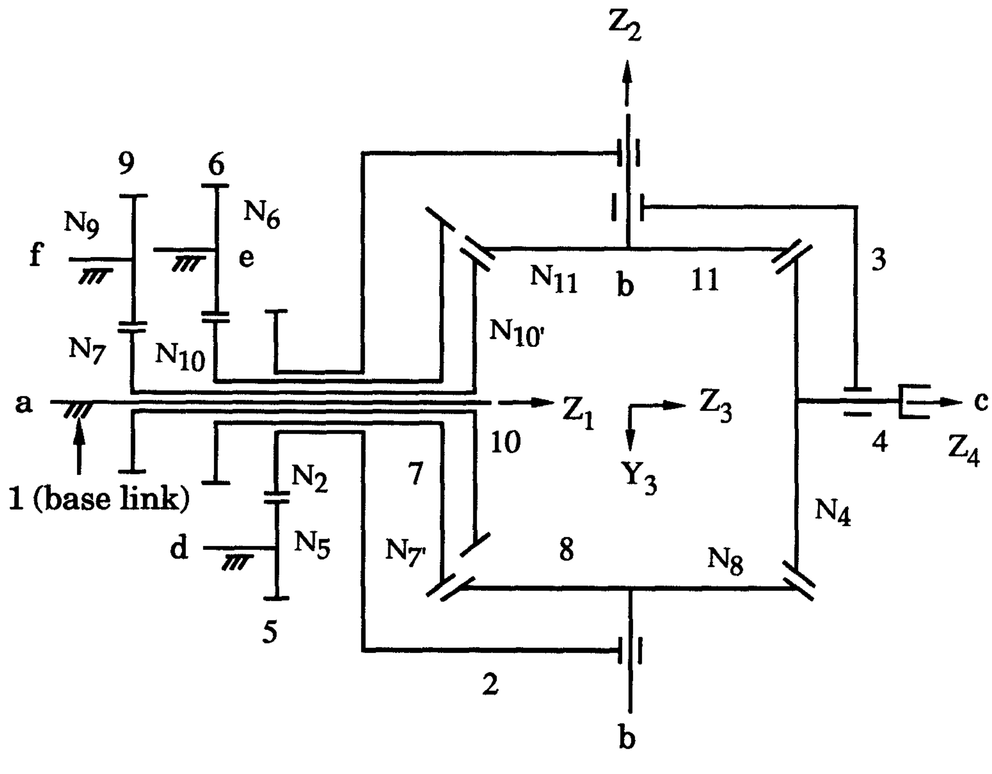

Fig. 3-1: Schematic Drawing of Bendix Wrist Mechanism.

Neglecting frictional forces in a perfect gear meshing, the contact load of one gear on the other can be replaced by a single force normal to the contacting surfaces (Spotts, 1985; Shigly and Mitchell, 1983). The gear tooth profiles are usually designed to have this normal force acting along a fixed direction, know as the line of action, relative to the carrier of the meshing gears. Hence, only one unknown quantity is necessary for the specification of the constraint force in a gear pair.

In the absence of friction, perfect revolute joints cannot transmit any torques about their joint axes. Hence, modeling the constraint forces in a revolute joint requires five unknown quantities: three forces and two torques.

Applying the above arguments on the graph representation of a mechanism, such as the PUMA wrist mechanism shown in Fig. 3-2, it become apparent that breaking each heavy edge requires the introduction of one unknown quantity while breaking each thin edge requires five unknown quantities. This observation can be useful in guiding the evaluation of constraint forces and/or torques.

Define link constraint connectivity (LCC) for link i as

$$LCC = N_{ig} + 5 \cdot N_{ir} \tag{3.1}$$

where N_{ig}, denotes the number of gear pairs incident with link i, and N_{ir}, the number of revolute joints incident with link i. LCC represents the number of constraint forces and torques associated with the link.

Then, a link with LCC equal to or less than six is identified and the unknown reaction forces and torques are solved. The above mentioned process is applied until all the reaction forces are determined.

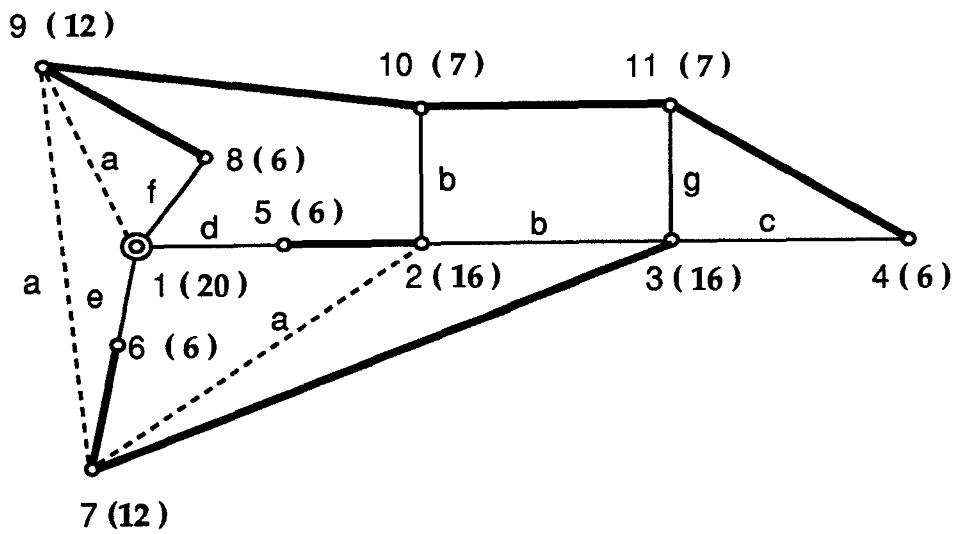

Fig. 3-2: Actual Graph Rep. of PUMA Wrist Mechanism(LCC).

Figure 3-2 shows the actual graph representation of the PUMA wrist where the number in parenthesis denotes the LCC associated with each link. It can be shown that, for the mechanism shown in Fig. 3-2, the link-by-link evaluation procedure can follow the sequence of { 4 -> 11 -> 3 -> 10 -> 2 -> 7 -> 9 -> 5 -> 8 -> 6 }. Figure 3-3 show the actual graph representation of the Bendix wrist. It can be shown that, for the mechanism shown in Fig. 3-3, the link-by-link evaluation procedure can start with links { 5 }, { 6 }, and { 9 } independently, but the remaining reaction forces have to be evaluated simultaneously.

From the above two examples, it seems that there are no systematic approach for the reaction forces analysis. However, Tsai (1989) suggested that revolute joints in a set of coaxial links can be reconfigured to form a canonic graph representation without affecting the functionality of a mechanism. This shed some light on the development of a systematic methodology.

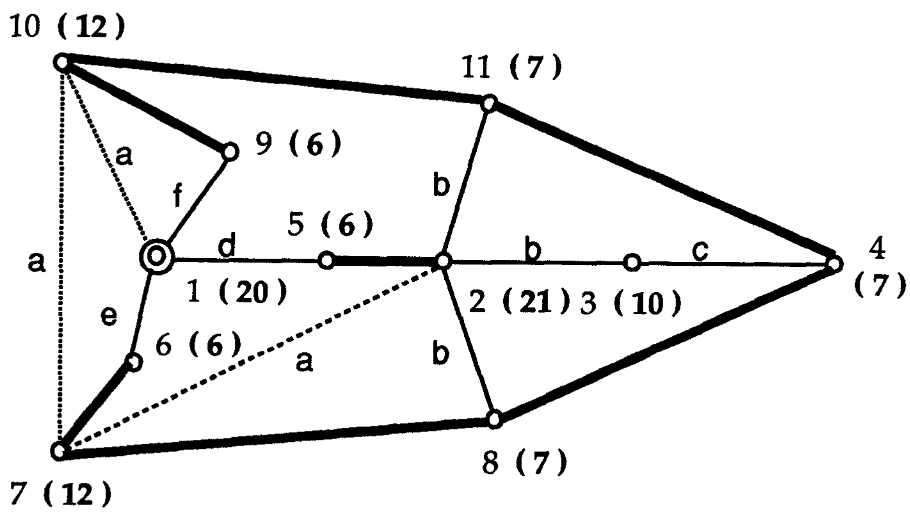

Fig. 3-3: Actual Graph Rep. of Bendix Wrist Mechanism(LCC).

Figures 3-4 and 3-5 show the canonic graph representations of the PUMA and Bendix wrist mechanisms, respectively, with their LCC given in the parenthesis. Using canonic graph representation, the link-by-link evaluation sequence for the PUMA wrist example, can now be accomplished in three independent paths: { 5 }, { 6 -> 7 }, and { 8 -> 9 -> 10 -> 11 }, followed by the path { 4 -> 3 -> 2 -> 1 }. The evaluation sequence for the Bendix wrist example can also be arranged in three independent paths: { 5 }, { 6 -> 7 -> 8 }, and { 9 -> 10 -> 11 }, followed by the path { 4 -> 3 -> 2 -> 1 }. It can be concluded that the evaluation sequence can always be carried out in two steps. The first step is a link-by-link *forward* evaluation of the reaction forces acting on the carried links in each transmission line, starting from the input link. The second step is a link-by-link *backward* evaluation of the reaction forces acting on the major links of the equivalent open-loop chain, starting from the output link. Note that the evaluation sequence in the first step consists of as many independent paths as the number of transmission lines, provided that gears are used only for the purpose of transmitting power and the number of transmission lines is equal to the number of degrees of freedom in the mechanism.

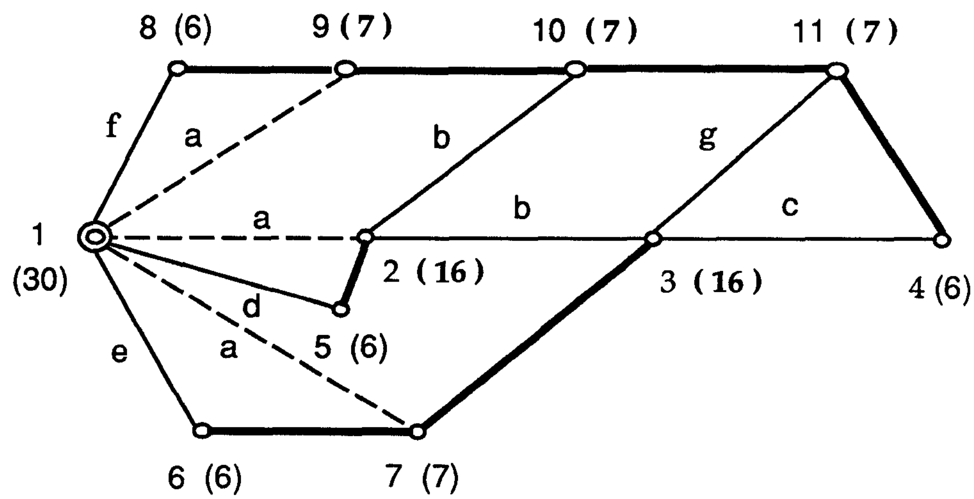

Fig. 3-4: Canonic Graph Rep. of PUMA Wrist Mechanism(LCC).

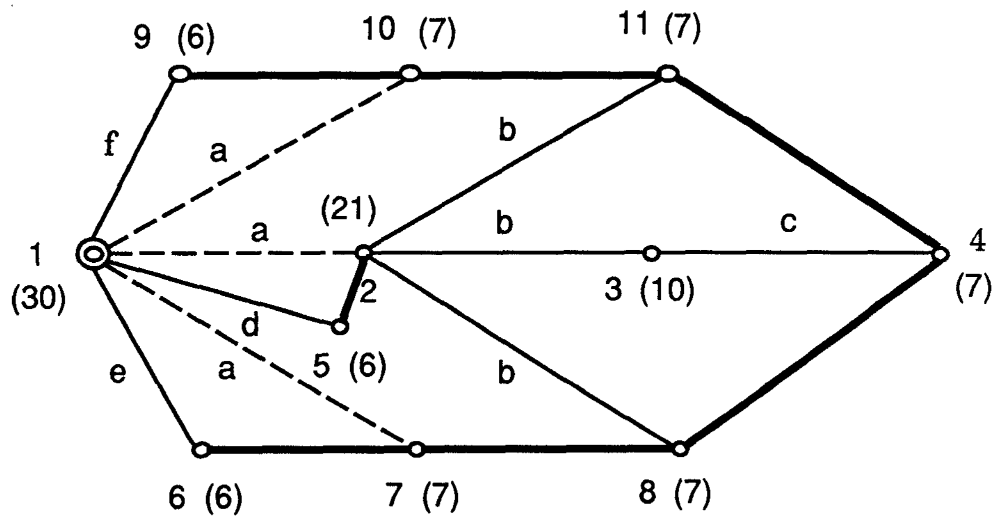

Fig. 3-5: Canonic Graph Rep. of Bendix Wrist Mechanism(LCC).

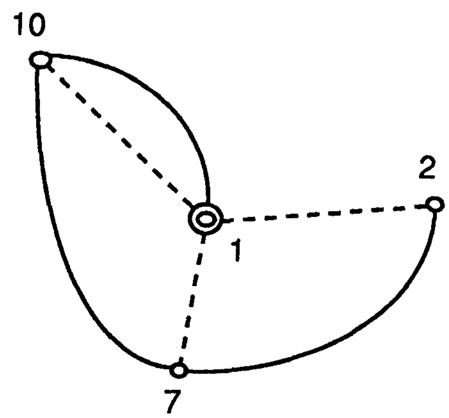

Fig. 3-6: Connection between coaxial links of Bendix Wrist Mechanism.

The reaction forces determined for the canonic graph representation of a mechanism can be called *canonic reactions* and the *actual* reaction forces have yet to be determined. This can be accomplished by identifying an equivalent force system in a set of coaxial links. For the Bendix wrist example, Fig. 3-6 shows the interconnection between the coaxial links in graph notation, where the doted lines denote the solved canonic reactions and solid lines the actual reactions. Considering the system being at equilibrium, six force balance equations can be written for each link shown in Fig. 3-6. Hence, the actual reactions can be determined from the equivalent force system in the sequence of { 2 -> 7 -> 10 -> 1 } or in the reverse order.

In conclusion, the reaction force in geared robotic mechanisms can be solved in a systematic manner. The procedure is as follows:

1. Construct canonic graph of the mechanism;
2. Perform forward evaluation of the reaction forces acting on the carried links along each transmission lines, starting from the input links;
3. Perform backward evaluation of the reaction forces acting on the major links along the EOLC, starting from the output link;
4. Find the actual reactions by solving the equivalent force system of coaxial links, if any.

3.3 Dynamic Force Analysis

3.3.1 Coordinate Systems

Before force/moment balance equations can be evaluated, coordinate systems for the carried links have to be established and the associated gear contact forces have to be described in compact and convenient forms. Figure 3-7 shows the coordinate systems for a carried link j containing a compound gear, where gear "ja" is on the input side and gear "jb" is on the output side of a transmission line. According to Tsai (1987), there is a carrier for each gear pair. Let major link k1 be the carrier for the gear pair [j, j-1], major link k2 be the carrier for the gear pair [j+1, j]. A coordinate system will be defined for each major link, in accordance with the D-H convention (Denavit and Hartenberg, 1955), in the equivalent open-loop chain. Two coordinate systems will be defined for each carried link, one on the input side and the other one for the output side of a compound gear. The Z-axis is defined along a pre-selected positive axis of rotation for that link. Specifically, they are defined as follows:

$[OXZ]_k$ Coordinate system for a major link k, established according to the D-H convention (Hartenberg and Denavit, 1955),

$[OXZ]_{ja}$ Local coordinate system of a carried link j defined on the input side of a transmission line, where X_{ja} is a unit vector pointing from O_{ja} to the contact point of the gear pair [j, j-1], and Z_{ja} is a unit vector along the positive direction of rotation of link j,

$[OXZ]_{jb}$ Local coordinate system of a carried link j defined on the output side of a transmission line, where X_{jb} is a unit vector pointing from O_{jb} to the contact point of the gear pair [j+1, j], and Z_{jb} is a unit vector along the positive direction of rotation of link j.

Although coordinate system $[OXZ]_{ja}$ is defined in the carried link j, its x-axis is always pointing from O_{ja} to the contact point of the gear pair [j, j-1]. Similarly, the x-axis of $[OXZ]_{jb}$ is always pointing from O_{jb} to the contact point of the gear pair [j+1, j].

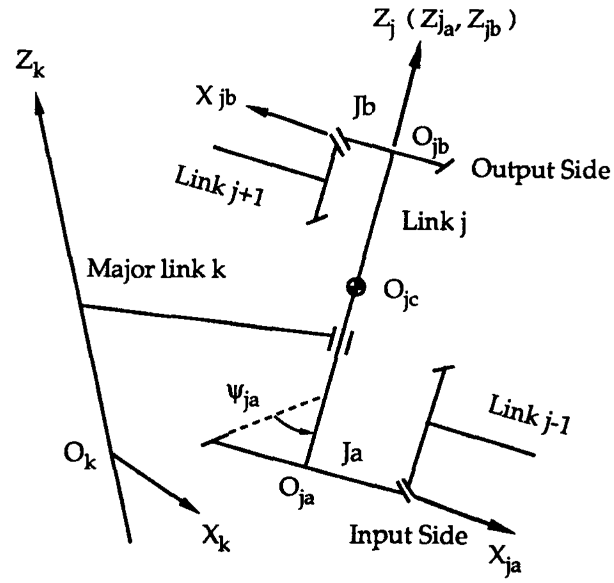

Fig. 3-7: Coordinate system of carried link j.

Note that if the carried link j is one of the input links, only one local coordinate system at output side is needed. Also note that from the definition of canonic graph, the following facts can be stated:

1): the carrier for the input side gear pair always supports the carried link j directly,

2). the carrier for the output side gear pair, does not necessary support the carried link j,

Since link k1 is the carrier for the gear pair [j, j-1], coordinate system $[OXZ]_{ja}$ is fixed in coordinate system $[OXZ]_{k1}$, and any vector Y in $[OXZ]_{ja}$ can be transformed to $[OXZ]_{k1}$ by

$$ {}^{k1}Y = {}^{k1}E_{ja}\, {}^{ja}Y \tag{3.2} $$

where

$$ {}^{k1}E_{ja} = \begin{bmatrix} C_{ja3}C_{ja2} & C_{ja3}S_{ja2}S_{ja1} - S_{ja3}C_{ja1} & C_{ja3}S_{ja2}C_{ja1} + S_{ja3}S_{ja1} \\ S_{ja3}C_{ja2} & S_{ja3}S_{ja2}S_{ja1} + C_{ja3}C_{ja1} & S_{ja3}S_{ja2}C_{ja1} - C_{ja3}S_{ja1} \\ -S_{ja2} & C_{ja2}S_{ja1} & C_{ja2}C_{ja1} \end{bmatrix} \tag{3.3} $$

and where $C_{jai} = \cos(\varepsilon_{jai})$, $S_{jai} = \sin(\varepsilon_{jai})$ and ε_{jai}, i= 1, 2, 3 are the Euler's heading, attitude and bank angles defined between $[OXZ]_{ja}$ and $[OXZ]_{k1}$ coordinate systems (Greenwood, 1965).

Similarly, since link k2 is the carrier for the gear pair [j+1, j], $[OXZ]_{jb}$ is fixed in $[OXZ]_{k2}$, and any vector in $[OXZ]_{jb}$ can be transformed to $[OXZ]_{k2}$ with the Euler's angles ε_{jbi}, i= 1, 2, 3 by

$$ {}^{k2}Y = {}^{k2}E_{jb}\, {}^{jb}Y \tag{3.4} $$

The gear force exerted on link j by link j-1 will be denoted by $\gamma_{j,\,j-1}$. Let [j, j-1] be the k-th gear pair in the i-th transmission line, then $\gamma_{j,\,j-1}$ can be expressed as

$$ {}^{ja}\gamma_{j,j-1} = \begin{bmatrix} -h_{i,k}\alpha_{i,k} \\ \mathrm{sign}(\delta_{i,k})\, h_{i,k} \\ \mathrm{sign}(B_{ja})\, h_{i,k}\, \beta_{i,k} \end{bmatrix} \tag{3.5} $$

where

$$ \alpha_{i,k} = \tan(\phi)\cos(\psi_{ja}) \tag{3.6} $$

$$ \beta_{i,k} = \tan(\phi)\sin(\psi_{ja}) \tag{3.7} $$

and where $h_{i,k}$ denotes the positive tangential measure of the contact force at the k-th gear pair of the i-th transmission line, ϕ the pressure angle, ψ_{ja} the pitch cone angle of the gear on the input side of link j. The sign(B_{ja}) is positive if the apex of the gear pair [j, j-1] lies on the negative side of the Z_{ja} axis, and is negative if it lies on the positive side of Z_{ja} axis. The sign of $\delta_{i,k}$ is given by

$$\mathrm{sign}(\delta_{i,k}) = -\zeta_{i,m} \cdot \mathrm{sign}(\xi_i) \tag{3.8}$$

where $\zeta_{i,m}$ is the sign of m-th gear pair of the i-th transmission line. Hence, the sign($\delta_{i,k}$), in the concept of power transmission, is determined by the direction of i-th input torque, ξ_i, and the gear transmission arrangement.

From eq. (3.5), it can be seen that the contact force $\gamma_{j,j-1}$ always has a component acting in the negative X_{ja} direction, and the component in the Z_{ja} direction depends on the location of the cone apex.

Note that, for spur gear pairs in which the cone angle is zero, eq. (3.5) can be simplified as

$${}^{ja}\gamma_{j,j-1} = \begin{bmatrix} -h_{i,k}\mathrm{Tan}(\phi) \\ \mathrm{sign}(\delta_{i,k})h_{i,k} \\ 0 \end{bmatrix} \tag{3.9}$$

3.3.2 Inertial Forces Formulation

The inertial forces can be formulated by using the Newton and

Euler equations. In the following, these inertial forces will be formulated in two different category, namely, the major links and the carried links.

(a). major links

The inertia force and torque of a major link k, expressed in its own center-of-mass coordinate system can be written by Newton-Euler equations as

$$ {}^{k}F_{k}^{*} = m_{k}\, {}^{k}\dot{v}_{sk} \tag{3.10}$$

$$ {}^{k}T_{k}^{*} = {}^{k}I_{k}\, {}^{k}\dot{\omega}_{k} + {}^{k}\omega_{k} \times ({}^{k}I_{k}\, {}^{k}\omega_{k}) \tag{3.11}$$

where I_k is the inertia matrix of link k in its own center-of mass coordinate system and the kinematic properties can be found from eqs. (2.1-6).

(b). Carried links

From eqs. (2.9) and (2.1), the angular velocity of a carried link j, supported by a major link k and expressed in its own coordinate system, can be written as

$$ {}^{j}\omega_{j} = {}^{x}E_{k}\, {}^{k}\omega_{k} + \dot{\theta}_{j,k}\, {}^{j}Z_{j} \tag{3.12}$$

$$ {}^{j}\dot{\omega}_{j} = {}^{x}E_{k}\, {}^{k}\dot{\omega}_{k} + \ddot{\theta}_{j,k}\, {}^{j}Z_{j} + {}^{x}E_{k}\, {}^{k}\omega_{k} \times \dot{\theta}_{j,k}\, {}^{j}Z_{j} \tag{3.13}$$

where x = jb, if link j is one of the input links, otherwise, x = ja.

Assuming the carried links are axisymmetric with respect to its own axis of rotation, then, the position vector for the center-of-mass of a carried link j, s_j is a fixed vector in its carrier's coordinate system. Hence, the mass center linear acceleration of a carried link j can be considered as a fixed point on its carrier. From eq. (2-6), we have

$$ {}^k\dot{v}_{sj} = {}^k\dot{\omega}_k \times {}^k s_j + {}^k\dot{v}_k + {}^k\omega_k \times ({}^k\omega_k \times {}^k s_j) \tag{3.14} $$

Thus, the inertial force and torque of a carried link j expressed in its carrier's coordinate system, can be written as

$$ {}^k F^*_j = m_j \, {}^k\dot{v}_{sj} \tag{3.15} $$

and

$$ {}^k T^*_j = {}^k E_x ({}^j I_j \, {}^j\dot{\omega}_j + {}^j\omega_j \times ({}^j I_j \, {}^j\omega_j)) \tag{3.16} $$

where I_j is the inertia matrix of link j in its own center-of mass coordinate system.

3.3.3 Forward Evaluation along Transmission Lines

With the gear contact forces and their associated position vectors properly expressed, the forces/moments equilibrium can now be discussed. Figure 3-8 shows the free-body-diagram of a carried link j supported by a major link k, where O_{jc} is the mass center of link j, d_{jk} the position vector from O_{jc} to the location of the revolute joint [j, k], d_{ja} and d_{jb} the position vectors from O_{jc} to the contact points of the gear pairs [j, j-1] and [j+1, j], respectively. Let $f_{j,k}$ and $t_{j,k}$ be the force and moment exerted on link j by link k in the revolute joint, then the force/moment balance equations for the carried link j can be written as follows.

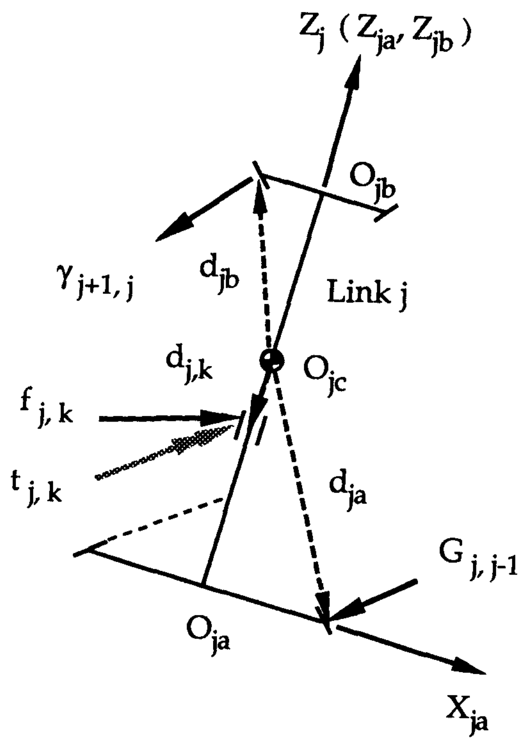

Fig. 3-8: Free-Body-Diagram of carried link j.

(a). If link j is not the first link of a transmission line, then

$$F^*_j = \gamma_{j,j-1} + f_{j,k} - \gamma_{j+1,j} \tag{3.17}$$

$$T^*_j = d_{ja} \times \gamma_{j,j-1} + t_{j,k} + d_{jk} \times f_{j,k} - d_{jb} \times \gamma_{j+1,j} \tag{3.18}$$

Note that perfect revolute joints cant not transmit torque along their axes of rotation. Hence, in the absence of friction, the component of $t_{j,k}$ in Z_j-direction must be equal to zero, i.e.

$$t_{j,k} \cdot Z_j = 0 \tag{3.19}$$

(b). If link j is the first link of a transmission line, there is no gear pair on the input side of link j and link j is directly connected to the rotor of an actuator. Then eqs. (3.17-18) reduce to

$$F^*_j = f_{j,k} - \gamma_{j+1,j} \tag{3.20}$$

$$T^*_j = t_{j,k} + d_{jk} \times f_{j,k} - d_{jb} \times \gamma_{j+1,j} \tag{3.21}$$

In this case, the component of $t_{j,k}$ in the Z_j direction is equal to the input torque, i.e.

$$t_{j,k} \cdot Z_j = \xi_i \tag{3.22}$$

Equation set (3.17-19) and (3.20-22) can also be expressed in its carrier's coordinate system to improve computational efficiency. Using from eqs. (2.7), (3.2) and (3.4), these equations can be rewritten as follows.

(a). If link j is not the first link of a transmission, then

$${}^kF^*_j = {}^kR_{k1}\,{}^{k1}E_{ja}\,{}^{ja}\gamma_{j,j-1} + {}^kf_{j,k} - {}^kR_{k2}\,{}^{k2}E_{jb}\,{}^{jb}\gamma_{j+1,j} \tag{3.23}$$

$$\begin{aligned} {}^kT^*_j = {}&{}^kR_{k1}\,{}^{k1}E_{ja}\,{}^{ja}d_{ja} \times {}^kR_{k1}\,{}^{k1}E_{ja}\,{}^{ja}\gamma_{j,j-1} + {}^kd_{j,k} \times {}^kf_{j,k} \\ &+ {}^kt_{j,k} - {}^kR_{k2}\,{}^{k2}E_{jb}\,{}^{jb}d_{jb} \times {}^kR_{k2}\,{}^{k2}E_{jb}\,{}^{jb}\gamma_{j+1,j} \end{aligned} \tag{3.24}$$

and

$${}^kt_{j,k} \cdot {}^kZ_j = 0 \tag{3.25}$$

(b). If link j is the first link of a transmission line, then

$${}^kF^*_j = {}^kf_{j,k} - {}^kR_{k2}\,{}^{k2}E_{jb}\,{}^{jb}\gamma_{j+1,j} \tag{3.26}$$

$$\begin{aligned} {}^kT^*_j = {}&{}^kt_{j,k} + {}^kd_{j,k} \times {}^kf_{j,k} \\ &- {}^kR_{k2}\,{}^{k2}E_{jb}\,{}^{jb}d_{jb} \times {}^kR_{k2}\,{}^{k2}E_{jb}\,{}^{jb}\gamma_{j+1,j} \end{aligned} \tag{3.27}$$

and

$$ {}^{k}t_{j,k} \cdot {}^{k}Z_{j} = \xi_{i} \tag{3.28} $$

Applying the equation sets to the aforementioned link-by-link forward evaluation procedure, all the gear contact forces and reaction forces on the revolute joints of carried links can be determined systematically and efficiently. The analysis begins at an input link and proceeds link-by-link along each transmission line until all the carried links on all transmission lines are evaluated.

3.3.4 Backward Evaluation along EOLC

Figure 3-9 shows the free-body-diagram of a major link k which is preceded by the major link k-1 and followed by another major link k+1. Assume that link k supports m carried links, and is the last link of p transmission lines. Let O_{kc} be the mass center of link k, $d_{k,k-1}$ the position vector from O_{kc} to the location of the revolute joint [k, k-1], $d_{k,k+1}$ the position vector from O_{kc} to the location of revolute joint [k+1, k], $d_{k\,j}$ (j= 0, 1, ···, m) the position vector from O_{kc} to the location of the revolute joint [k, j], and $d_{k\,i}$ (i= 0, 1, ···, p) the position vector from O_{kc} to the contact point of the gear pair [k, i]. Then the force/moment balance equations for the major link k can be written as

$$ F^{*}_{k} = f_{k,k-1} - f_{k+1,k} + \sum_{i=0}^{p} \gamma_{k,i} - \sum_{j=0}^{m} f_{j,k} \tag{3.29} $$

$$ T^{*}_{k} = t_{k,k-1} + d_{k,k-1} \times f_{k,k-1} - t_{k+1,k} - d_{k,k+1} \times f_{k+1,k} $$

$$+\sum_{i=0}^{p}(d_{k,i}\times\gamma_{k,i})-\sum_{j=0}^{m}t_{j,k}-\sum_{j=0}^{m}(d_{k,j}\times f_{j,k}) \tag{3.30}$$

Noted that the torque component of $t_{k,\,k\text{-}1}$ in the direction of $Z_{k\text{-}1}$ is equal to zero since a revolute joint cannot transmit torque in its axial direction, i.e.,

$$t_{k,k-1}\cdot Z_{k-1}=0 \tag{3.31}$$

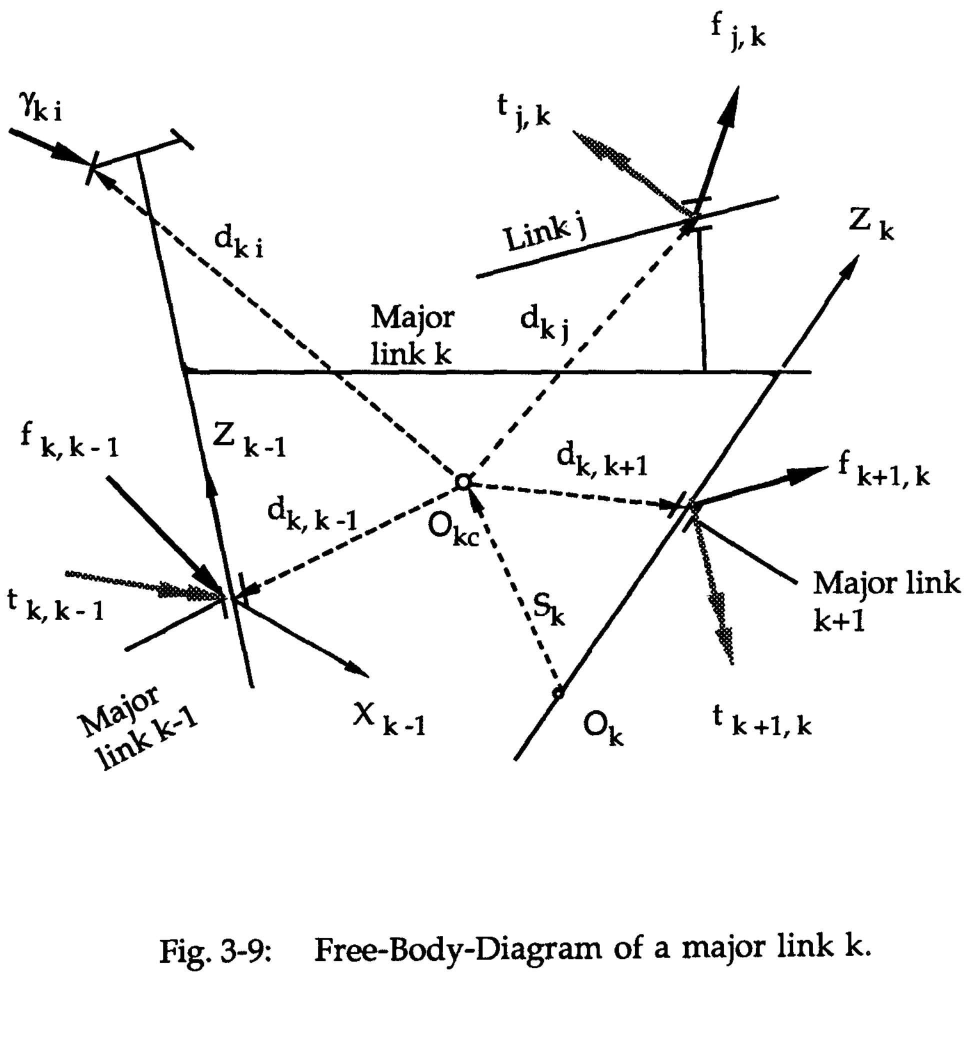

Fig. 3-9: Free-Body-Diagram of a major link k.

Equations (3.29-31), can also be expressed in link coordinate system of a major link k to improve computational efficiency. Applying eqs. (2.6), (3.2) and (3.4), these equations can be rewritten as

$$ {}^{k}F_{k}^{*} = {}^{k}f_{k,k-1} - {}^{k}f_{k+1,k} + \sum_{i=0}^{p} {}^{k}R_{k-1} {}^{k-1}\gamma_{k,i} - \sum_{j=0}^{m} {}^{k}f_{j,k} \tag{3.32} $$

$$ \begin{aligned} {}^{k}T_{k}^{*} = {}^{k}t_{k,k-1} + {}^{k}d_{k,k-1} \times {}^{k}f_{k,k-1} - {}^{k}d_{k,k+1} \times {}^{k}f_{k+1,k} \\ - {}^{k}t_{k+1,k} + \sum_{i=0}^{p} ({}^{k}d_{k,i} \times {}^{k}R_{k-1} {}^{k-1}\gamma_{k,i}) \\ - \sum_{j=0}^{m} {}^{k}t_{j,k} - \sum_{j=0}^{m} ({}^{k}d_{k,j} \times {}^{k}f_{j,k}) \end{aligned} \tag{3.33} $$

and

$$ {}^{k}t_{k,k-1} \cdot {}^{k}Z_{k-1} = 0 \tag{3.34} $$

Applying eqs. (3.32-34) to the link-by-link backward evaluation procedure, all the reaction forces on the bearings of the equivalent open-loop chain can be determined systematically and efficiently.

3.3.5 Canonic and Actual Reaction Forces

From the previous two sections, canonic reaction forces can be determined systematically and efficiently. The remaining task now is to solve the equivalent force systems for all coaxial links which have been reconfigured into the canonic representation.

Take the Bendix wrist mechanism shown in Figs. 3-1 as an example.

The equivalent force system for the four coaxial links is shown in Fig. 3-6. Let $d_{2,7}$ be the position vector from O_{2c} to the actual location of the revolute joint [2, 7]. Then, from Fig. 3-6, the actual forces/moments exerted on link 2 by link 7, $f_{2,7}$ and $t_{2,7}$, can be determined by solving the following two equations.

$$^{2}f_{2,7} = {}^{2}f_{2,1} \tag{3.35}$$

and

$$^{2}t_{2,7} + {}^{2}d_{2,7} \times {}^{2}f_{2,7} = {}^{2}t_{2,1} + {}^{2}d_{2,1} \times {}^{2}f_{2,1} \tag{3.36}$$

Similarly, the reaction forces, $f_{7,10}$, $t_{7,10}$, $f_{10,1}$ and $t_{10,1}$, can also be determined.

3.4 Summary

In this chapter, it is shown that the analysis of reaction forces in geared robotic mechanisms can be systematically and efficiently performed. The evaluation can be carried out in two steps. The first step is a link-by-link forward evaluation of the carried links, starting from the input link of each transmission line. The second step is a link-by-link backward evaluation of the major links, starting from the output link of the equivalent open-loop chain. The procedure can be the basis for a computer program to provide automated analysis of a general class of articulated gear mechanisms. Numerical examples will be given in chapter seven to illustrate the principle.

CHAPTER 4

Performance Indices

4.1 Introduction

The velocity ratio and the mechanical advantage are the two most commonly used criteria for evaluating the performance of a single-input and single-output mechanism such as a four bar linkage. The velocity ratio is the ratio of the output velocity to the input velocity and the mechanical advantage is the ratio of the output torque to the input torque of a mechanism at the instant of interest. For multi-D.O.F. mechanisms such as a manipulator, these concepts need to be modified.

Various performance measures have been proposed for the evaluation of kinematic and/or dynamic performance of a manipulator. Most of the kinematic performance measures, such as the velocity ellipsoid and the generalized velocity ratio (Asada and Cro Granlto, 1985; Dubey and Luh, 1986), the manipulability measure (Yoshikawa, 1985a), and the condition number (Gosselin and Angeles, 1988), are based on the relation between velocity vectors in the joint-space and end-effector-space of an open-loop manipulator. As for the dynamic performance measure, Asada (1983) proposed an approach for the manipulator design by modifying the link lengths and mass distribution such that the generalized moment of inertia is uniform in all directions and the nonlinear forces are eliminated. Using the relation between the joint torques and end-effector acceleration, Yoshikawa (1985b) proposed a dynamic manipulability index, which is the volume of dynamic manipulability ellipsoid, for the design of manipulators. Since these performance measures are based on the transformation between the *joint-space* and *end-effector-space,* they are only useful for the evaluation or design of *direct-drive manipulators.* However, they are not very helpful in evaluating manipulators which use gear trains or other means for power transmission.

For geared robotic mechanisms, the transformation between the *actuator-space* and joint-space must also be taken into consideration. That is, the transformation has to be extended from "end-effector-space to joint-space" to "end-effector-space to actuator-space." The structure matrix, defined by Chang and Tsai (1990), transforms the velocity vector from the joint-space to the actuator-space while the Jacobian matrix transforms the velocity vector from the joint-space to the end-effector-space. Together, they give the overall transformation from the actuator-space to the end-effector-space.

In this chapter, the definitions of various performance measures will be extended from direct-drive manipulators to non-direct drive manipulators and, in particular, gear-coupled manipulators.

4.2 Kinematic Characteristics

Kinematic characteristics can be best understood by viewing the manipulator as a mechanical transformer, with velocity or force vector in the actuator-space as the input and velocity or force vector in the end-effector-space as the output. In this section, the concepts of generalized velocity ratio and velocity capacity will be defined.

4.2.1 Actuator-Space, Joint-Space and End-Effector-Space

Figure 4-1 shows a geared robotic mechanism in conceptual form, where the inputs to the mechanism are the actuators and the output is the end-effector.

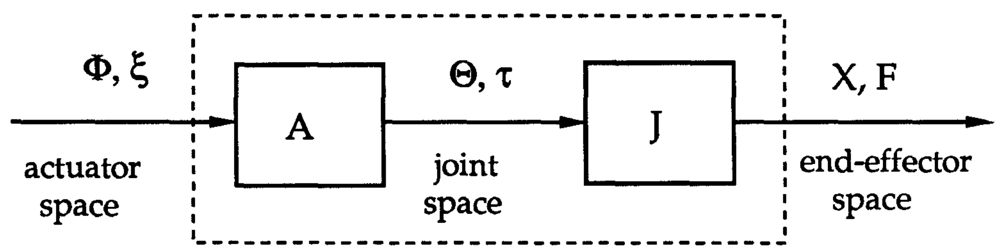

Fig. 4-1: Conceptual block diagram of a geared robotic mechanism.

Let Φ, Θ, and X be the displacement vectors associated with the actuators, joints, and the end-effector. Let $\dot{\Phi}$, $\dot{\Theta}$ and $\dot{X}$ be the time derivatives of Φ, Θ, and X. And let ξ, τ, and F be the generalized force vectors in the actuator-space, joint-space and end-effector-space, respectively. Then, the joint and output velocity vectors are related by the Jacobian matrix, J, as

$$\dot{X} = J\,\dot{\Theta} \tag{4.1}$$

and the joint torque and output force vectors are related by

$$\tau = J^T F \tag{4.2}$$

where $(\;)^T$ denotes the transpose of $(\;)$.

The actuator and joint velocity vectors are related by the structure matrix, A, as

$$\dot{\Phi} = A^T \dot{\Theta} \tag{4.3}$$

and the joint and actuator torque vectors are related by

$$\tau = A\,\xi \tag{4.4}$$

where the elements of A are functions of gear ratios in a mechanism. The i-th row of the structure matrix A describes how the resultant torque about joint "i" is affected by the input actuators and, on the other hand, the j-th column of matrix A describes how the torque of an input actuator "j" is transmitted to various joints of a mechanism. We note that the velocity vector, $\dot{X}$, in eq. (4.1) contains both linear and angular velocities of a point in the end-effector. Similarly, the force vector, F, in eq. (4.2) contains both forces and couples acting on a point in the end-effector.

In general, the elements in a velocity vector may have different units. Hence, it is necessary to define a weighted norm for the magnitude of a velocity vector. In the following, quadratic forms are defined for the square of the norms:

$$|\dot{X}|^2 \equiv \dot{X}^T W_x \dot{X} \tag{4.5}$$

and

$$|\dot{\Phi}|^2 \equiv \dot{\Phi}^T W_\phi \dot{\Phi} \tag{4.6}$$

where W_X and W_ϕ are diagonal, positive definite, weighting matrices.

4.2.2 Generalized Velocity Ratio

As an extension of velocity ratio, the square of the generalized velocity ratio K_V is defined as the ratio of the two quadratics:

$$K_v^2 \equiv \frac{|\dot{X}|^2}{|\dot{\Phi}|^2} \tag{4.7}$$

Substituting eq. (4.1) into eq. (4.5) , yields

$$|\dot{X}|^2 = \dot{\Theta}^T J^T W_x J \dot{\Theta} \tag{4.8}$$

Substituting eq. (4.3) into eq. (4.8), yields

$$|\dot{X}|^2 = \dot{\Phi}^T A^{-1} J^T W_x J A^{-T} \dot{\Phi} \tag{4.9}$$

where $(\,)^{-1}$ denotes the inverse of ( ), and $(\,)^{-T}$ the inverse of $(\,)^{T}$.

Substituting eq. (4.3) into eq. (4.6) , yields

$$|\dot{\Phi}|^2 = \dot{\Theta}^T A \, W_\phi A^T \dot{\Theta} \tag{4.10}$$

Substituting eq. (4.1) into eq. (4.10), yields

$$|\dot{\Phi}|^2 = \dot{X}^T J^{-T} A \, W_\phi \, A^T J^{-1} \dot{X} \tag{4.11}$$

Thus, from eqs. (4.6), (4.7), and (4.9), the generalized velocity ratio can be expressed in the actuator-space as

$$K_v^2 = \frac{\dot{\Phi}^T A^{-1} J^T W_x \, J \, A^{-T} \dot{\Phi}}{\dot{\Phi}^T W_\phi \, \dot{\Phi}} \tag{4.12}$$

Alternatively, from eqs. (4.7), (4.8) and (4.10), the generalized velocity ratio can also be expressed in the joint-space as

$$K_v^2 = \frac{\dot{\Theta}^T J^T W_x \, J \, \dot{\Theta}}{\dot{\Theta}^T A \, W_\phi \, A^T \dot{\Theta}} \tag{4.13}$$

or from eqs. (4.5), (4.7) and (4.11), K_V can be expressed in the end-effector-space as

$$K_v^2 = \frac{\dot{X}^T W_x \, \dot{X}}{\dot{X}^T J^{-T} A \, W_\phi \, A^T J^{-1} \dot{X}} \tag{4.14}$$

Equations (4.12), (4.13) and (4.14) are known as Rayleigh's quotient. The value of the generalized velocity ratio, K_V, depends on the position as well as direction of motion of the end-effector. The values of K_V are the square root of the eigenvalues of the following eigenvalue problem (Strang, 1980):

$$(W_{\phi}^{-1} A^{-1} J^{T} W_{x} J A^{-T}) \dot{\Phi} = \lambda \dot{\Phi} \tag{4.15}$$

or

$$(J^{T} W_{x} J) \dot{\Theta} = \lambda (A W_{\phi} A^{T}) \dot{\Theta} \tag{4.16}$$

or

$$(W_{x}^{-1} J^{-T} A W_{\phi} A^{T} J^{-1}) \dot{X} = \frac{1}{\lambda} \dot{X} \tag{4.17}$$

Equations (4.15) and (4.16) have the same eigenvalues, λ's, and their eigenvectors are related by eq. (4.3). Eigenvalues of eq. (4.17) are equal to the inverse of that of eq. (4.16), i.e. $1/\lambda$'s. Eigenvectors of eq. (4.16) and (4.17) are related by eq. (4.1). Hence, the eigenvalues and the corresponding eigenvectors of eq. (4.15) or (4.16) or (4.17) completely characterize the kinematic performance of a manipulator at a given end-effector position. The eigenvalues of eqs. (4.15-4.17) are function of the structure matrix A, which is a function of gear ratios, at a given configuration. Deriving an explicit expression for λ in terms of its arguments is very cumbersome and even impractical. In fact, one could proceed to derive the said expression for a particular robotic architecture using symbolic algebra. However, doing it for robot of arbitrary architecture may be nearly impossible. This would lead to a highly nonlinear expression whose stationary points have to be computed numerically. To avoid this, the velocity capacity is defined as follow.

4.2.3 Velocity Capacity and Kinematic Condition Number

Equations (4.12), (4.13) or (4.14) can also be interpreted geometrically. Constraining $|\dot{\Phi}|^2 = 1$, at a given posture, eq. (4.11) yields an velocity ellipsoid in the end-effector-space as shown in Fig. 4-2. The velocity capacity, V.C., is defined to be proportional to the volume of the ellipsoid, i.e.

$$V.C. \equiv \prod_{i=1}^{n} \sqrt{\lambda_i} \tag{4.18}$$

where λ_i, i = 1, 2, 3, ..., n, are the eigenvalues of eqs. (4.15), or (4.16).

It can also be shown (Strang, 1980) that the velocity capacity, V.C., is equal to the determinant of the matrix product on the left-handed side of eq. (4.15), i.e.

$$V.C. = [\det(W_{\phi}^{-1} A^{-1} J^T W_x J A^{-T})]^{1/2} \tag{4.19}$$

The velocity capacity, V.C., by rearranging eq. (4.19), can also be expressed as

$$V.C. = \left[\frac{\det(J^T W_x J)}{\det(A W_{\phi} A^T)}\right]^{1/2} \tag{4.20}$$

As an index for measuring the directional sensitivity, the kinematic condition number (KCN) can be defined as the ratio of the maximum to the minimum eigenvalues of eq. (4.15), or eq. (4.16) as

$$\mathrm{KCN} = \sqrt{\frac{\lambda_i)_{max}}{\lambda_i)_{min}}} \tag{4.21}$$

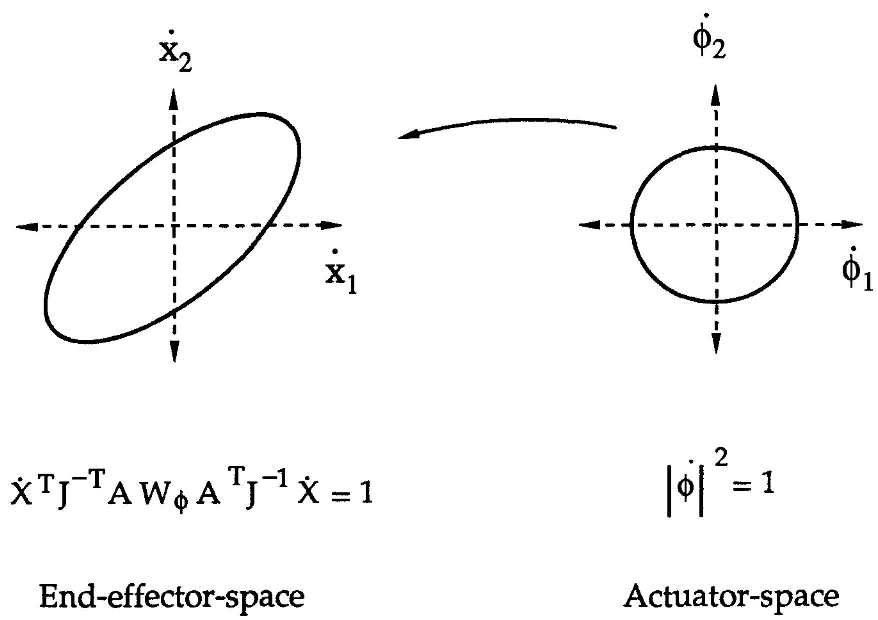

Fig. 4-2: Velocity Transformation between actuator-space and end-effector-space.

The velocity capacity, V.C., can be used as an index to indicate the ability of a manipulator to respond to a given set of input velocity. The larger the velocity capacity, the more responsive the system is. At a given end-effector position the determinant of the product of Jacobian matrix, det ($J^T W_x J$), is a constant while the determinant of the product of structure matrix A, which is a function of gear ratios, depends on the gearing configuration. Hence, the selection of gearing configuration plays an important role in determining the velocity capacity.

4.3 Dynamic Characteristics

Robot designer usually neglects the highly complicated dynamic characteristics of a multi-D.O.F. system in the design of a manipulator. It is essential to overcome this "dynamic blind" design practice by taking the manipulator dynamics into consideration so that optimal dynamic performance can be achieved.

4.3.1 Generalized Effective Inertia

Figure 4-3 shows a one-D.O.F. mechanism. The dynamic equation can be written as

$$(r_{2,1}^2 I_i + I_L)\ddot{q} = r_{2,1}\,\xi_i \tag{4.22}$$

where q is the output displacement, ξ_i the input actuator torque, I_i the inertia of the input shaft and rotor, I_L the load inertia and $r_{2,1} = N_2/N_1$ the gear reduction ratio.

The effective inertia, I_{eff}, is defined as the ratio of the input torque to the output acceleration, i.e.

$$I_{eff} = \frac{r_{2,1}^2 I_i + I_L}{r_{2,1}} \tag{4.23}$$

It is clear that the smaller the effective inertia is, the larger the output acceleration will be. Thus, the value of effective inertia can be used as a quantitative measure of dynamic responsiveness.

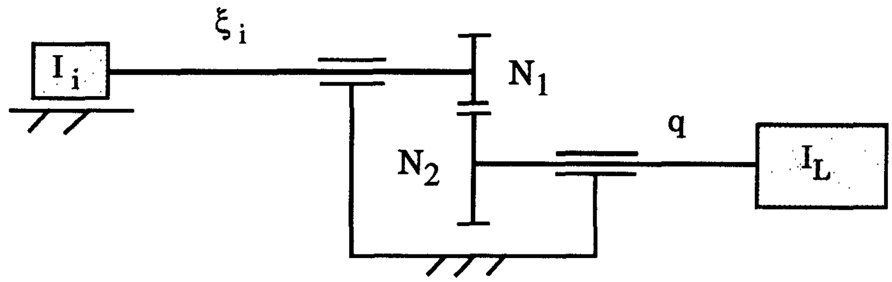

Fig. 4-3: A one-D.O.F. geared mechanism.

The equations of motion for an n-D.O.F. geared robotic mechanism, from eq. (2.55), can be written in the joint-space as

$$M\ddot{\Theta} + \dot{\Theta}^T C\dot{\Theta} + G(\Theta) = A\ \xi \tag{4.24}$$

In what follows, we shall neglect the coriolis and centrifugal effects, and we shall also assume that there are no gravitational forces and external loads. Under these assumptions, eq. (4.24) can be simplified as

$$M\ \ddot{\Theta} = A\ \xi \tag{4.25}$$

Differentiating eq. (4.1) and neglecting the coriolis and centrifugal accelerations, yields

$$\ddot{X} = J\,\ddot{\Theta} \tag{4.26}$$

Eliminating $\ddot{\Theta}$ from eqs. (4.25) and (4.26), yields

$$A^{-1} M\, J^{-1} \ddot{X} = \xi \tag{4.27}$$

Equation (4.27) provides a torque transformation from the end-effector-space to the actuator-space. The norms of the input torque and end-effector acceleration are defined as follow:

$$|\xi|^2 \equiv \xi^T W_\xi\, \xi \tag{4.28}$$

and

$$|\ddot{X}|^2 = \ddot{X}^T W_x\, \ddot{X} \tag{4.29}$$

where W_ξ is a diagonal, positive definite, weighting matrix. In general, W_ξ is chosen as the inverse of W_ϕ.

Substituting eq. (4.25) into (4.28), yields

$$|\xi|^2 = \ddot{\Theta}^T M^T A^{-T} W_\xi\, A^{-1} M\, \ddot{\Theta} \tag{4.30}$$

or from eq. (4.27) and (4.28), yields

$$|\xi|^2 = \ddot{X}^T J^{-T} M^T A^{-T} W_\xi\, A^{-1} M\, J^{-1} \ddot{X} \tag{4.31}$$

Substituting eq. (4.26) into eq. (4.29), we have

$$\left|\ddot{X}\right|^2 = \ddot{\Theta}^T J^T W_x J \ddot{\Theta} \tag{4.32}$$

As an extension of effective inertia, the generalized effective inertia K_d is defined as the ratio of the two quadratics:

$$K_d^2 \equiv \frac{\left|\xi\right|^2}{\left|\ddot{X}\right|^2} \tag{4.33}$$

From eqs. (4.29), (4.31) and (4.33) the square of the generalized effective inertia can be expressed as

$$K_d^2 = \frac{\ddot{X}^T J^{-T} M^T A^{-T} W_\xi A^{-1} M J^{-1} \ddot{X}}{\ddot{X}^T W_x \ddot{X}} \tag{4.34}$$

And from eqs. (4.30), (4.32) and (4.33), we can have

$$K_d^2 = \frac{\ddot{\Theta}^T M^T A^{-T} W_\xi A^{-1} M \ddot{\Theta}}{\ddot{\Theta}^T J^T W_x J \ddot{\Theta}} \tag{4.35}$$

The value of K_d depends on the position as well as direction of motion of the end-effector. The extreme values of K_d are the square root of the maximum and minimum eigenvalues of the following problem:

$$(M^T A^{-T} W_\xi A^{-1} M) \ddot{\Theta} = \mu (J^T W_x J) \ddot{\Theta} \tag{4.36}$$

or

$$(W_x^{-1} J^{-T} M^T A^{-T} W_\xi A^{-1} M J^{-1}) \ddot{X} = \mu \ddot{X} \tag{4.37}$$

Equations (4.36) and (4.37) have the same eigenvalues, μ's, and their eigenvectors are related by eqs. (4.1). Hence, the eigenvalues and the corresponding eigenvectors of eq. (4.36) or (4.37) can be used to characterize the dynamic performance of a manipulator at a given end-effector position. Similar to the kinematic case, to derive explicit expressions for eigenvalue μ in terms of gear ratios at a given configuration is cumbersome and even impractical. To avoid this, the acceleration capacity is defined as follow.

4.3.2 Acceleration Capacity and Dynamic Condition Number

Equations (4.34) or (4.35) can also be interpreted geometrically. Constraining actuator torques to $|\xi|^2 = 1$ at a given posture, eq. (4.31) yields an acceleration ellipsoid in the end-effector-space as shown in Fig. 4-4. The acceleration capacity, A.C., is defined to be proportional to the volume of the ellipsoid, i.e.

$$\text{A.C.} \equiv 1 / \left(\prod_{i=1}^{n} \sqrt{\mu_i} \right) \tag{4.38}$$

where μ_i, i = 1, 2, 3, ..., n, are the eigenvalues of eqs. (4.36) or (4.37).

It can be shown that (Strang, 1980) the acceleration capacity, A.C., is inversely proportional to the square root of determinant of the matrix, i.e.

$$\text{A.C.} = 1 / [\det (W_x^{-1} J^{-T} M^T A^{-T} W_\xi A^{-1} M J^{-1})]^{1/2} \tag{4.39}$$

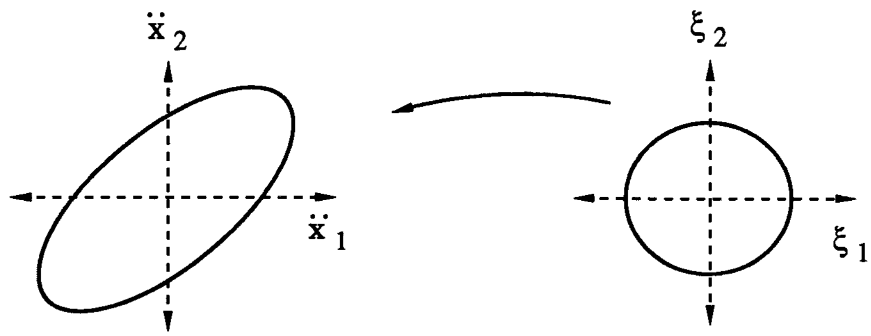

$$\ddot{X}^{T} J^{-T} M^{T} A^{-T} W_{\xi} A^{-1} M J^{-1} \ddot{X} = 1 \qquad\qquad |\xi|^{2} = 1$$

End-effector-space   Actuator-space

Fig. 4-4: Force Transformation between actuator-space and end-effector-space.

By rearranging eq. (4.39), A.C. can also be written as

$$\text{A.C.} = \frac{[\det(J^{T} W_{x} J) \det(A W_{\phi} A^{T})]^{1/2}}{\det(M)} \tag{4.40}$$

As an index for measuring the directional sensitivity, the dynamic condition number (DCN) can be defined as the ratio of the maximum to the minimum eigenvalues of eq. (4.36) or (4.37) as

$$DCN = \sqrt{\frac{\mu_i)_{max}}{\mu_i)_{min}}} \tag{4.41}$$

The acceleration capacity, A.C., can be used as an index to indicate the ability of a manipulator to respond to a given set of input torques. The larger the acceleration capacity, the more responsive the system is. At a given end-effector position the determinant of the product of Jacobian matrix, det ($J^T W_X J$), is a constant while the determinant of inertia matrix, det (M), and the product of structure matrix are function of gear ratios. Hence, the value of A.C. and the direction sensitivity of generalized effective inertia are highly affected by the selection of gearing configuration.

4.4 Summary

In this chapter, the concepts of velocity ratio and effective inertia are extended from one-D.O.F. system to multi-D.O.F. geared robotic mechanisms. Performance indices, such as generalized velocity ratio, velocity capacity, generalized effective inertia and acceleration capacity are defined. With these performance indices, gearing configuration selection and gear ratios determination which are critical design factors will be discussed in the following two chapters.

CHAPTER 5

Gearing Configuration Determination Based on Kinematic Isotropy and Maximum Acceleration Capacity

5.1 Introduction

It has been shown that there are four two-D.O.F. basic geared robotic mechanisms and thirty three-D.O.F. basic geared robotic mechanisms (Chang and Tsai, 1990). It has also been known that there are various different ways of constructing the transmission lines from a basic geared robotic mechanisms. From such a large variety of different gearing configurations, the designer must be able to choose a suitable one for his own application. This motivates the research of this chapter.

The equation of motion of the one-D.O.F. geared mechanism shown in Fig. 4-3 can be written as

$$(I_r + I_L)\ddot{q} = r_{2,1}\,\xi_i \tag{5.1}$$

where $I_r = I_i\, r_{21}^2$ denotes the inertia of the input link reflected at the output shaft, I_i the inertia of the input link, I_L the inertia of the output link, ξ_i the input torque, q the angular displacement of the output shaft.

Assume that I_i and I_L remain constant regardless of the change in gear ratio and assume that there is no power loss in the gear mesh. Figure 5-1 shows the relation between the output shaft acceleration, $\ddot{q}$, and the gear ratio, $r_{2,1}$. It is clear that, given ξ_i, I_i and I_L, there exists an optimum gear ratio which yields a maximum output acceleration. At the optimum design, the output acceleration and the gear ratio are given by

$$\ddot{q})_{max} = \frac{\xi_i}{2\sqrt{I_i I_L}} \tag{5.2}$$

$$r_{2,1}^2)_{opt} = \frac{I_L}{I_i} \tag{5.3}$$

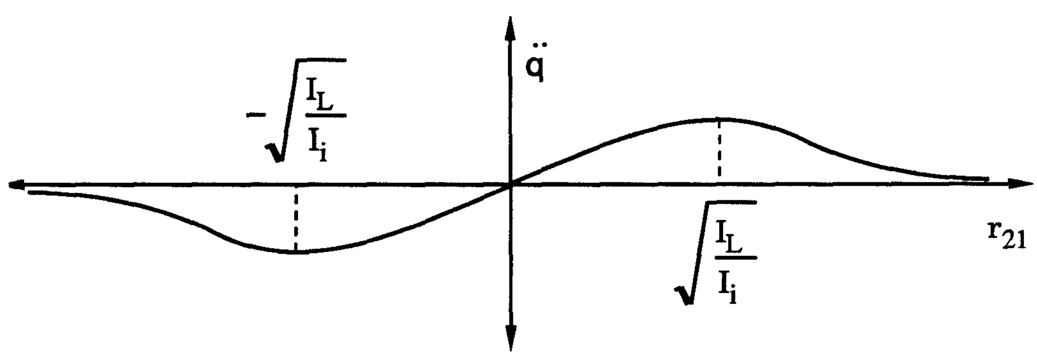

Fig. 5-1: Variation of output acceleration vs. gear ratio.

Equations (5.2) and (5.3) can be simply stated as follows. At the optimum design, the gear ratio is chosen such that the reflected input inertia is "matched" with the output inertia. This is known as the "principle of inertia match" (Klafter, et at. 1989, Stockdale, 1968) .

The principle of inertia match serves as a solid guideline in the gear ratio selection for one-D.O.F. geared mechanism. However, for multi-D.O.F. geared mechanisms, which can be commonly found in robotic applications, the selection of gearing configuration and determination of gear ratios still depend on the designer's intuition.

In this chapter and in the following chapter, design criteria will be established using the performance indices defined in chapter four and methodologies for the selection of gearing configuration and determination of gear ratios will be developed.

5.2 Kinematic Isotropic Condition

It has been shown that the kinematic characteristics of a manipulator is dependent on the kinematic condition number of its Jacobian matrix (Salisbury and Craig, 1982). This number should be kept as small as possible. The smallest value that can be attained is one which results in a kinematic isotropy. Kinematic isotropy is a local property since the Jacobian matrix is position dependent. Various approaches have been proposed to achieve the isotropic condition (Asada and Cro Granito, 1985; Dubey and Luh, 1986; Grosselin and Angles, 1985a). Most of them suggested the use of special linkage proportions which are difficult and sometimes even impractical to implement. Nevertheless, these approaches are merely useful for direct-drive manipulators since the Jacobian matrix only relates the velocity in the joint-space to the end-effector-space. In the following, a novel approach for achieving a kinematically isotropic condition will be developed for a general class of geared robotic mechanisms. The approach will be based on the transformation between the actuator-space and the end-effector-space.

5.2.1 Proportional Condition

Suppose the kinematic structure of a manipulator has already been selected and the problem is to determine the gear ratios such that the generalized velocity ratio defined in chapter four is less directional sensitive. The problem can be stated as:

How to choose the gear ratios of a manipulator such that the mechanism can possess kinematically isotropic property at a predetermined end-effector position ?

This problem can be solved by minimizing the difference between the maximum and minimum eigenvalues of eq. (4.15), or (4.16) or (4.17). Equations (4.15) and (4.17) contain both Jacobian and structure matrices on the left-hand-side of the equation, while (4.16) contains the Jacobian matrix on the left-hand-side and the structure matrix on the right-hand-side. Since the Jacobian matrix is determined by the dimensions and joint angles of the equivalent open-loop chain, it is configuration dependent and is not a function of gear ratio. The separation of Jacobian matrix from structure matrix makes it more convenient to use eq. (4.16) for the purpose of design optimization.

For eq. (4.16) to have non-trivial solutions, the following condition must be satisfied:

$$\det\,(P - \lambda Q) = 0 \tag{5.4}$$

where $P = J^T W_x J$ and $Q = A\, W_\phi\, A^T$.

Since both P and Q are positive definite matrices, the eigenvalues, λ's, are all positive real numbers. It has been shown that for λ to be a r-fold root, all the principal minors of $(P-\lambda Q)$ starting from order n to order n-r+1 must vanish (Jeffreys, 1956; Goldstein, 1981). If λ is an n-fold root for an n-D.O.F. geared robotic mechanism, then the mechanism is said to be kinematically isotropic at the given end-effector position. For λ to be an n-fold root, the following proportional condition must be satisfied

$$(J^T W_x J)_{i,j} = \lambda\,(A W_\phi\, A^T)_{i,j} \tag{5.5}$$

or

$$(J^T W_x J)_{i,j} = K_v^2\,(A\, W_\phi\, A^T)_{i,j} \tag{5.6}$$

where $(\ )_{i,j}$ denotes the (i, j) element of the matrix enclosed in the parenthesis.

Under this condition, the generalized velocity ratio defined in eq. (4.13), $K_v = \sqrt{\lambda}$, is independent of the direction of motion. Taking determinant of both sides of eq. (5.6), yields

$$\det (J^T W_x J) = K_v^{2n} \det (A\, W_\phi\, A^T) \tag{5.7}$$

From eqs. (4.20) and (5.7), it can be concluded that, for n-D.O.F. manipulators with kinematic isotropy property, the velocity capacity is equal to the generalized velocity ratio to the n-th power, i.e.

$$V.C. = K_v^n \tag{5.8}$$

5.2.1 Individual-Joint Drive Manipulators

If every moving link in a manipulator is driven by an actuator mounted on its preceding link through a gear-reduction unit such as the one shown in Fig. 5-2, then the joint motions are independent of each other. We call this type of manipulators *individual joint-drive manipulators.*

The structure matrix for an individual joint-drive manipulator has the following form:

$$A = \begin{bmatrix} g_{11} & & & 0 \\ & g_{22} & & \\ & & \ddots & \\ 0 & & & g_{nn} \end{bmatrix} \tag{5.9}$$

where g_{ii} is the gear reduction for the i-th actuator. Hence,

$$A\, W_\phi\, A^T = \begin{bmatrix} w_1 g_{11}^2 & & & 0 \\ & w_2 g_{22}^2 & & \\ & & \ddots & \\ 0 & & & w_n g_{nn}^2 \end{bmatrix} \tag{5.10}$$

where w_i is the (i,i) element of W_ϕ.

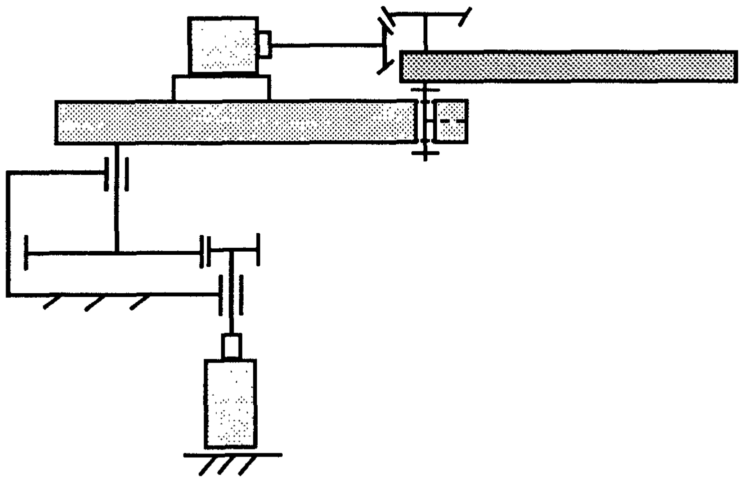

Fig. 5-2: A two-D.O.F. planar individual joint-drive manipulator.

At a given end-effector position the product of Jacobian matrix can be written in following form:

$$J^T W_x J = \begin{bmatrix} \varepsilon_{11} & \varepsilon_{12} & \cdots & \varepsilon_{1n} \\ \varepsilon_{12} & \varepsilon_{22} & \cdots & \varepsilon_{2n} \\ \vdots & \vdots & \ddots & \vdots \\ \varepsilon_{1n} & \varepsilon_{2n} & \cdots & \varepsilon_{m} \end{bmatrix} \tag{5.11}$$

Substituting eqs. (5.10) and (5.11) into (5.6), yields

$$\varepsilon_{ij} = \lambda \begin{cases} w_i\, g_{ii}^2, & i = j, \\ 0, & i \neq j \end{cases} \tag{5.12}$$

It is obvious that eq. (5.12) can not be satisfied by any choice of g_i, unless $\varepsilon_{ij} = 0$ for all i not equal to j which requires special linkage proportions and joint parameters. This leads to the following theorem.

Theorem 1. Individual joint-drive manipulators can not possess a kinematically isotropic property unless the product of Jacobian matrix, $J^T W_x J$*, is a diagonal matrix at the position of interest.*

5.2.2 Gear-Coupled Manipulators

If some of the links in a manipulator are driven by actuators mounted on links other than their preceding links through the use of gear trains, then the joint motions are coupled. We call this type of mechanisms *gear-coupled manipulators*. For example, Fig. 5-3 shows a planar gear-coupled manipulator.

The structure matrix A for a gear-coupled manipulator is no-longer diagonal (Chang and Tsai, 1990). For an n-D.O.F. gear-coupled manipulator, eq. (5.6) yields n(n+1)/2 nonlinear equations. However, the number of unknowns contained in eq. (5.6) depends on the arrangement of transmission lines, i.e. the number of non-zero elements in the structure matrix. It is essential that the number of unknowns is not less than the number of equations. If the number of unknowns is less than the number of equations, then special linkage geometry is required to yield an isotropic condition. If the number of unknowns is greater than the number of equations, then there exist some free choices among the non-zero elements of the structure matrix. This leads to the second theorem.

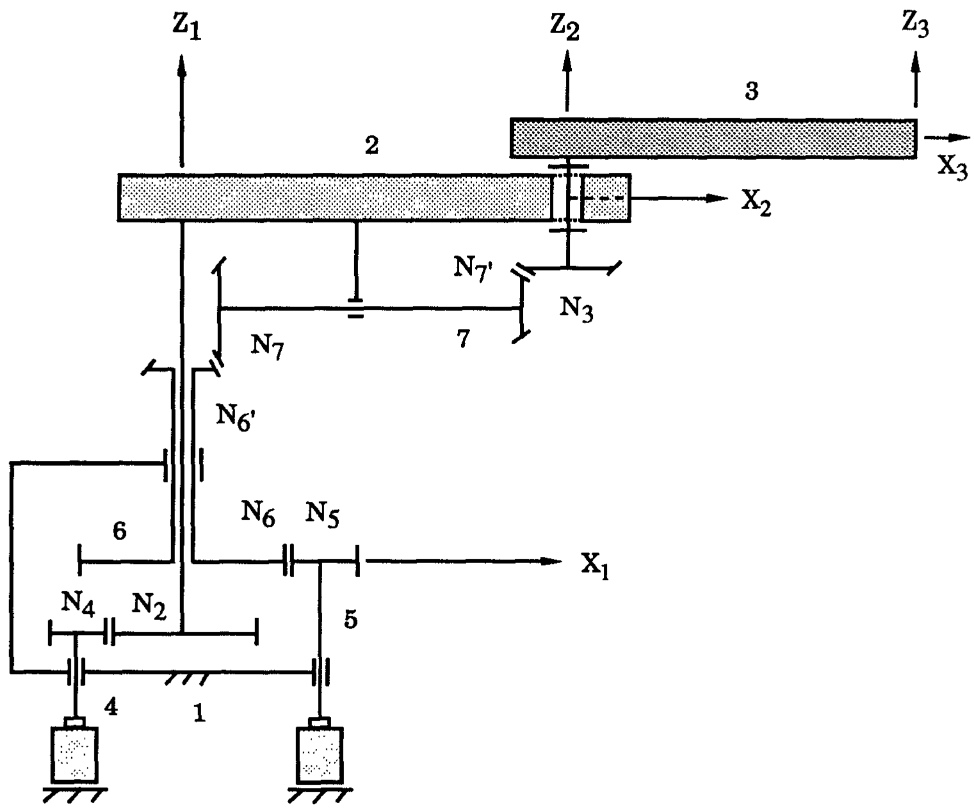

Fig. 5-3: A two-D.O.F. planar gear-coupled manipulator.

Theorem 2. Gear-coupled manipulators can be designed to possess the kinematically isotropic property at a given end-effector position, if and only if the number of non-zero elements in the structure matrix is equal to or greater than n(n+1)/2.

5.2.3 Two-Stage Gear Reduction

From eq. (5.6), it can be shown that for those gear-coupled manipulators, if the kinematic isotropic property is achievable through proper choice of gear ratios, then the elements of the structure matrix can be written as

$$A = K_v^{-1} \begin{bmatrix} \alpha_{11} & \alpha_{12} & \cdots & \alpha_{1n} \\ \alpha_{12} & \ddots & & \vdots \\ \vdots & & & \\ \alpha_{1n} & & \cdots & \alpha_{m} \end{bmatrix} \tag{5.13}$$

where $\alpha_{i,j}$ is a function of $J^T W_x J$ and W_ϕ .

Note that the value of $\alpha_{i,j}$ depends only on the Jacobian and the weighting matrices. Hence, from eq. (5.13), the train value in each transmission line can be thought of as a product of two-stage gear reductions, i.e. K_v^{-1} and $\alpha_{i,j}$'s. This leads to the following theorem.

Theorem 3: For gear-coupled manipulators, if the kinematic isotropy condition can be made at a given end-effector position through proper choice of gear ratios , then the gearing system can be viewed as composed of a two-stage gear reductions. The first-stage gear reduction, which is common to all transmission lines, provides the desired overall reduction to the system while the second-stage gear reduction provides the necessary condition for a kinematically isotropic transformation

Example:

Referring to the two-D.O.F. planar manipulator shown in Fig. 5-3, both actuators of the manipulator are mounted on the ground, and there are two transmission lines. The first transmits an actuator torque through the (4, 2) gear pair to link 2. The second transmits another actuator torque through the (5, 6), (6, 7) and (7, 3) gear pairs to link 3. The structure matrix is given by

$$A = \begin{bmatrix} g_{11} & g_{12} \\ 0 & g_{22} \end{bmatrix} \tag{5.14}$$

where $g_{11} = r_{2,4}$, $g_{12} = r_{6,5}$, $g_{22} = g_{12}\, r_{7,6}'\, r_{3,7}'$.

Assuming at a given end-effector position, the product of Jacobian matrix takes the following form:

$$J^T W_x J = \begin{bmatrix} \varepsilon_{11} & \varepsilon_{12} \\ \varepsilon_{12} & \varepsilon_{22} \end{bmatrix} \tag{5.15}$$

and W_ϕ is an identity matrix, then it follows from eqs. (5.6), (5.14) and (5.15) that

$$K_v^2\,(g_{11}^2 + g_{12}^2) = \varepsilon_{11} \tag{5.16}$$

$$K_v^2\, g_{12}\, g_{22} = \varepsilon_{12} \tag{5.17}$$

$$K_v^2\, g_{22}^2 = \varepsilon_{22} \tag{5.18}$$

Solving eqs. (5.16)-(5.18), yields

$$|g_{11}| = \frac{\sqrt{(\varepsilon_{11}\varepsilon_{22} - \varepsilon_{12}^2)/\varepsilon_{22}}}{K_v} \tag{5.19}$$

$$|g_{12}| = \varepsilon_{12}/(\sqrt{\varepsilon_{22}}\,K_v) \tag{5.20}$$

$$|g_{22}| = \sqrt{\varepsilon_{22}}\,/K_v \tag{5.21}$$

and where the signs of g_1, g_2 and e in matrix A can have one of the following combinations:

$$A = \begin{bmatrix} + & + \\ 0 & + \end{bmatrix}, \text{ or } \begin{bmatrix} + & - \\ 0 & - \end{bmatrix}, \text{ or } \begin{bmatrix} - & + \\ 0 & + \end{bmatrix}, \text{ or } \begin{bmatrix} - & - \\ 0 & - \end{bmatrix}$$

Hence, a sign change along any transmission line does not change the isotropic condition. Equations (5.19) to (5.21) can be written in the following form:

$$g_{11} = \alpha k \tag{5.22}$$

$$g_{12} = \beta k \tag{5.23}$$

$$r_{7,6'} r_{3,7'} = g_{22}/g_{12} = \varepsilon_{22}/\varepsilon_{12} \tag{5.24}$$

or

$$A = k \begin{bmatrix} \alpha & \beta \\ 0 & \beta \dfrac{\varepsilon_{22}}{\varepsilon_{12}} \end{bmatrix} \tag{5.25}$$

where

$$k = \frac{\sqrt{(\varepsilon_{11}\varepsilon_{22} - \varepsilon_{12}^2)/\varepsilon_{22}}}{\alpha K_v} = \frac{\sqrt{\det(J^T W_x J)}}{\alpha K_v \sqrt{\varepsilon_{22}}} \tag{5.26}$$

$$\beta = \alpha\, \varepsilon_{12} / \sqrt{(\varepsilon_{11}\varepsilon_{22} - \varepsilon_{12}^2)} = \alpha\, \varepsilon_{12} / \sqrt{\det(J^T W_x J)} \tag{5.27}$$

We note that α can be chosen arbitrarily. But, once α is chosen, β is determined by eq. (5.27). It follows, from eqs. (5.22) to (5.27), that k, which is inversely proportional to the generalized velocity ratio K_V, can be considered as a scaling factor and the train value for each transmission line can be thought of as a product of two-stage gear reductions as shown in Fig. 5-4. The first-stage gear reduction, k, which is common to all transmission lines, provides the desired overall reduction while the second-stage gear reduction provides the necessary condition for an isotropic transformation.

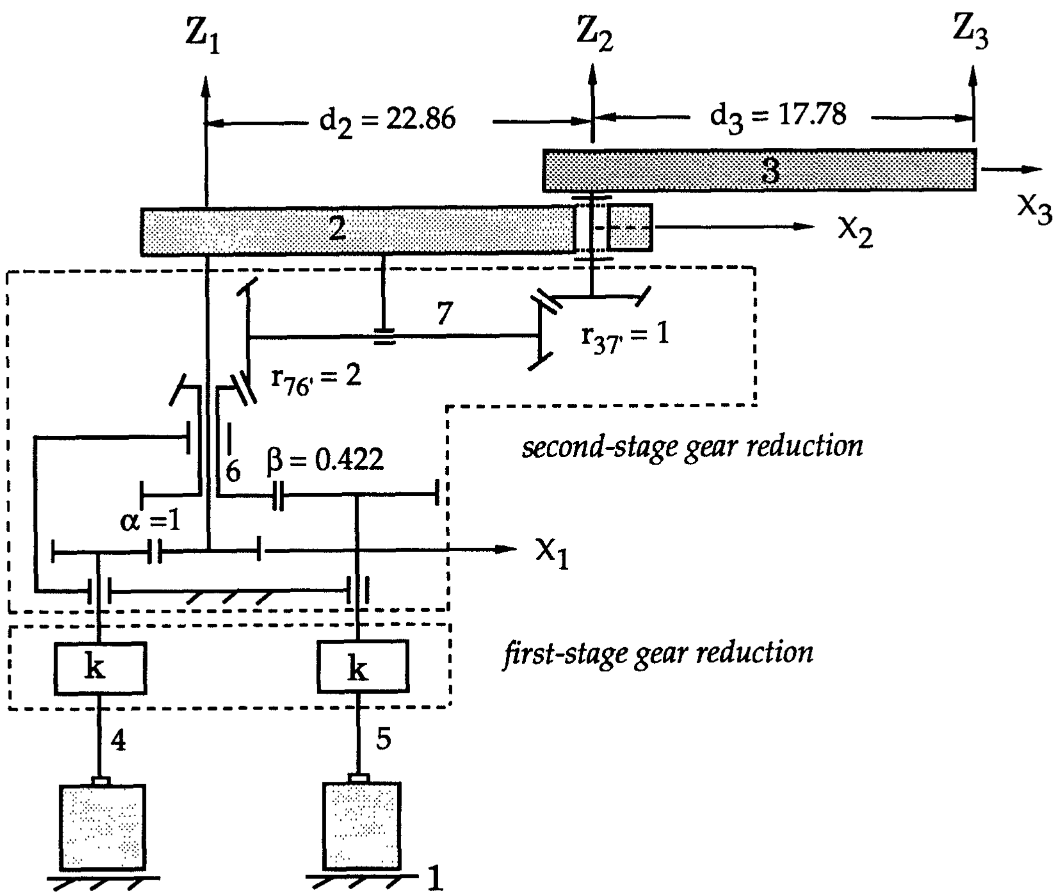

Fig. 5-4: Illustration of two-stage gear reductions of the manipulator shown in Fig. 5-3.

For the manipulator shown in Fig. 5-4, it can be shown that the Jacobian matrix is given by

$$J = \begin{bmatrix} -d_3S_{12} - d_2S_1 & -d_3S_{12} \\ d_3C_{12} + d_2C_1 & d_3C_{12} \end{bmatrix} \tag{5.28}$$

where d_2 and d_3 are the lengths of link 2 and link 3, respectively, and where S_i, C_i, S_{12}, and C_{12} denote $\sin(\theta_i)$, $\cos(\theta_i)$, $\sin(\theta_1+\theta_2)$, and $\cos(\theta_1+\theta_2)$, respectively. Hence, with the end-effector positioned at $[X_1, Y_1] = [22.86, 0]$, and assuming $d_2 = 22.86$ cm and $d_3 = 17.78$ cm, the Jacobian becomes:

$$J = \begin{bmatrix} 0 & 16.38 \\ 22.86 & 6.91 \end{bmatrix} \tag{5.29}$$

Assuming W_x and W_ϕ are both identity matrices, yields

$$J^T W_x J = \begin{bmatrix} 522.58 & 157.96 \\ 157.96 & 316.05 \end{bmatrix} \tag{5.30}$$

Substituting eq. (5.30) into eqs. (5.22-5.27), yields

$$k = 21.063/(\alpha K_v) \tag{5.31}$$

$$\beta = 0.422\,\alpha \tag{5.32}$$

$$r_{7,6'} r_{3,7'} = 2 \tag{5.33}$$

or

$$A = \frac{21.063}{K_v} \begin{bmatrix} \alpha & 0.422\,\alpha \\ 0 & 0.844\,\alpha \end{bmatrix} \tag{5.34}$$

For example, we can choose $\alpha = 1$ and $r_{3,7'} = 1$, then $\beta = 0.422$ and $r_{7,6'} = 2$. Hence, a designer can finalize the second-stage gear reduction without concerning the generalized velocity ratio, K_v.

5.3 Dynamic Optimization

In the previous section, we have shown that infinite many sets of gear ratios can be used to produce a kinematically isotropic condition for those gear-coupled manipulators which satisfy theorem 2. This leaves room for dynamic optimization.

From eqs. (4.40) and (5.7), the acceleration capacity can be simplified as

$$A.C. = \frac{\det(J^T W_x J)}{K_v^n \det(M)} \tag{5.35}$$

The acceleration capacity, A.C., can be used as an index to indicate the ability of a manipulator to respond to a given set of input torques. The larger the acceleration capacity, the more responsive the system is. At a given end-effector position the determinant of the product of Jacobian matrix, $\det(J^T W_x J)$, is a constant while the determinant of inertia matrix, $\det(M)$, is function of gear ratios. Hence, the unknown gear ratios can then be used to optimize the acceleration capacity.

Taking the manipulator shown in Fig. 5-4 as an example, the mass matrix M contributed by the major links and the carried links is given by

$$M = M_m + M_c \tag{5.36}$$

where

$$M_m = \begin{bmatrix} M_{m11} & M_{m12} \\ M_{m12} & M_{m22} \end{bmatrix} \tag{5.37a}$$

$$M_c = M_r + M_g \tag{5.37b}$$

$$M_r = \begin{bmatrix} I_4 g_{11}^2 + I_5 g_{12}^2 & I_5 g_{12} g_{22} \\ I_5 g_{12} g_{22} & I_5 g_{22}^2 \end{bmatrix} \tag{5.37c}$$

and

$$M_g = \begin{bmatrix} I_6 & I_6 r_{7,6'} r_{3,7'} \\ I_6 r_{7,6'} r_{3,7'} & I_6 (r_{7,6'} r_{3,7'})^2 + I_7 r_{3,7'}^2 \end{bmatrix} \tag{5.37d}$$

is given by eq. (2.65).

Substituting eqs. (5.22)-(5.24) into (5.37c),

$$M_r = k^2 \begin{bmatrix} \delta_1 & \delta_2 \\ \delta_2 & \delta_3 \end{bmatrix} \tag{5.38}$$

where

$$\delta_1 = I_4 \alpha^2 + I_5 \beta^2 \tag{5.39}$$

$$\delta_2 = I_5 \beta^2 r_{7,6'} r_{3,7'} \tag{5.40}$$

$$\delta_3 = I_5 (\beta r_{7,6'} r_{3,7'})^2 \tag{5.41}$$

Note that $r_{7,6'} r_{3,7'} = 2$, eq. (5.33), is determined by link properties and M_g is not a function of k^2. Hence, the contribution of axial moment of inertias of gears 6 and 7 to the overall inertia can be neglected due to the small values of I_6, I_7, and $r_{7,6'} r_{3,7'}$, i.e. $M_g \simeq 0$. However, I_4 and I_5 can have significant effect on the overall inertia due to the k^2 term in eq. (5.38). Hence, $M_r \simeq M_c$.

In what follows, we shall assume that adjusting gear ratios will not have significant effect on the M_m matrix. Under this assumption, the determinant of inertia matrix can be written as

$$\det(M) = \det(M_m) + k^2 \rho_1 + k^4 \rho_2 \tag{5.42}$$

where

$$\rho_1 = M_{m11}\delta_3 - 2M_{m12}\delta_2 + M_{m22}\delta_1 \tag{5.43}$$

$$\rho_2 = \delta_1\delta_3 - \delta_2^2 \tag{5.44}$$

Substituting k_v, from eq. (5.26) and det(M) from eq. (5.42) into eq.(5.35), yields

$$A.C. = \varepsilon_{22}\,\alpha^2 \left[\frac{\det(M_m)}{k^2} + \rho_1 + k^2\rho_2\right]^{-1} \tag{5.45}$$

It follows from eq. (5.45) that, at a given end-effector position, the acceleration capacity is a function of the first-stage gear reduction, k. Taking the derivative of eq. (5.45) with respect to k and equating the resulting equation to zero, yields

$$k^4 = \det(M_m)/\rho_2 \tag{5.46a}$$

Note that $k^4\,\rho_2 = \det(M_r)$. Hence, eq. (5.46a) can also be written as

$$\det(M_r) = \det(M_m) \tag{5.46b}$$

Taking second derivative of eq. (5.45) with respect to k and substituting eq. (5.46a) into it, we obtain

$$\left.\frac{\partial}{\partial k}\left(\frac{\partial A.C.}{\partial k}\right)\right|_{k^4 = \frac{\det(M_m)}{\rho_2}} = -\frac{8\,\alpha^2\varepsilon_{22}\,\rho_2\sqrt{\det(M_m)}}{\left[\rho_1 + 2\sqrt{\rho_2\det(M_m)}\right]^2} \tag{5.47}$$

It is clear that eq. (5.47) is always negative. Thus, eq. (5.46a) or (5.46b) provides the optimum condition for the maximum acceleration capacity of this planar two-D.O.F. manipulator. At the optimum condition, the acceleration capacity is given by

$$A.C.)_{max} = \varepsilon_{22}\, \alpha^2 \left[\rho_1 + 2\sqrt{\rho_2 \det(M_m)} \right]^{-1} \tag{5.48}$$

Assuming that m_2 = 2600 g, m_3 = 1156 g, p_{2x} = -12.872 cm, p_{3x} = -10.201 cm, I_{2z} = 142900 g-cm^2, I_{3z} = 40940 g-cm^2, $I_4 = I_5$ =87.9 g-cm^2, for the manipulator shown in Fig. 5-4, then with the end-effector positioned at $[X_1, Y_1]$ = [22.86, 0], the mass matrix contributed by the major links, M_m, is given by

$$M_m = \begin{bmatrix} 905.763 & 24.953 \\ 24.953 & 104.113 \end{bmatrix} \quad (10^{-4}\ \mathrm{kg-m^2}) \tag{5.49}$$

Assuming that $\alpha = 1$, $\beta = 0.422$, $r_{3,7'} = 1$, and $r_{7,6'} = 2$, then from eq. (5.46), we obtain k = 65.54 as the first-stage gear reduction. Hence, from eq. (5.31), the generalized velocity ratio K_V is found to be $3.2136 \cdot 10^{-3}$ m and, from eq. (5.8), the velocity capacity (V.C.) is equal to 0.10327.

Since the Jacobian matrix and the inertia matrix are position dependent, the isotropic condition, the acceleration capacity, generalized velocity ratio, and the velocity capacity obtained under the optimal condition are only local properties. Usually, a reference position within the workspace is selected for design optimization. The performance of a manipulator will then vary from position to position. Hence, the reference position must be chosen carefully in order to achieve a good compromise between extreme positions. It seems that this can only be accomplished by an iterative process.

Figure 5-5 shows the workspace of the example manipulator shown in Fig. 5-4. Since the Jacobian matrix and inertia matrix are symmetric about the first joint axis, it is only necessary to investigate the kinematic and dynamic performance along the X_1-axis. As a first approximation, the middle point of the workspace is chosen as the reference position for design optimization.

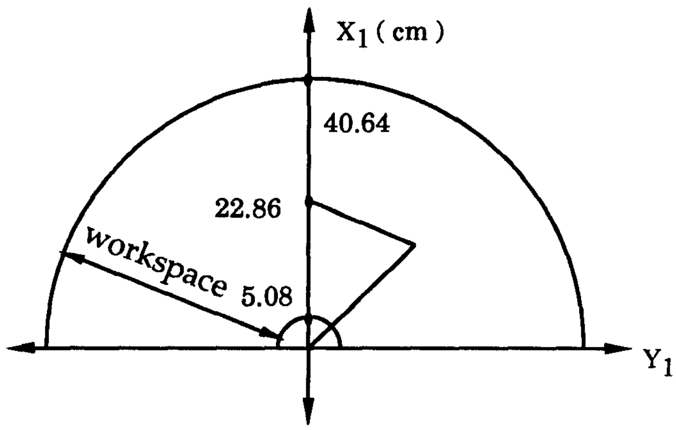

Fig. 5-5: Workspace of the manipulator shown in Fig. 5-4.

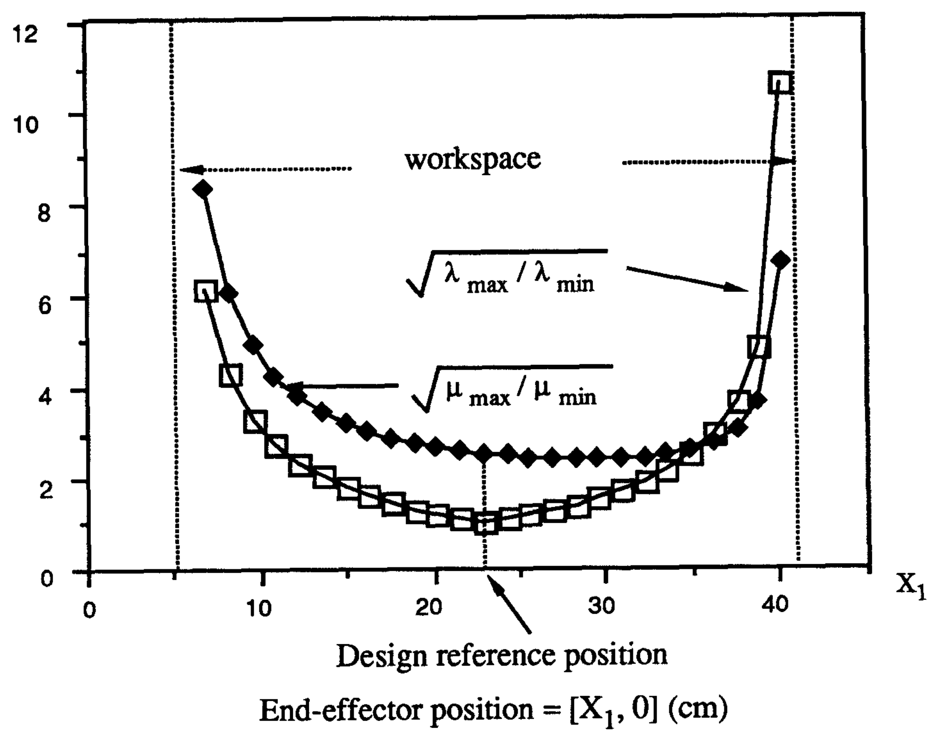

Fig. 5-6: Performance indices Vs. End-Effector Positions.

Figure 5-6 shows the variation of the kinematic condition number ($\sqrt{\lambda_{max}/\lambda_{min}}$) and dynamic condition number ($\sqrt{\mu_{max}/\mu_{min}}$) as functions of the end-effector position. Since $X_1 = 22.86$ cm is chosen as the reference position, the global minimum kinematic condition number occurs at this reference position. However, the global minimum dynamic condition number does not occur at the reference position.

Figure 5-7 shows the variation of the determinants of M and J^TJ, and the variation of the acceleration capacity, A.C., as functions of the end-effector position. As can be seen from Fig. 5-7, the global maximum acceleration capacity occurs at $X_1 = 29.53$ cm, instead of the reference position. This is due to the influence of the determinant of the product of the Jacobian matrix, J^TJ. Note that the maximum value of $\det(J^TJ)$ occurs at $X_1 = 29.53$ cm coincidently.

5.4 Summary

In this chapter, a methodology for the determination of train values in geared robotic mechanisms based on the kinematic isotropy condition followed by an optimization of the acceleration capacity has been developed. It is shown that individual-joint drive manipulators cannot be designed to possess an isotropic condition unless it has special linkage proportions and joint parameters. It is also shown that certain gear-coupled manipulators can be designed to possess an isotropic condition through proper choice of gear ratios. The train values of these gear-coupled manipulators can be thought of as a product of two-stage gear reductions. The second-stage gear reduction is determined from the kinematic isotropic condition while the first-stage gear reduction is used for the optimization of acceleration capacity.

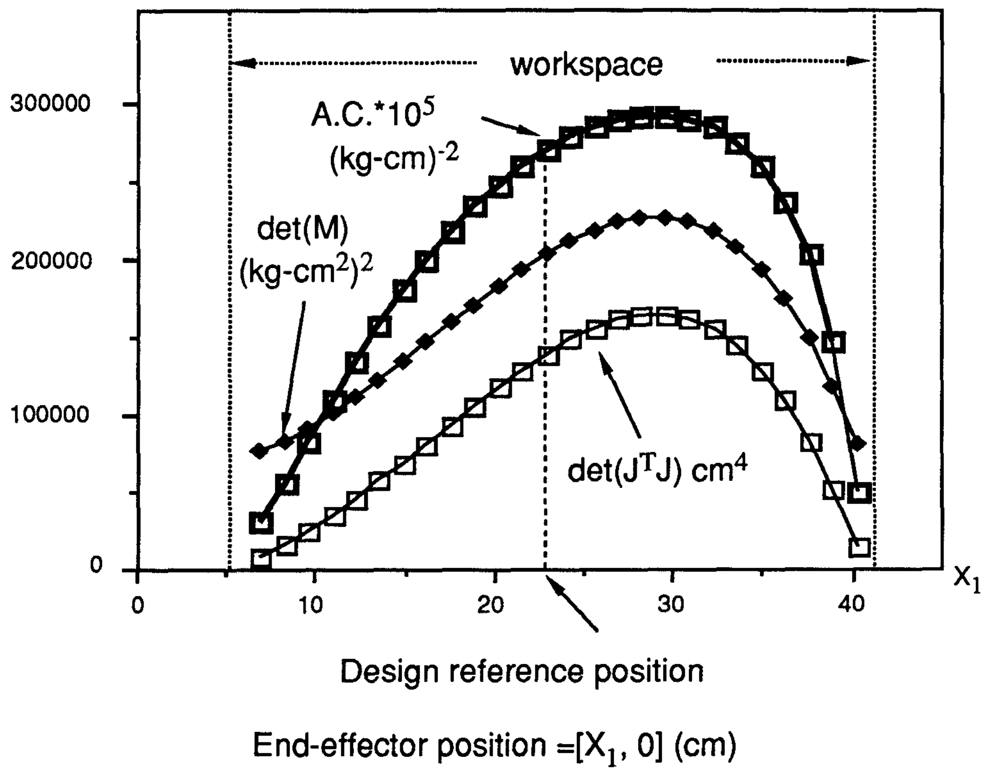

Fig. 5-7: Acceleration Capacity Vs. End-Effector Positions.

CHAPTER 6

Gearing Configuration Determination Based on Maximum Acceleration Capacity

6.1 Introduction and Problem Formulation

In Chapter five, an approach based on kinematic isotropy followed by acceleration capacity optimization is developed and the concept of two-stage gear reduction is introduced for multi-D.O.F. gear-coupled manipulators. In this chapter, a different approach based on the optimization of acceleration capacity alone will be developed. Design equations and optimality conditions will be derived. Several two-D.O.F. geared robotic mechanisms will be used as numerical examples to demonstrate the principle.

The question we want to answer is

$$\text{Given } \quad |\xi|^2 \equiv \xi^T W_\xi \xi = 1, \tag{6.1}$$

as a constraint on actuator torques, what gear ratios yield the optimum dynamic performance?

Using the concept of acceleration capacity defined in chapter four, the problem can be restated as

$$\text{Given} \quad |\xi|^2 = 1,$$

what gear ratios yield the optimum acceleration capacity?

To answer this question, we will first examine the inertia matrix M, and then seek for the optimum solution.

6.2 Inertia Matrix

Neglecting the Coriolis and centrifugal terms, the generalized inertia force contribution due to relative rotation of a carried link i with respect to its carrier j, and associated with the generalized coordinate q_r, eqs. (2.31) and (2.32), can be written as

$$F^*_{ir} = I_i\, b_{ir} [\sum_{s=j}^{n} (b_{is}\, \ddot{q}_s) + \sum_{s=1}^{j-1} (U_{js}\, \ddot{q}_s) \cdot {}^j\upsilon_i], \qquad \text{for } r \geq j \tag{6.2a}$$

and

$$F^*_{ir} = I_i [\sum_{s=j}^{n} (b_{is}\, \ddot{q}_s)(U_{jr} \cdot {}^j\upsilon_i)], \qquad \text{for } r < j \tag{6.2b}$$

Note that the order-of-magnitude for ($U_{js} \cdot {}^j\upsilon_i$) ranges from -1 to +1, while the b_{is}'s are usually one order-of-magnitude larger than ($U_{js} \cdot {}^j\upsilon_i$) . Hence, in general, the first term in eq. (6.2a) dominates the equation and eqs. (6.2a-b) can be approximated as:

$$F^*_{ir} = \begin{cases} I_i\, b_{ir} \sum_{s=j}^{n} (b_{is}\, \ddot{q}_s), & \text{for } r \geq j \\ 0, & \text{for } r < j \end{cases} \tag{6.3}$$

Recalling that b_{ij} is the element of the structure matrix A. Hence, the contribution of input links to the inertia matrix M_r can be obtained by assembling the coefficients of $\ddot{q}_s$ in eq. (6.3), for all combinations of i and r, as

$$M_r = I_m A\, V\, A^T \tag{6.4}$$

where

$$I_m = \sqrt[n]{\prod_{i=1}^{n} I_i} \tag{6.5}$$

and where I_i is the axial moment of inertia of the i-th input link, V is a diagonal scaling matrix with its (i, i) element equal to I_i/I_m and its determinant equal to unity. Note that the contribution to the inertia matrix due to the intermediate carried links, M_g, can be neglected, since they are usually one order-of-magnitude smaller than that due to the input links. Hence, the overall inertia matrix can be written as:

$$M = M_m + M_r \tag{6.6}$$

where M_m is the inertia matrix contributed by the major links in the equivalent open-loop chain.

It should also be noted that M_r is a function of gear ratios while M_m is a function of the joint angles and link mass properties. Hence, we can optimize the design of a manipulator only at a predetermined manipulator posture.

6.3 The Generalized Principle of Inertia Match

Taking the determinant of eq. (6.4), yields

$$\det(M_r) = \det(I_m A V A^T) = I_m^n \det(A A^T) \tag{6.7}$$

With eq. (6.7), the acceleration capacity, eq. (4.40) can be reduced to

$$A.C. = \frac{\sqrt{\det(J^T W_x J) \det(W_\phi) \det(M_r)}}{\sqrt{I_m^n} \det(M)} \tag{6.8}$$

or simply,

$$A.C. = \alpha \eta \tag{6.9}$$

where

$$\alpha = \sqrt{\frac{\det(J^T W_x J) \det(W_\phi)}{I_m^n}} \tag{6.10}$$

and

$$\eta = \frac{\sqrt{\det(M_r)}}{\det(M)} \tag{6.11}$$

Note that to maximize the acceleration capacity is equivalent to maximize η, since α is a constant at a given posture.

6.3.1 Two-D.O.F. Systems:

Assume that the structure matrix A takes following general form:

$$A = \begin{bmatrix} g_{11} & g_{12} \\ g_{21} & g_{22} \end{bmatrix} \tag{6.12}$$

Then, from eq. (6.4), the inertia matrix M_r can be written as

$$M_r = \begin{bmatrix} \kappa_{11} & \kappa_{12} \\ \kappa_{12} & \kappa_{22} \end{bmatrix} \tag{6.13}$$

where

$$\kappa_{11} = I_1 g_{11}^2 + I_2 g_{12}^2 \tag{6.14}$$

$$\kappa_{12} = I_1 g_{11} g_{21} + I_2 g_{12} g_{22} \tag{6.15}$$

$$\kappa_{22} = I_1 g_{21}^2 + I_2 g_{22}^2 \tag{6.16}$$

Note that the matrix M_r contains only three independent parameters, although the number of non-zero elements in the structure matrix can be as many as four. Also note that the structure matrix must have at least three non-zero elements in order for M_r to be non-singular and to have non-zero κ_{12}.

Similarly, the inertia matrix M_m can also be expressed in terms of three independent parameters as shown below:

$$M_m = \begin{bmatrix} M_{m11} & M_{m12} \\ M_{m12} & M_{m22} \end{bmatrix} \tag{6.17}$$

Hence, from eq. (6.6), the inertia matrix M is given by

$$M = \begin{bmatrix} M_{m11} + \kappa_{11} & M_{m12} + \kappa_{12} \\ M_{m12} + \kappa_{12} & M_{m22} + \kappa_{22} \end{bmatrix} \tag{6.18}$$

Substituting determinants of eqs. (6.17) and (6.18) into eq. (6.11), yields

$$\eta = \frac{\sqrt{\kappa_{11}\kappa_{22} - \kappa_{12}^2}}{(M_{m11} + \kappa_{11})(M_{m22} + \kappa_{22}) - (M_{m12} + \kappa_{12})^2} \tag{6.19}$$

Taking derivative of η with respect to κ_{ij} and equating them to zero, yields

$$(M_{m22}+\kappa_{22})[\kappa_{22}(M_{m11}-\kappa_{11})+2\kappa_{12}^2]-\kappa_{22}(M_{m12}+\kappa_{12})^2=0 \tag{6.20}$$

$$(M_{m12}+\kappa_{12})[\kappa_{12}(M_{m12}-\kappa_{12})+2\kappa_{11}\kappa_{22}]$$
$$-\kappa_{12}(M_{m11}+\kappa_{11})M_{m22}+\kappa_{22})=0 \tag{6.21}$$

and

$$(M_{m11}+\kappa_{11})[\kappa_{11}(M_{m22}-\kappa_{22})+2\kappa_{12}^2]-\kappa_{11}(M_{m12}+\kappa_{12})^2=0 \tag{6.22}$$

Two non-trivial solutions to eqs. (6.20-22) are:

$$\begin{cases} \kappa_{11}=M_{m11} \\ \kappa_{12}=M_{m12} \\ \kappa_{22}=M_{m22} \end{cases} \tag{6.23a}$$

and

$$\begin{cases} \kappa_{11}=-M_{m11} \\ \kappa_{12}=-M_{m12} \\ \kappa_{22}=-M_{m22} \end{cases} \tag{6.23b}$$

Since the inertias must be non-negative real numbers, only the former set is a feasible solution. The Hessian matrix of η evaluated with the condition of eq. (6.23a) can be written as

$$H(\eta)=\begin{bmatrix} -M_{m22}^2 & 2M_{m12}M_{m22} & -M_{m12}^2 \\ 2M_{m12}M_{m22} & -2(M_{m11}M_{m22}+M_{m12}^2) & 2M_{m11}M_{m12} \\ -M_{m12}^2 & 2M_{m11}M_{m12} & -M_{m11}^2 \end{bmatrix} \tag{6.24}$$

It can be shown that the Hessian matrix is negative semidefinite. Thus, for two-D.O.F. systems, the optimality condition for maximum acceleration capacity is

$$M_r)_{i,j} = M_m)_{i,j} \tag{6.25}$$

provided M_r and M_m have the same number of independent parameters. Substituting eq. (6.25) into eq. (6.6) and the resulting equation into eq. (6.11), yields

$$\eta)_{max} = \frac{1}{2^2\sqrt{\det\,(M_m)}} \tag{6.26}$$

From eqs. (6.10) and (6.26), we note that, given J, I_1 and I_2, the maximum acceleration capacity of a manipulator at a prescribed posture is independent of the gearing configuration, i.e. the arrangement of transmission lines.

6.3.2 N-D.O.F. Systems

It has been shown (Beckenbach and Bellman, 1965) that for positive definite matrices X and Y of order n, the following inequality holds

$$[\det(X+Y)]^{1/n} \geq [\det(X)]^{1/n} + [\det(Y)]^{1/n} \tag{6.27}$$

Squaring both sides of eq. (6.27), yields

$$[\det(X+Y)]^{2/n} \geq [\det(X)]^{2/n} + [\det(Y)]^{2/n} + 2[\det(X)\det(Y)]^{1/n} \tag{6.28}$$

Since it is always true that

$$[\det(X)]^{2/n} + [\det(Y)]^{2/n} \geq 2[\det(X)\det(Y)]^{1/n} \tag{6.29}$$

It follows, from eqs. (6.28) and (6.29), that

$$[\det(X+Y)]^{2/n} \geq 2^2 [\det(X)\det(Y)]^{1/n} \tag{6.30}$$

Taking n/2 power to both sides of eq. (6.30), we obtain

$$\det(X+Y) \geq 2^n [\det(X)\det(Y)]^{1/2} \tag{6.31}$$

Dividing both sides of eq. (6.31) by { det(X+Y) [det (Y) $]^{1/2}$ }, yields

$$\frac{[\det(X)]^{1/2}}{\det(X+Y)} \leq \frac{1}{2^n [\det(Y)]^{1/2}} \tag{6.32}$$

Replacing X and Y by M_r and M_m in eq. (6.32), respectively, and using eq. (6.6), it can be shown that

$$\frac{[\det(M_r)]^{1/2}}{\det(M)} \leq \frac{1}{2^n [\det(M_m)]^{1/2}} \tag{6.33}$$

For $M_r = M_m$, we have

$$\det(M_r + M_m) = \det(2M_r) = 2^n \det(M_r) \tag{6.34}$$

From eq. (6.34), it can be concluded that $M_r = M_m$ is a sufficient condition for the equality sign in eq. (6.33) to hold. This leads to the following theorem.

Theorem 4: For n-D.O.F. geared robotic systems, the acceleration capacity is bounded by the following inequality:

$$A.C. \leq \frac{1}{2^n} \sqrt{\frac{\det(J^T W_x J)\det(W_\phi)}{I_m^n \det(M_m)}} \tag{6.35}$$

And, a sufficient condition for the equality to hold is

$$M_r = M_m \tag{6.36}$$

Equation (6.36) requires the forms of M_r and M_m to be compatible. When the equality sign holds, the optimum value of acceleration capacity at a given posture is independent of the gearing configuration.

Equation (6.36) implies that, at the optimum design, the mass inertia matrix of the input links reflected at the joint-space is equal to that of the major links. We shall call above theorem the *generalized principle of inertia match* for multi-D.O.F. geared robotic systems.

6.4 Case Study: Two D.O.F. Systems

Figures 6-1 to 6-3 show three different two-D.O.F. planar manipulators. Assume that, at a given posture, the inertia matrix M_m takes the form of eq. (6.17) and the product of Jacobian matrix is:

$$J^T W_x J = \begin{bmatrix} \varepsilon_{11} & \varepsilon_{12} \\ \varepsilon_{12} & \varepsilon_{22} \end{bmatrix} \tag{6.37}$$

The effect of gearing configuration on the optimum gear ratios is discussed as follows.

6.4.1 Individual-Joint Drive Manipulator

Figure 6-1 shows a manipulator in which every moving link is driven by an actuator mounted on its preceding link through a gear-reduction unit. The structure matrix A can be written as

$$A = \begin{bmatrix} g_{11} & 0 \\ 0 & g_{22} \end{bmatrix} \tag{6.38}$$

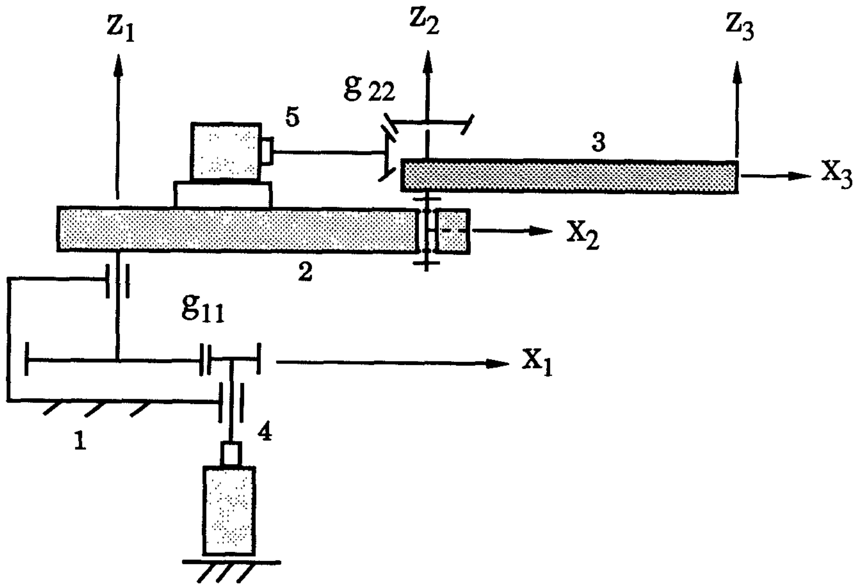

Fig. 6-1: A Two-D.O.F. Planar Individual Joint-Drive Manipulator.

Substituting eq. (6.38) into eqs. (6.14)-(6.16) and the resulting equations into eq. (6.13), yields

$$M_r = \begin{bmatrix} \kappa_{11} & 0 \\ 0 & \kappa_{22} \end{bmatrix} \tag{6.39}$$

where $\kappa_1 = I_1\, g_{11}^2$ and $\kappa_3 = I_2\, g_{22}^2$.

Since $\kappa_{12} = 0$, the forms of M_r and M_m are not compatible with each other and, therefore, eq. (6.23) can not be used as a valid solution.

With $\kappa_{12} = 0$, eqs. (6.20) and (6.22) reduce to

$$[(M_{m11} M_{m22} - M_{m12}^2) - \kappa_{11} \kappa_{22}] - (\kappa_{11} M_{m22} - \kappa_{22} M_{m11}) = 0 \tag{6.40}$$

$$[(M_{m11} M_{m22} - M_{m12}^2) - \kappa_{11} \kappa_{22}] + (\kappa_{11} M_{m22} - \kappa_{22} M_{m11}) = 0 \tag{6.41}$$

From eqs. (6.40-41), we have

$$\begin{cases} M_{m11} M_{m22} - M_{m12}^2 = \kappa_{11} \kappa_{22} \\ \kappa_{11} M_{m22} = \kappa_{22} M_{m11} \end{cases} \tag{6.42}$$

Solving eq. (6-42), yields

$$\kappa_{11} = \sqrt{\frac{\zeta_1 M_{m11}}{M_{m22}}} \tag{6.43}$$

$$\kappa_{22} = \sqrt{\frac{\zeta_1 M_{m22}}{M_{m11}}} \tag{6.44}$$

where

$$\zeta_1 = M_{m11} M_{m22} - M_{m12}^2 \tag{6.45}$$

Hence, the structure matrix can be written as:

$$A = \begin{bmatrix} \frac{1}{\sqrt{I_1}} [\frac{\zeta_1 M_{m11}}{M_{m22}}]^{1/4} & 0 \\ 0 & \frac{1}{\sqrt{I_2}} [\frac{\zeta_1 M_{m22}}{M_{m11}}]^{1/4} \end{bmatrix} \tag{6.46}$$

Assume that W_ϕ is an identity matrix. Substituting eqs. (6.43) and (6.44) into eq. (6.19), and the resulting equation as well as eq. (6.10) into eq. (6.9), yields the optimum A.C. as

$$A.C.)_{opt} = \frac{\sqrt{(\varepsilon_{11}\varepsilon_{22} - \varepsilon_{12}^2)}}{2\sqrt{I_1 I_2}(\sqrt{\zeta_1} + \sqrt{M_{m11}M_{m22}})} \tag{6.47}$$

Note that the individual joint drive manipulator can be designed to possess a optimum acceleration capacity, although it can not possess a kinematic isotropic property.

6.4.2 Gear-Coupled Manipulator: One Joint Coupled Case

Figure 6-2 shows a gear-coupled manipulator having three non-zero elements in its structure matrix as given below:

$$A = \begin{bmatrix} g_{11} & g_{12} \\ 0 & g_{22} \end{bmatrix} \tag{6.48}$$

where $g_{11} = r_{2,4}$, $g_{12} = r_{6,5}$, $g_{22} = g_{12}\, r_{7,6'}\, r_{3,7'}$.

In this case, the optimality condition, eq. (6.25), applies, since the matrices M_m and M_r are compatible. Substituting eq. (6.48) in eq. (6.25) and solving the resulting equations for the gear ratios, yields

$$A = \begin{bmatrix} \sqrt{\dfrac{\zeta_1}{I_1 M_{m22}}} & \dfrac{M_{m12}}{\sqrt{I_2 M_{m22}}} \\ 0 & \sqrt{\dfrac{M_{m22}}{I_2}} \end{bmatrix} \tag{6.49}$$

Substituting eqs. (6.10) and (6.26) into (6.9), yields

$$A.C.)_{max} = \frac{1}{4}\sqrt{\frac{\varepsilon_{11}\varepsilon_{22} - \varepsilon_{12}^2}{I_1 I_2 \zeta_1}} \tag{6.50}$$

where ζ_1 is given in eq. (6.45).

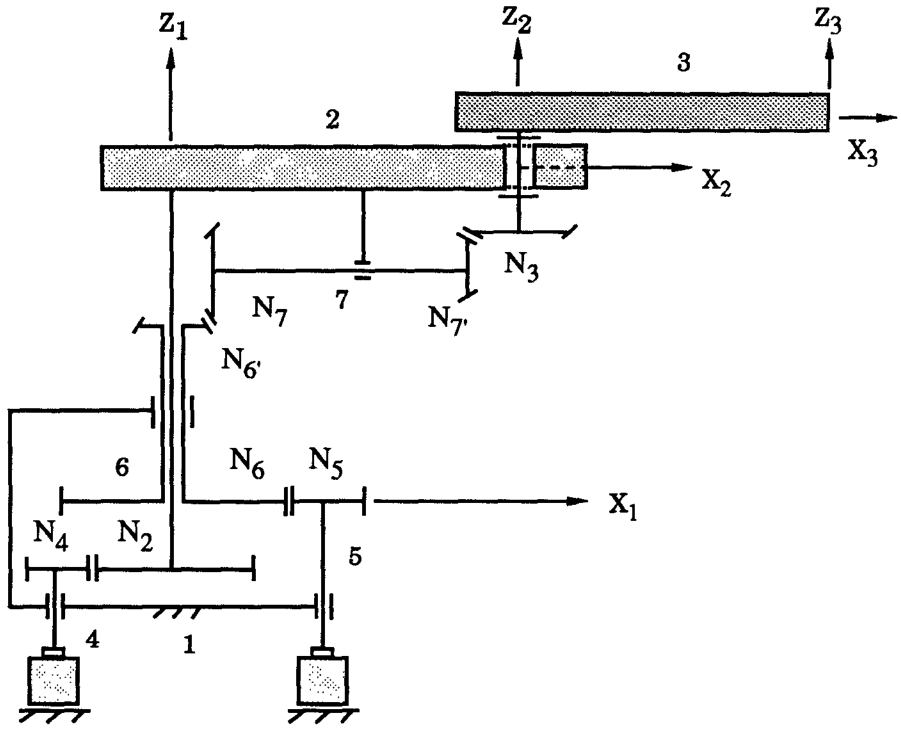

Fig. 6-2: A Two-D.O.F. Planar Gear-Coupled Manipulator.

6.4.3 Gear-Coupled Manipulator: Fully Coupled Case

Figure 6-3 shows another gear-coupled manipulator having four non-zero elements in its structure matrix as shown below:

$$A = \begin{bmatrix} g_{11} & g_{12} \\ g_{21} & g_{22} \end{bmatrix} \tag{6.51}$$

where $g_{11} = r_{5,4}$, $g_{12} = r_{8,7}$, $g_{21} = g_{11}\, r_{6,5'}\, r_{3,6'}$ and $g_{22} = g_{12}\, r_{9,8'}\, r_{3,9'}$.

Again, matrices M_m and M_r are compatible. Substituting eq. (6.51) into eq. (6.25), yields

$$\begin{cases} M_{m11} = I_1 g_{11}^2 + I_2 g_{12}^2 \\ M_{m12} = I_1 g_{11} g_{21} + I_2 g_{12} g_{22} \\ M_{m22} = I_1 g_{21}^2 + I_2 g_{22}^2 \end{cases} \tag{6.52}$$

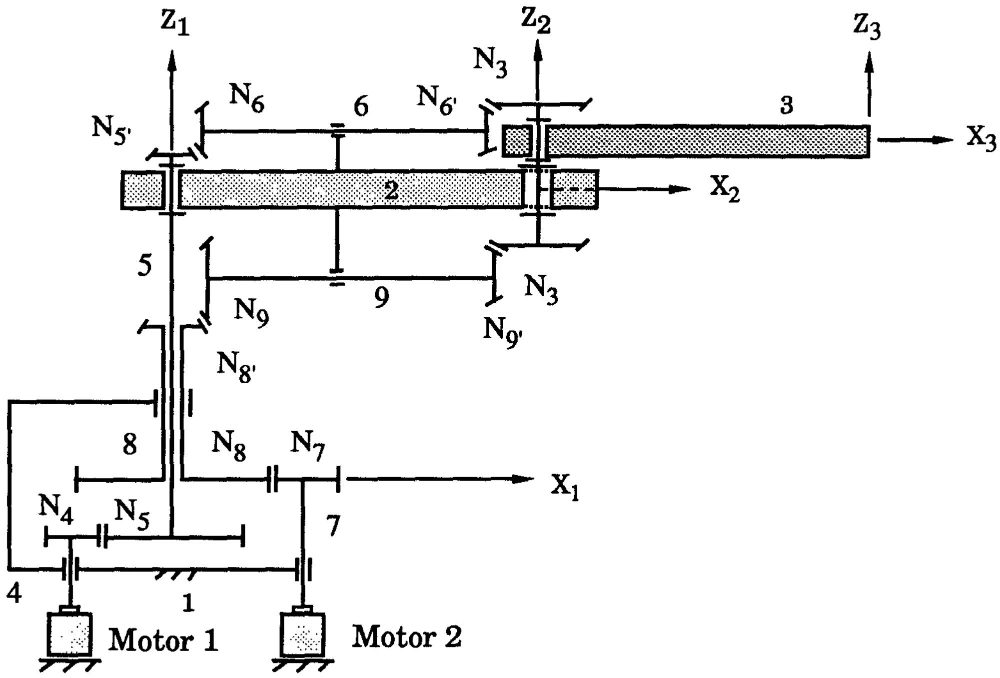

Fig. 6-3: Another Two-D.O.F. Planar Gear-Coupled Manipulator.

Equations (6.52) represents three non-linear equations in four unknown parameters, g_{11}, g_{12}, g_{21}, and g_{22}. Hence, one of the four unknown parameters can be chosen arbitrarily. Once a parameter is chosen, eq. (6.52) can be solved for the remaining unknowns. Alternatively, we can choose the ratio $h = g_{11}/g_{12}$ arbitrarily. Then, the remaining parameters can be solved in terms of h. Two sets of solutions are given as follows:

$$A = \begin{bmatrix} h\sqrt{\dfrac{M_{m11}}{\zeta_2}} & \sqrt{\dfrac{M_{m11}}{\zeta_2}} \\ \dfrac{\sqrt{\zeta_1 I_2} + h M_{m12}\sqrt{I_1}}{\sqrt{\zeta_2 I_1 M_{m11}}} & -\dfrac{h\sqrt{\zeta_1 I_1} - M_{m12}\sqrt{I_2}}{\sqrt{\zeta_2 I_2 M_{m11}}} \end{bmatrix} \tag{6.53}$$

and

$$A = \begin{bmatrix} h\sqrt{\dfrac{M_{m11}}{\zeta_2}} & \sqrt{\dfrac{M_{m11}}{\zeta_2}} \\ -\dfrac{\sqrt{\zeta_1 I_2} - h M_{m12}\sqrt{I_1}}{\sqrt{\zeta_2 I_1 M_{m11}}} & \dfrac{h\sqrt{\zeta_1 I_1} + M_{m12}\sqrt{I_2}}{\sqrt{\zeta_2 I_2 M_{m11}}} \end{bmatrix} \tag{6.54}$$

where ζ_1 is given in eq. (6.45), and

$$\zeta_2 = I_2 + h^2 I_1 \tag{6.55}$$

Note that the value of acceleration capacity will not be affected by the choice of the free parameter and is given exactly as eq. (6.50). Also note that a sign change along any column of the structure matrices as given by eqs. (6.46), (6.49), (6.53) and (6.54) does not change the optimum acceleration capacity.

6.5 Performance Comparison

From eq. (6.36), it can be concluded that if the forms of inertia matrices of the input links and the major links are compatible, then the acceleration capacity can always reach a maximum value through proper choice of gear ratios and its maximum value is independent of the gearing configuration. This has been demonstrated by the above case study. It has also been shown that an individual joint drive manipulator can also be designed to optimize its acceleration capacity although it is only a local optimal.

For the two-D.O.F. planar manipulators shown in Figs. 6-1 to 6-3, it can be shown that the Jacobian matrix is given by eq. (5,28). With the end-effector positioned at $[X_1, Y_1] = [22.86, 0]$ as the design reference point, the inertia matrix contributed by major links, the Jacobian Matrix, and the product of Jacobian matrix can be found in eqs, (5.49), (5.29) and (5.30), respectively. Let the axial moment of inertia of the input links, I_1 and I_2, be equal to $8.8*10^{-2}$ kg-cm^2 and 0.1 kg-cm^2, respectively. The optimal structure matrices for the above three manipulators and their maximum acceleration capacities are shown in Table 6-1. Note that in the fully-coupled case, there are two solution sets of train values for each choice of h ($h = g_{11}/g_{12}$). Also note that the signs in each structure matrix shown in Table 6-1 can be changed along each transmission line.

6.6 Summary

In this chapter, the principle of inertia match has been extended from one degree-of-freedom system to multi-degree-of-freedom systems. Based on the concept of maximum acceleration capacity, a methodology for the determination of gear ratios in geared robotic mechanisms have been developed. It has been shown that at the optimum design, the mass inertia matrix of the input links reflected at the joint-space is equal to that of the major links, and the maximum acceleration capacity is independent of the gearing configuration. Several two degree-of-freedom geared robotic mechanisms have been used as design examples to illustrated the principle. Using this methodology, mechanisms can be designed to yield optimum dynamic performance.

Examples	Structure Matrix (A)	A. C.
1	$\begin{bmatrix} 104.1171 & 0 \\ 0 & -32.6417 \end{bmatrix}$	3.12344
2	$\begin{bmatrix} 103.8970 & 8.9879 \\ 0 & 32.7109 \end{bmatrix}$	3.13062
3	$h=1$ $\begin{bmatrix} 71.3845 & 71.3845 \\ 27.5148 & -20.0944 \end{bmatrix}$	3.13062
	$h=1$ $\begin{bmatrix} 71.3845 & 71.3845 \\ -23.1334 & 24.4758 \end{bmatrix}$	3.13062
	$h=3$ $\begin{bmatrix} 98.3155 & 32.7719 \\ 14.6432 & -29.6868 \end{bmatrix}$	3.13062
	$h=3$ $\begin{bmatrix} 98.3155 & 32.7719 \\ -8.6088 & 31.6983 \end{bmatrix}$	3.13062

Table 6-1: Structure Matrices and Acceleration Capacities of Two-D.O.F. Planar Manipulators.

CHAPTER 7

Illustrative Design Examples

7.1 Introduction

In this chapter, two design examples are given to illustrate the force analysis techniques and the gearing configuration methodologies developed in the previous chapters. The gear ratios of a two-D.O.F. planar manipulator will be selected based on kinematic isotropy and maximum acceleration capacity conditions, while the gearing configuration of a Bendix-type wrist mechanism will be determinated based on maximum acceleration capacity alone. Reaction force analysis for these design examples will also be performed.

7.2 A Two-D.O.F. Planar Manipulator

In this section, a two-D.O.F. planar manipulator, as shown in Fig. 7-1, will be used as an example to mimic a actual size design. The gear ratios will be determined based on the kinematic isotropy and maximum acceleration capacity conditions. Reaction force analysis will be evaluated at a prescribed motion state. The actual and canonical graph representations of the manipulator are shown in Figs. 2-7 and 2-8, respectively. Assuming the end-effector is positioned at [X_1, Y_1] = [0.2286, 0] (m), gear ratios for the second-stage gear reduction can be determined according the kinematic isotropy condition, eqs. (5.22)-(5.24), as illustrated in chapter five. By choosing the gear ratios as close to the isotropic condition as possible as shown in Fig. 7-1, the structure matrix, eq. (5.34), with first-stage gear reduction excluded, can be written as

$$A = \begin{bmatrix} -1 & -0.42168675 \\ 0 & -0.84045525 \end{bmatrix} \tag{7.1}$$

The kinematic condition number (KCN) is equal to 1.004727, slightly larger than one due the the actual gear sizes.

Let the diametral pitch of all gears be 32 and the effective gear width be $3.175 \cdot 10^{-3}$ m. Dimensions and inertia properties of the major links and carried links are given in Tables 7-1 to 7-4 in accordance with the dimensions and material for the parts shown in Fig. 7-1. Table 7-5 shows the inertia properties of the equivalent open-loop chain. Note that link inertias are evaluated with respect to the mass center.

Revolute joint [j, k] between a carried link j and its supporting major link k is assumed to be located at midpoint of the shaft. Position vectors associated with each carried link and major link are shown in Tables 7-6 and 7-7 respectively. Position vectors associated actual and canonic joint locations are shown in Table 7-8. Note that vectors associated with the major links are expressed in their respective link coordinate system and those associated with the carried links are expressed in their input side local coordinate system for input links and in its output side local coordinate system for intermediate carried links. Refer to chapter three for the definitions of the vectors shown in Tables 7-3 to 7-8.

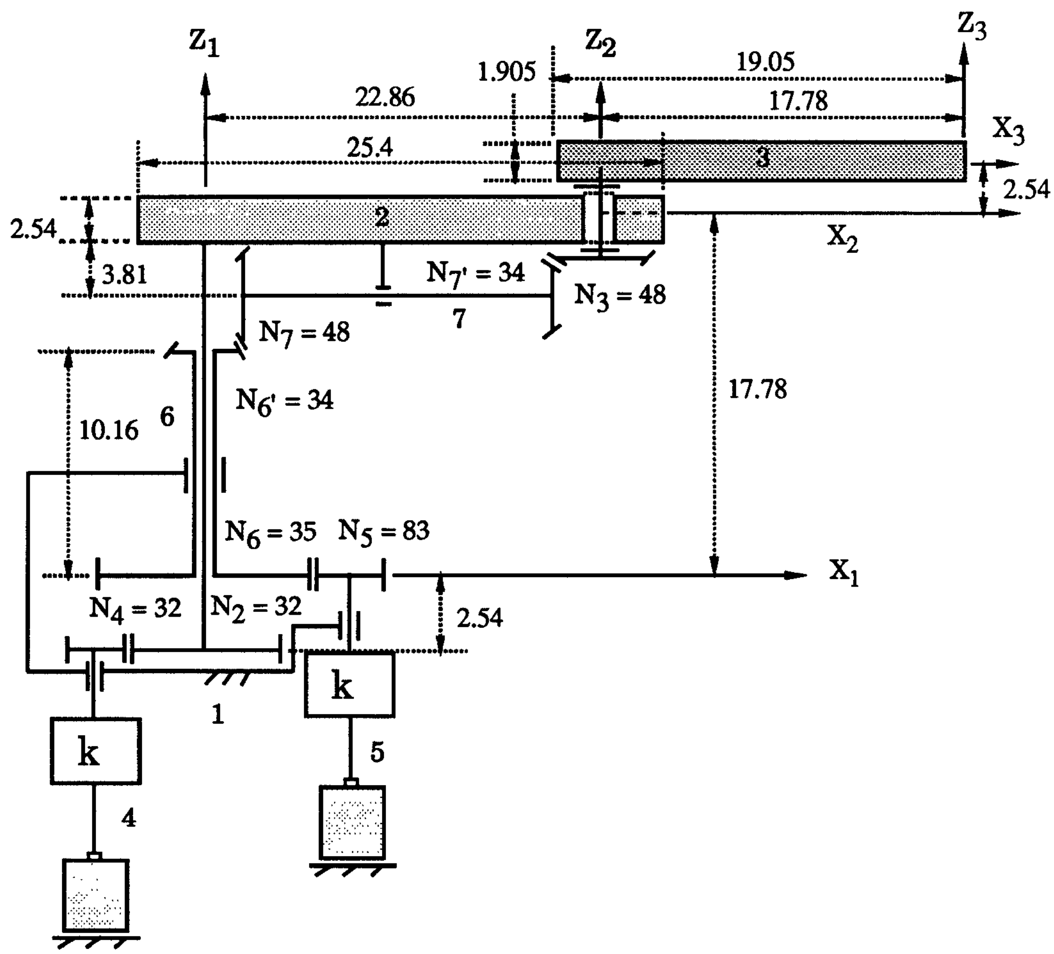

Fig. 7-1 Design Example: A Two-D.O.F. Mechanism.

Link	N	Length (cm)	Hight (cm)	Width (cm)	Shaft Dia. (cm)
2	35	25.4	2.54	5.08	0.9525
3	48	19.05	1.905	3.81	0.9525

Table 7-1 Dimensions of Major Links

Link	N_j	$N_{j'}$	Shaft Dia. (cm)	Shaft Length (cm)
4	NA	32	0.79375	2.54
5	NA	83	0.79375	2.54
6	35	34	inner: 1.349375 outer: 1.11125	10.16
7	48	34	0.79375	18.25625

Table 7-2 Dimensions of Carried Links

Link	Mass(g)	S_i (cm)	I (g-cm^2)
2	2667.73202	$\begin{bmatrix} -11.9071621 \\ 0.0 \\ -0.4659611 \end{bmatrix}$	$\begin{bmatrix} 23661.32699 & 0.0 & 13615.02771 \\ 0.0 & 169544.724107 & 0.0 \\ 13615.02771 & 0.0 & 156899.81418 \end{bmatrix}$
3	1132.72858	$\begin{bmatrix} -9.920451 \\ 0.0 \\ -0.21617 \end{bmatrix}$	$\begin{bmatrix} 2831.63171 & 0.0 & 1924.46467 \\ 0.0 & 37662.46345 & 0.0 \\ 1924.46467 & 0.0 & 37494.20143 \end{bmatrix}$

Table 7-3 Mass Properties of Major Links

Link	Mass (g)	S_i (cm)	I (g-cm^2)
4	22.3521	$\begin{bmatrix} 0.0 \\ 0.0 \\ -0.55702 \end{bmatrix}$	$\begin{bmatrix} 19.593644 & 0.0 & 0.0 \\ 0.0 & 19.593644 & 0.0 \\ 0.0 & 0.0 & 10.891856 \end{bmatrix}$
5	94.22442	$\begin{bmatrix} 0.0 \\ 0.0 \\ -0.13214 \end{bmatrix}$	$\begin{bmatrix} 248.83321 & 0.0 & 0.0 \\ 0.0 & 248.83321 & 0.0 \\ 0.0 & 0.0 & 458.791029 \end{bmatrix}$
6	65.64705	$\begin{bmatrix} 0.0 \\ 0.0 \\ 5.014568 \end{bmatrix}$	$\begin{bmatrix} 1087.06144 & 0.0 & 0.0 \\ 0.0 & 1087.06144 & 0.0 \\ 0.0 & 0.0 & 41.309261 \end{bmatrix}$
7	118.07156	$\begin{bmatrix} 0.0 \\ 0.0 \\ 8.634818 \end{bmatrix}$	$\begin{bmatrix} 6372.3165 & 0.0 & 0.0 \\ 0.0 & 6372.3165 & 0.0 \\ 0.0 & 0.0 & 70.0878 \end{bmatrix}$

Table 7-4 Mass Properties of Carried Links

Link (EOLC)	Mass(g)	S_i (cm)	I (g-cm^2)
2	2785.80385	$\begin{bmatrix} -11.94822 \\ 0.0 \\ -0.63461 \end{bmatrix}$	$\begin{bmatrix} 25521.58111 & 0.0 & 14040.82134 \\ 0.0 & 177813.29497 & 0.0 \\ 14040.82134 & 0.0 & 163378.21871 \end{bmatrix}$
3	1132.72858	$\begin{bmatrix} -9.920451 \\ 0.0 \\ -0.21617 \end{bmatrix}$	$\begin{bmatrix} 2831.63171 & 0.0 & 1924.46467 \\ 0.0 & 37662.46345 & 0.0 \\ 1924.46467 & 0.0 & 37494.20143 \end{bmatrix}$

Table 7-5 Mass Properties of Equivalent Open-Loop Chain

Link j	d_{ja} (cm)	d_{jb} (cm)	$d_{j,k}$ (cm)
4	N/A	${}^{1}d_{4b} = \begin{bmatrix} 1.27 \\ 0.0 \\ 0.55702 \end{bmatrix}$	${}^{1}d_{4,1} = \begin{bmatrix} 0.0 \\ 0.0 \\ -0.71298 \end{bmatrix}$
5	N/A	${}^{1}d_{5b} = \begin{bmatrix} -3.29406 \\ 0.0 \\ 0.31214 \end{bmatrix}$	${}^{1}d_{5,1} = \begin{bmatrix} 0.0 \\ 0.0 \\ -1.13786 \end{bmatrix}$
6	${}^{1}d_{6a} = \begin{bmatrix} 1.38906 \\ 0.0 \\ -5.01457 \end{bmatrix}$	${}^{1}d_{6b} = \begin{bmatrix} 0.94123 \\ -0.96690 \\ 5.14543 \end{bmatrix}$	${}^{1}d_{6,1} = \begin{bmatrix} 0.0 \\ 0.0 \\ 0.06543 \end{bmatrix}$
7	${}^{2}d_{7a} = \begin{bmatrix} -8.63482 \\ 0.0 \\ -1.905 \end{bmatrix}$	${}^{2}d_{7b} = \begin{bmatrix} 10.97081 \\ 0.0 \\ 1.34938 \end{bmatrix}$	${}^{2}d_{7,2} = \begin{bmatrix} 1.168 \\ 0.0 \\ 0.0 \end{bmatrix}$

Table 7-6 Position Vectors Associated with Carried Links

Link	2	3
$d_{k,k+1}$ (cm)	${}^{2}d_{2,3} = \begin{bmatrix} 11.90716 \\ 0.0 \\ 0.46596 \end{bmatrix}$	NA
$d_{k,k-1}$ (cm)	NA	${}^{3}d_{3,2} = \begin{bmatrix} -7.85955 \\ 0.0 \\ 2.32383 \end{bmatrix}$
$d_{k,i}$ (cm)	${}^{2}d_{2,7} = \begin{bmatrix} 0.19935 \\ 0.0 \\ -3.97904 \end{bmatrix}$	NA
$d_{k,j}$ (cm)	${}^{2}d_{2,4} = \begin{bmatrix} -11.83870 \\ -0.91002 \\ -18.58404 \end{bmatrix}$	${}^{2}d_{3,7} = \begin{bmatrix} -7.11872 \\ 1.75505 \\ -5.41946 \end{bmatrix}$

Table 7-7 Position Vectors Associated with Major Links

Canonic	Actual
$^{2}d_{2,1}=\begin{bmatrix}-10.95284\\0.0\\-10.96404\end{bmatrix}$	$^{2}d_{2,6}=\begin{bmatrix}-10.95284\\0.0\\-10.96404\end{bmatrix}$
	$^{1}d_{6,2}=\begin{bmatrix}0.0\\0.0\\0.06543\end{bmatrix}$

Table 7-8 Position Vectors Associated Canonic and Actual Joint.

Substituting all the inertia properties, link dimensions, and gear ratios into eq. (2.59) to (2.67), the dynamic equation can be written as

$$(M_m + M_r)\,[\ddot{\Theta}] + C_m(\Theta,\dot{\Theta}) = \begin{bmatrix} -\tau_1 - 0.42168675\ \tau_2 \\ -0.84045525\ \tau_2 \end{bmatrix} \tag{7.2}$$

where

$$M_m = \begin{bmatrix} 1036191.4453745 & 28320.370237 \\ 28320.370237 & 107465.694 \end{bmatrix} \tag{7.3}$$

$$C_m = \begin{bmatrix} -187496.673\ \dot{\theta}_2^2 - 374993.347\ \dot{\theta}_1\dot{\theta}_2 \\ 187496.673\ \dot{\theta}_1^2 \end{bmatrix} \tag{7.4}$$

and where τ_1 and τ_2 are the torques seen at the axes of gear 4 and 5, respectively, i.e. they are the actuator torques multiplies by the first-stage gear reduction, k.

Assuming the motor-rotor inertias, I_4 and I_5 are both equal to 87.9 g-cm^2, then eqs. (5.38-41) yield

$$M_r = k^2 \begin{bmatrix} 103.53035 & 31.15254 \\ 31.15254 & 62.08949 \end{bmatrix} \tag{7.5}$$

From eq. (5.46b), the optimal condition for maximum acceleration capacity is to make the determinant of M_m and M_r equal to each other. Taking determinant of eqs. (7.3) and (7.5) and equating them yields

$$5457.66577\ k^4 = 1.1055 \cdot 10^{11} \tag{7.6}$$

Solving eq. (7.6), yields the first-stage gear reduction, k= 67.0872.

Let the joint velocity and joint acceleration vectors be $[\dot{\theta}_1, \dot{\theta}_2] = [\ 0.5,\ 0.5\ ]$ (rad/sec) and $[\ddot{\theta}_1, \ddot{\theta}_2] = [\ 8.0, -8.0\ ]$ (rad/sec^2), respectively. Then, the associated end-effector velocity and acceleration vectors are as follows

$$\dot{X} = \begin{bmatrix} -8.19022 \\ 14.88722 \end{bmatrix} \quad (10^{-2}\ \text{m/sec}) \tag{7.7}$$

$$\ddot{X} = \begin{bmatrix} 120.1427 \\ 115.2791 \end{bmatrix} \quad (10^{-2}\ \text{m/sec}^2) \tag{7.8}$$

The required input torque τ_1 and τ_2 with the prescribed motion can be evaluated from eq. (7.2) as

$$\begin{bmatrix} \tau_1 \\ \tau_2 \end{bmatrix} = \begin{bmatrix} -11382042.90427 \\ 2026584.23719 \end{bmatrix} \quad (10^{-7}\ \text{N}-\text{m}) \tag{7.9}$$

and the input actuator torques are

$$\begin{bmatrix} \xi_1 \\ \xi_2 \end{bmatrix} = \begin{bmatrix} -169660.4256 \\ 30208.21017 \end{bmatrix} \quad (10^{-7}\ \text{N}-\text{m}) \tag{7.10}$$

Using the inertia properties and from eqs. (3.10-11) and (3.15-16), the inertial forces of all links can first be evaluated for the assumed motion state. Then, the force evaluation process can be performed. The reaction forces associated with the carried and major links are given in Tables 7-9 and 7-10, respectively. Actual reaction forces in journal bearings are given in Table 7-11.

Link	$\gamma_{i,j}$ (10^{-5} N)	$f_{i,j}$ (10^{-5} N)	$t_{i,j}$ (10^{-7} N-m)
4	${}^1\gamma_{2,4} = \begin{bmatrix} 2354935.81258 \\ -6470132.96933 \\ 0.0 \end{bmatrix}$	${}^1f_{4,1} = \begin{bmatrix} 2354935.81258 \\ -6470132.96933 \\ 0.0 \end{bmatrix}$	${}^1t_{4,1} = \begin{bmatrix} 8217068.87105 \\ 2990768.48197 \\ -11382042.90427 \end{bmatrix}$
5	${}^1\gamma_{6,5} = \begin{bmatrix} -77310.96894 \\ -212410.14143 \\ 0.0 \end{bmatrix}$	${}^1f_{5,1} = \begin{bmatrix} -77310.96894 \\ -212410.14143 \\ 0.0 \end{bmatrix}$	${}^1t_{5,1} = \begin{bmatrix} 269760.87961 \\ -98184.93055 \\ 2026584.23719 \end{bmatrix}$
6	${}^1\gamma_{7,6} = \begin{bmatrix} 64870.92554 \\ -218414.28440 \\ 45950.23892 \end{bmatrix}$	${}^1f_{6,1} = \begin{bmatrix} -33945.34879 \\ 13575.86778 \\ 45950.23892 \end{bmatrix}$	${}^1t_{6,1} = \begin{bmatrix} 2044692.29427 \\ -1001171.59223 \\ 0.0 \end{bmatrix}$
7	${}^2\gamma_{3,7} = \begin{bmatrix} 64747.51030 \\ 307762.95098 \\ 91408.24984 \end{bmatrix}$	${}^2f_{7,2} = \begin{bmatrix} -418.12755 \\ 535608.02930 \\ 45458.01091 \end{bmatrix}$	${}^2t_{7,2} = \begin{bmatrix} 0.0 \\ -1135526.98886 \\ 0.0 \end{bmatrix}$

Table 7-9 Reaction Forces Associated with Carried Links.

Link	2	3
$f_{i,j}$ (10^{-5} N)	${}^1f_{2,1} = \begin{bmatrix} -6354326.66705 \\ 3486227.44433 \\ -45950.23892 \end{bmatrix}$	${}^1f_{3,2} = \begin{bmatrix} -73895.69261 \\ 104740.80009 \\ -91408.24984 \end{bmatrix}$
$t_{i,j}$ (10^{-7} N- m)	${}^1t_{2,1} = \begin{bmatrix} 15163363.88646 \\ 47456371.01706 \\ 5.35510\ E-09 \end{bmatrix}$	${}^1t_{3,2} = \begin{bmatrix} 568080.70421 \\ 1298080.46678 \\ 4.65661\ E-10 \end{bmatrix}$

Table 7-10 Reaction Forces Associated with Major Links.

Link	6	
$f_{i,j}$ (10^{-5} N)	${}^{1}f_{6,1} = \begin{bmatrix} 1900320.82740 \\ -6971398.25850 \\ 91900.47784 \end{bmatrix}$	${}^{1}f_{6,2} = \begin{bmatrix} -6354326.66705 \\ 3486227.44433 \\ -45950.23892 \end{bmatrix}$
$t_{i,j}$ (10^{-7} N- m)	${}^{1}t_{6,1} = \begin{bmatrix} -42537309.55333 \\ -23238074.83262 \\ -1.5578\,E-08 \end{bmatrix}$	${}^{1}t_{6,2} = \begin{bmatrix} 15163363.88646 \\ 47456371.01706 \\ 5.35510\,E-09 \end{bmatrix}$

Table 7-11 Actual Reaction Forces.

7.3 A Bendix-Type Wrist Mechanism

In this section, gear ratios for the Bendix-type wrist mechanism as shown schematically in Fig. 3-1, will be determined to optimize the maximum acceleration capacity. Reaction forces will also be analyzed at for given motion state. The structure matrix A for this type of mechanism can be represented as

$$A = \begin{bmatrix} g_{11} & g_{12} & g_{13} \\ 0 & g_{22} & g_{23} \\ 0 & g_{32} & g_{33} \end{bmatrix} \qquad (7.11)$$

where $g_{11} = r_{2,5}$, $g_{12} = r_{7,6}$, $g_{13} = r_{10,9}$, $g_{22} = g_{12}\, r_{8,7'}$, $g_{23} = g_{13}\, r_{11,10'}$, $g_{32} = g_{22}\, r_{4,8'}$, and $g_{33} = g_{23}\, r_{4,11'}$.

Assuming major links 3 and 4 are symmetric with respect to Z_3 and Z_4 axes, respectively, then from eq. (2.24), inertia matrix of the equivalent open-loop chain, M_m, can be written in the following form

$$M_m = \begin{bmatrix} M_{m11} & 0 & M_{m13} \\ 0 & M_{m22} & 0 \\ M_{m13} & 0 & M_{m33} \end{bmatrix} \tag{7.12}$$

where M_{mij} is a function of link mass properties and the end-effector position or joint angles.

The contribution of the input links to the inertia matrix, M_r, from eq. (6.4), can be written as

$$M_r = I_m \begin{bmatrix} M_{r11} & M_{r12} & M_{r13} \\ M_{r12} & M_{r22} & M_{r23} \\ M_{r13} & M_{r23} & M_{r33} \end{bmatrix} \tag{7.13}$$

where

$$M_{r11} = g_{11}^2 + g_{12}^2 + g_{13}^2 \tag{7.14a}$$

$$M_{r12} = g_{12}^2 r_{8,7'} + g_{13}^2 r_{11,10'} \tag{7.14b}$$

$$M_{r13} = g_{12}^2 r_{8,7'} r_{4,8'} + g_{13}^2 r_{11,10'} r_{4,11'} \tag{7.14c}$$

$$M_{r22} = g_{12}^2 r_{8,7'}^2 + g_{13}^2 r_{11,10'}^2 \tag{7.14d}$$

$$M_{r23} = g_{12}^2 r_{8,7'}^2 r_{4,8'} + g_{13}^2 r_{11,10'}^2 r_{4,11'} \tag{7.14e}$$

$$M_{r33} = g_{12}^2 r_{8,7'}^2 r_{4,8'}^2 + g_{13}^2 r_{11,10'}^2 r_{4,11'}^2 \tag{7.14f}$$

and where I_m is defined in eq. (6.5).

From eq. (6.36), at the maximum acceleration capacity, $M_m = M_r$. Thus, by equating eqs. (7.12) and (7.13), we obtain six scalar equations in seven unknowns, from which we can solve six variables in terms of the seventh, e.g.

$$|g_{11}| = \sqrt{\frac{M_{m11} M_{m33} - M_{m22}^2}{I_m M_{m33}}} \tag{7.15a}$$

$$|g_{12}| = \frac{M_{m13}}{\sqrt{I_m (M_{m33} + r_{4,11'}^2 M_{m22})}} \tag{7.15b}$$

$$|g_{13}| = \frac{r_{4,11'} M_{m13} M_{m22}}{\sqrt{I_m M_{m22} M_{m33} (M_{m33} + r_{4,11'}^2 M_{m22})}} \tag{7.15c}$$

$$r_{8,7'} = -\frac{M_{m22}}{r_{4,11'} M_{m13}} \tag{7.15d}$$

$$r_{11,10'} = \frac{M_{m33}}{r_{4,11'} M_{m13}} \tag{7.15e}$$

$$r_{4,8'} = -\frac{M_{m33}}{r_{4,11'} M_{m22}} \tag{7.15f}$$

Since M_{m22} and M_{m33} are always positive number and, from eq. (2.24), $M_{m13} = M_{m33} C_2$ is also a positive number within the range of $-\pi/2 < q_2 < \pi/2$, the following sign relations can be derived from eqs. (7.15d-f):

$$\mathrm{sign}(r_{8,7'}) = -\,\mathrm{sign}(r_{11,10'}) \tag{7.16}$$

$$\mathrm{sign}(r_{4,8'}) = -\,\mathrm{sign}(r_{4,11'}) \tag{7.17}$$

$$\mathrm{sign}(r_{8,7'}) = \mathrm{sign}(r_{4,8'}) \tag{7.18}$$

$$\mathrm{sign}(r_{11,10'}) = \mathrm{sign}(r_{4,11'}) \tag{7.19}$$

Hence, eqs. (7.16) and (7.17) relate the gearing configuration arrangement between two transmissions and eqs. (7.18) and (7.19) specify that within the same transmission line.

Inertia properties of the major links are given in Table 7-12. The inertia property of link 4 includes an object of 1204.6608 (g) attached to the end-effector. As an approximation, it is assumed that the contribution of major links to the inertia matrix, M'_m, dominates that of the equivalent open-loop chain, M_m. The dimension of major links are shown in Fig. 7-2, where the effective gear width is assumed to be 0.47625 cm and the diametral pitch is assumed to be 32 for all gears. Assuming the pitch diameters for the gears attached to major links 2 and 4 are 4.7625 cm and 4.365625 cm, respectively, the inertia matrix, M'_m can be written as

$$M_{m'} = \begin{bmatrix} 55512.1116 S_2^2 + 33926.1858 & 0 & 15766.10279 C_2 \\ 0 & 75252.99493 & 0 \\ 15766.10279 C_2 & 0 & 15766.10279 \end{bmatrix} \quad (7.20)$$

Link	Mass(g)	S_i (cm)	I (g-cm^2)
2	873.52556	$\begin{bmatrix} 0.0 \\ -3.81986 \\ 0.0 \end{bmatrix}$	$\begin{bmatrix} 12518.22101 & 0.0 & 0.0 \\ 0.0 & 12494.76862 & 0.0 \\ 0.0 & 0.0 & 6776.21136 \end{bmatrix}$
3	562.94922	$\begin{bmatrix} 0.0 \\ 0.0 \\ 3.30489 \end{bmatrix}$	$\begin{bmatrix} 5443.9765 & 0 & 0 \\ 0 & 3753.4426 & 0 \\ 0 & 0 & 5665.31436 \end{bmatrix}$
4	1437.905	$\begin{bmatrix} 0.0 \\ 0.0 \\ -0.1546 \end{bmatrix}$	$\begin{bmatrix} 17664.73613 & 0 & 0 \\ 0 & 17664.73613 & 0 \\ 0 & 0 & 15766.10279 \end{bmatrix}$

Table 7-12 Estimated mass Properties of Major Links.

Let $r_{4,8'} = - r_{4,11'}$, $I_m = 87.9$ g-cm^2, and the end-effector be positioned

positioned at [q_1, q_2, q_3] = [0.0, 15, 0.0] (degrees), the values of M_{mij}, in eq. (7-20) can be found. Solving eqs. (7.15a-f), yields $g_{11} = \pm$ 16.153, $g_{12} = \pm$ 9.14738, $g_{13} = \pm$ 9.14738, n_{21} = 2.26181, n_{22} = - 2.26181, n_{31} = 0.45772, and n_{32} = - 0.45772. Hence, The structure matrix can be written as

$$A = \begin{bmatrix} 16.15300 & 9.14738 & 9.14738 \\ 0.0 & -20.68962 & 20.68962 \\ 0.0 & 9.47006 & 9.47006 \end{bmatrix} \tag{7.21}$$

Figure 7-2 shows the design of a three-D.O.F. bendix-type wrist mechanism by selecting the gear ratios as close to the optimal values as possible. The resulting structure matrix is

$$A = \begin{bmatrix} 16.14706 & 9.15 & 9.15 \\ 0.0 & -20.71698 & 20.69643 \\ 0.0 & 9.48488 & 9.47547 \end{bmatrix} \tag{7.22}$$

Note that tooth number for the gears attached to major links 2 and 4 are 61 and 38, respectively. Also note that the gear ratios optimization are based on M_m' instead of M_m. Hence, an iterative procedure is recommended to fine tune the gear ratios. However, for the purpose of illustration, these gear ratios are used for the following force analysis. Figures 7-3 and 7-4 show the actual and canonic graph representations of the wrist mechanism. Dimensions of the carried links are shown in Tables 7-13. Inertia properties of the major links, carried links and equivalent open-loop chain are shown in Tables 7-14, 7-15 and 7-16, respectively. Position vectors associated with the major links and carried links are shown in Tables 7-17 and 7-18, respectively. Position vectors associated actual and canonic joints are shown in Table 7-19.

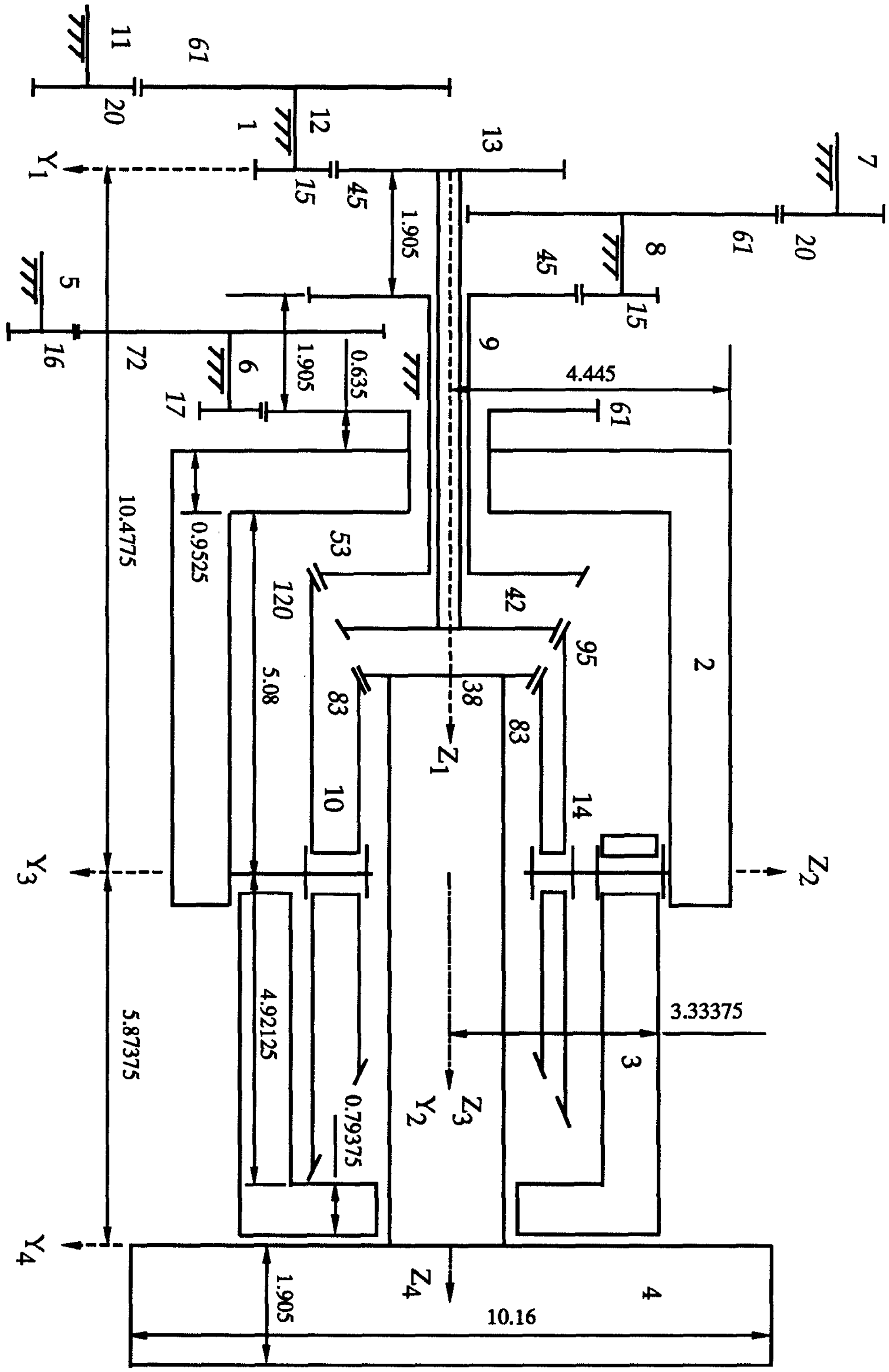

Fig. 7-2 Design Example: A Three-D.O.F. Mechanism.

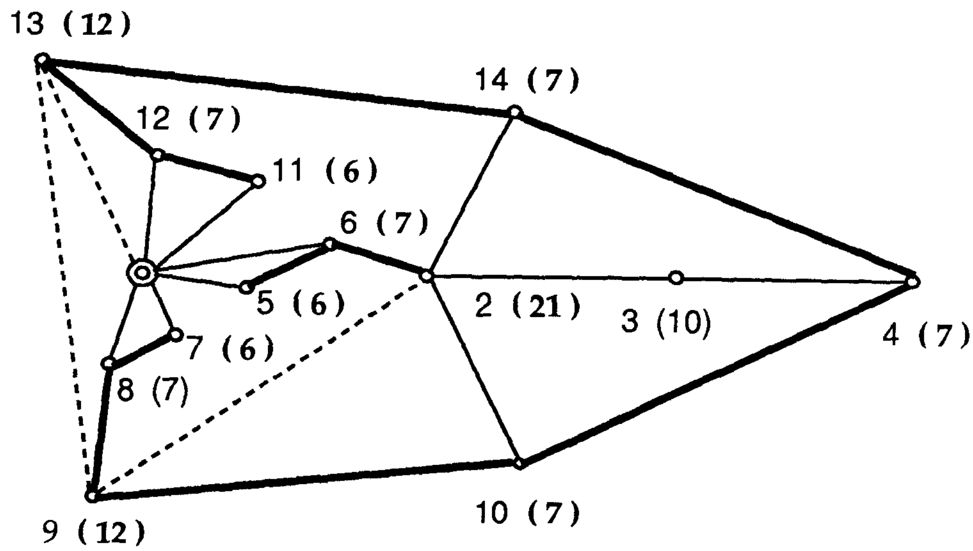

Fig. 7-3 Actual graph of the Three-D.O.F. Mechanism.

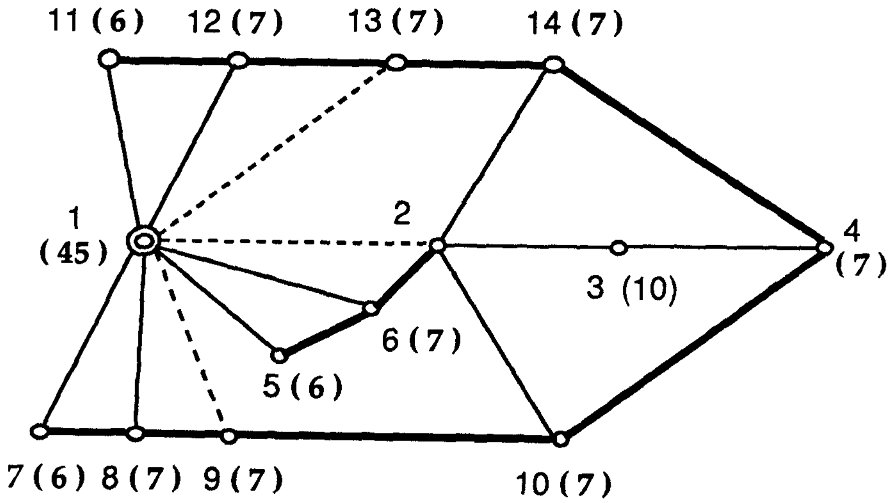

Fig. 7-4 Canonic graph of the Three-D.O.F. Mechanism.

Link	N_j	$N_{j'}$	Shaft Dia. (cm)	Shaft Length (cm)
5	NA	16	0.635	1.27
6	72	17	0.635	1.27
7	NA	20	0.635	1.27
8	61	15	0.635	1.27
9	45	53	0.79735	3.81
10	120	83	0.79735	0.5953125
11	NA	20	0.635	1.27
12	61	15	0.635	1.27
13	45	42	1.11125	6.7071875
14	95	83	0.79735	0.4365625

Table 7-13 Dimensions of Carried Links.

Link	Mass(g)	S_i (cm)	I (g-cm^2)
2	875.74934	$\begin{bmatrix} 0.0 \\ -3.82709 \\ 0.0 \end{bmatrix}$	$\begin{bmatrix} 12542.62314 & 0.0 & 0.0 \\ 0.0 & 12507.59246 & 0.0 \\ 0.0 & 0.0 & 6800.61350 \end{bmatrix}$
3	562.94922	$\begin{bmatrix} 0.0 \\ 0.0 \\ 3.30489 \end{bmatrix}$	$\begin{bmatrix} 5443.9765 & 0 & 0 \\ 0 & 3753.4426 & 0 \\ 0 & 0 & 5665.31436 \end{bmatrix}$
4	1435.01983	$\begin{bmatrix} 0.0 \\ 0.0 \\ -0.02103 \end{bmatrix}$	$\begin{bmatrix} 15865.09904 & 0 & 0 \\ 0 & 15865.09904 & 0 \\ 0 & 0 & 15666.62125 \end{bmatrix}$

Table 7-14 Mass Properties of Major Links.

Link	Mass (g)	s_i (cm)	I (g-cm ^{2})
5	7.84284	$\begin{bmatrix} 0.0 \\ 0.0 \\ -0.254 \end{bmatrix}$	$\begin{bmatrix} 1.65501 & 0.0 & 0.0 \\ 0.0 & 1.65501 & 0.0 \\ 0.0 & 0.0 & 88.84873 \end{bmatrix}$
6	103.7400	$\begin{bmatrix} 0.0 \\ 0.0 \\ 0.08424 \end{bmatrix}$	$\begin{bmatrix} 204.64240 & 0.0 & 0.0 \\ 0.0 & 204.64240 & 0.0 \\ 0.0 & 0.0 & 390.24736 \end{bmatrix}$
7	10.48980	$\begin{bmatrix} 0.0 \\ 0.0 \\ -0.18991 \end{bmatrix}$	$\begin{bmatrix} 2.46644 & 0.0 & 0.0 \\ 0.0 & 2.46644 & 0.0 \\ 0.0 & 0.0 & 90.21623 \end{bmatrix}$
8	75.67119	$\begin{bmatrix} 0.0 \\ 0.0 \\ 0.09574 \end{bmatrix}$	$\begin{bmatrix} 108.24960 & 0.0 & 0.0 \\ 0.0 & 108.24960 & 0.0 \\ 0.0 & 0.0 & 201.17167 \end{bmatrix}$
9	103.5623	$\begin{bmatrix} 0.0 \\ 0.0 \\ 2.17009 \end{bmatrix}$	$\begin{bmatrix} 419.76958 & 0.0 & 0.0 \\ 0.0 & 419.76958 & 0.0 \\ 0.0 & 0.0 & 173.58875 \end{bmatrix}$
10	393.62498	$\begin{bmatrix} 0.0 \\ 0.0 \\ 0.19325 \end{bmatrix}$	$\begin{bmatrix} 1847.88021 & 0.0 & 0.0 \\ 0.0 & 1847.88021 & 0.0 \\ 0.0 & 0.0 & 3688.86692 \end{bmatrix}$
11	10.48980	$\begin{bmatrix} 0.0 \\ 0.0 \\ -0.18991 \end{bmatrix}$	$\begin{bmatrix} 2.46644 & 0.0 & 0.0 \\ 0.0 & 2.46644 & 0.0 \\ 0.0 & 0.0 & 90.21623 \end{bmatrix}$
12	75.67119	$\begin{bmatrix} 0.0 \\ 0.0 \\ 0.095738 \end{bmatrix}$	$\begin{bmatrix} 108.24960 & 0.0 & 0.0 \\ 0.0 & 108.24960 & 0.0 \\ 0.0 & 0.0 & 201.17162 \end{bmatrix}$
13	95.53564	$\begin{bmatrix} 0.0 \\ 0.0 \\ 3.18518 \end{bmatrix}$	$\begin{bmatrix} 929.84760 & 0.0 & 0.0 \\ 0.0 & 929.84760 & 0.0 \\ 0.0 & 0.0 & 104.40887 \end{bmatrix}$
14	291.91310	$\begin{bmatrix} 0.0 \\ 0.0 \\ -0.06870 \end{bmatrix}$	$\begin{bmatrix} 934.88099 & 0.0 & 0.0 \\ 0.0 & 934.88099 & 0.0 \\ 0.0 & 0.0 & 1866.14504 \end{bmatrix}$

Table 7-15 Mass Properties of Carried Links.

Link (EOLC)	Mass (g)	S_i (cm)	I (g-cm^2)
2	1561.2878	$\begin{bmatrix} 0.0 \\ -2.1447 \\ -0.1828 \end{bmatrix}$	$\begin{bmatrix} 23114.1302 & 0.0 & 0.0 \\ 0.0 & 17447.0527 & -612.5914 \\ 0.0 & -612.5914 & 17987.6723 \end{bmatrix}$
3	562.94922	$\begin{bmatrix} 0.0 \\ 0.0 \\ 3.3049 \end{bmatrix}$	$\begin{bmatrix} 5443.9765 & 0.0 & 0.0 \\ 0.0 & 3753.4426 & 0.0 \\ 0.0 & 0.0 & 5665.3144 \end{bmatrix}$
4	1435.01983	$\begin{bmatrix} 0.0 \\ 0.0 \\ -0.0210 \end{bmatrix}$	$\begin{bmatrix} 15865.0990 & 0.0 & 0.0 \\ 0.0 & 15865.0990 & 0.0 \\ 0.0 & 0.0 & 15666.6213 \end{bmatrix}$

Table 7-16 Mass Properties of Equivalent Open-Loop Chain.

Link	2	3	4
$d_{k,k+1}$ (cm)	${}^2d_{2,3} = \begin{bmatrix} 0.0 \\ 3.82709 \\ 2.936875 \end{bmatrix}$	${}^3d_{3,4} = \begin{bmatrix} 0.0 \\ 0.0 \\ 2.01324 \end{bmatrix}$	NA
$d_{k,k-1}$ (cm)	${}^2d_{2,1} = \begin{bmatrix} 0.0 \\ -1.72916 \\ 0.0 \end{bmatrix}$	${}^3d_{3,2} = \begin{bmatrix} 0.0 \\ -2.936875 \\ -3.30489 \end{bmatrix}$	${}^4d_{4,3} = \begin{bmatrix} 0.0 \\ 0.0 \\ -0.53460 \end{bmatrix}$
$d_{k,i}$ (cm)	${}^2d_{2,6} = \begin{bmatrix} 0.0 \\ -2.84041 \\ -2.42094 \end{bmatrix}$	NA	${}^4d_{4,10} = \begin{bmatrix} 0.0 \\ 1.508125 \\ -9.14678 \end{bmatrix}$ ${}^4d_{4,14} = \begin{bmatrix} 0.0 \\ -1.508125 \\ -9.14678 \end{bmatrix}$
$d_{k,j}$ (cm)	${}^2d_{2,10} = \begin{bmatrix} 0.0 \\ 3.82709 \\ -1.80578 \end{bmatrix}$ ${}^2d_{2,14} = \begin{bmatrix} 0.0 \\ 3.82709 \\ 1.5875 \end{bmatrix}$	NA	NA

Table 7-17 Position Vectors Associated with Major Links.

Link j	${}^{k}d_{ja}$ (cm)	${}^{k}d_{jb}$ (cm)	${}^{k}d_{j,k}$ (cm)
5	N/A	$\begin{bmatrix} 0.0 \\ -0.635 \\ 0.254 \end{bmatrix}$	$\begin{bmatrix} 0.0 \\ 0.0 \\ -0.381 \end{bmatrix}$
6	$\begin{bmatrix} 0.0 \\ 2.8587 \\ -0.08424 \end{bmatrix}$	$\begin{bmatrix} 0.0 \\ -0.67469 \\ 1.18576 \end{bmatrix}$	$\begin{bmatrix} 0.0 \\ 0.0 \\ 0.55076 \end{bmatrix}$
7	N/A	$\begin{bmatrix} 0.0 \\ 0.79375 \\ 0.18991 \end{bmatrix}$	$\begin{bmatrix} 0.0 \\ 0.0 \\ -0.44509 \end{bmatrix}$
8	$\begin{bmatrix} 0.0 \\ -2.42094 \\ -0.09574 \end{bmatrix}$	$\begin{bmatrix} 0.0 \\ 0.59531 \\ 1.17426 \end{bmatrix}$	$\begin{bmatrix} 0.0 \\ 0.0 \\ 0.53926 \end{bmatrix}$
9	$\begin{bmatrix} 0.0 \\ -1.78594 \\ -2.17009 \end{bmatrix}$	$\begin{bmatrix} 0.0 \\ 2.10344 \\ 1.6400 \end{bmatrix}$	$\begin{bmatrix} 0.0 \\ 0.0 \\ -0.26510 \end{bmatrix}$
10*	$\begin{bmatrix} 0.0 \\ -4.7625 \\ -0.19325 \end{bmatrix}$	$\begin{bmatrix} 0.85257 \\ -3.18182 \\ 0.40206 \end{bmatrix}$	$\begin{bmatrix} 0.0 \\ 0.0 \\ 0.10440 \end{bmatrix}$
11	N/A	$\begin{bmatrix} 0.0 \\ -0.79375 \\ 0.18991 \end{bmatrix}$	$\begin{bmatrix} 0.0 \\ 0.0 \\ -0.44509 \end{bmatrix}$
12	$\begin{bmatrix} 0.0 \\ 2.42094 \\ -0.09574 \end{bmatrix}$	$\begin{bmatrix} 0.0 \\ -0.59531 \\ 1.17426 \end{bmatrix}$	$\begin{bmatrix} 0.0 \\ 0.0 \\ 0.53926 \end{bmatrix}$
13	$\begin{bmatrix} 0.0 \\ 1.78594 \\ -3.18518 \end{bmatrix}$	$\begin{bmatrix} 0.0 \\ -1.66688 \\ 3.52200 \end{bmatrix}$	$\begin{bmatrix} 0.0 \\ 0.0 \\ 0.16841 \end{bmatrix}$
14*	$\begin{bmatrix} 0.0 \\ -3.77031 \\ 0.06870 \end{bmatrix}$	$\begin{bmatrix} 0.85257 \\ -3.18182 \\ -0.09005 \end{bmatrix}$	$\begin{bmatrix} 0.0 \\ 0.0 \\ -0.01068 \end{bmatrix}$

* k=2 , otherwise k=1

Table 7-18 Position Vectors Associated with Carried Links.

Canonic	Actual
$^{2}d_{2,1} = \begin{bmatrix} 0.0 \\ -1.72916 \\ 0.0 \end{bmatrix}$	$^{2}d_{2,9} = \begin{bmatrix} 0.0 \\ -1.72916 \\ 0.0 \end{bmatrix}$
	$^{1}d_{9,2} = \begin{bmatrix} 0.0 \\ 0.0 \\ 0.84616 \end{bmatrix}$
	$^{1}d_{9,13} = \begin{bmatrix} 0.0 \\ 0.0 \\ -0.26509 \end{bmatrix}$
	$^{1}d_{13,9} = \begin{bmatrix} 0.0 \\ 0.0 \\ 0.62482 \end{bmatrix}$

Table 7-19 Position Vectors Associated Canonic and Actual Joint.

The dynamic equation, at the reference end-effector position, can be written as

$$(M_m + M_c)\left[\ddot{\Theta}\right] + C_m(\Theta,\dot{\Theta}) = \begin{bmatrix} 16.15385\,\xi_1 + 9.15\,\xi_2 + 9.15\,\xi_3 \\ -20.71698\,\xi_2 + 20.69643\,\xi_3 \\ 9.48488\,\xi_2 + 9.47547\,\xi_3 \end{bmatrix} \tag{7.23}$$

where ξ_1, ξ_2, and ξ_3 are the input torques as seen at links 5, 6 and 9 respectively, and

$$M_m = \begin{bmatrix} 42534.30528 & 0 & 15132.79407 \\ 0 & 74922.90126 & 0 \\ 15132.79407 & 0 & 15666.62125 \end{bmatrix} (10^{-7}\ \mathrm{kg-m^2}) \tag{7.24}$$

$$M_c = \begin{bmatrix} 47195.25524 & -177.90073 & 19691.18811 \\ -177.90073 & 102887.36158 & -1040.93445 \\ 19691.18811 & -1040.93445 & 21566.17072 \end{bmatrix} (10^{-7}\ \mathrm{kg-m^2}) \tag{7.25}$$

$$C_m = \begin{bmatrix} -4054.81963\ \dot{\theta}_2\dot{\theta}_3 + 106795.6475\ \dot{\theta}_1\dot{\theta}_2 \\ 4054.81963\ \dot{\theta}_1\dot{\theta}_3 - 13820.375\ \dot{\theta}_1^2 \\ -4054.81963\ \dot{\theta}_1\dot{\theta}_2 \end{bmatrix} (10^{-7}\ \mathrm{kg-m^2}) \tag{7.26}$$

Let the joint velocity and joint acceleration vectors be $[\dot{\theta}_1, \dot{\theta}_2, \dot{\theta}_3]$ = [1, 2, 5] (rad/sec) and $[\ddot{\theta}_1, \ddot{\theta}_2, \ddot{\theta}_3]$ = [40, -25, 10] (rad/sec^2), respectively. Then, the associated velocity and acceleration vectors at the end-effector center of mass are as follows.

$$\dot{X}_{linear} = \begin{bmatrix} -11.34721 \\ -1.52024 \\ -3.04048 \end{bmatrix} \quad (10^{-2}\ \mathrm{m/sec}) \tag{7.27}$$

$$\ddot{X}_{linear} = \begin{bmatrix} 149.44136 \\ -83.50396 \\ 15.31153 \end{bmatrix} \quad (10^{-2}\ \mathrm{m/sec^2}) \tag{7.28}$$

The associated angular velocity and acceleration vectors of the end-effector are as

$$\dot{X}_{angular} = \begin{bmatrix} -1.2941 \\ -2.0 \\ 5.82963 \end{bmatrix} \quad (\mathrm{rad/sec}) \tag{7.29}$$

$$\ddot{X}_{angular} = \begin{bmatrix} 5.0130 \\ 2.30557 \\ 26.96483 \end{bmatrix} \quad (\mathrm{rad/sec^2}) \tag{7.30}$$

The required input torques ξ_1, ξ_2 and ξ_3 to achieve the prescribed motion can be evaluated from eq. (7.23) as

$$\begin{bmatrix} \xi_1 \\ \xi_2 \\ \xi_3 \end{bmatrix} = \begin{bmatrix} 138507.25305 \\ 201554.81157 \\ -13563.74068 \end{bmatrix} \quad (10^{-7}\,\mathrm{N-m}) \tag{7.31}$$

Using the inertia properties and eqs. (3.10-11) and (3.15-16), the inertial forces of all links can first be evaluated for the assumed motion state. Then, the reaction force evaluation procedure can be performed. The reaction forces associated with the carried and major links are shown in Tables 7-20 and 7-21, respectively. The Actual reaction forces are shown in Table 7-22.

7.4 Summary

Dynamic analysis and synthesis methodologies developed in the previous chapters are illustrated via two examples. Gear ratios of a two D.O.F. planar manipulator are determined based on the kinematic isotropy and maximum acceleration capacity conditions. Gearing configuration and gear ratios of a three-D.O.F. Bendix-type wrist mechanism are investigated based on the optimal acceleration capacity condition alone. Reaction forces in the joints are also evaluated. It is shown that geared robotic mechanisms can be designed and analyzed systematically and efficiently.

	$\gamma_{i,j}$ (10^{-5}N)	$f_{i,j}$ (10^{-5}N)	$t_{i,j}$ (10^{-7} N - m)
5	$^{1}\gamma_{6,5} = \begin{bmatrix} 127750.27840 \\ -46497.29876 \\ 0.0 \end{bmatrix}$	$^{1}f_{5,1} = \begin{bmatrix} 127750.27840 \\ -46497.29876 \\ 0.0 \end{bmatrix}$	$^{1}t_{5,1} = \begin{bmatrix} 29525.78471 \\ 81121.42678 \\ 138507.25053 \end{bmatrix}$
6	$^{1}\gamma_{2,6} = \begin{bmatrix} -458040.86633 \\ -166713.24142 \\ 0.0 \end{bmatrix}$	$^{1}f_{6,1} = \begin{bmatrix} -585791.14473 \\ -120215.94267 \\ 0.0 \end{bmatrix}$	$^{1}t_{6,1} = \begin{bmatrix} 135388.69301 \\ -209734.52334 \\ 0.0 \end{bmatrix}$
7	$^{1}\gamma_{8,7} = \begin{bmatrix} -142681.65782 \\ 51931.87642 \\ 0.0 \end{bmatrix}$	$^{1}f_{7,1} = \begin{bmatrix} -142681.65782 \\ 51931.87642 \\ 0.0 \end{bmatrix}$	$^{1}t_{7,1} = \begin{bmatrix} -32976.74153 \\ -90602.85272 \\ 201554.81157 \end{bmatrix}$
8	$^{1}\gamma_{9,8} = \begin{bmatrix} 471795.12220 \\ 171719.38115 \\ 0.0 \end{bmatrix}$	$^{1}f_{8,1} = \begin{bmatrix} 614476.78002 \\ 119787.50473 \\ 0.0 \end{bmatrix}$	$^{1}t_{8,1} = \begin{bmatrix} -142018.54856 \\ 208987.04988 \\ 0.0 \end{bmatrix}$
9	$^{2}\gamma_{10,9} = \begin{bmatrix} -391752.95341 \\ 57607.12478 \\ -130431.22593 \end{bmatrix}$	$^{1}f_{9,1} = \begin{bmatrix} -863548.07561 \\ -41288.15523 \\ 57607.12478 \end{bmatrix}$	$^{1}t_{9,1} = \begin{bmatrix} -454423.91995 \\ 152480.33153 \\ 0.0 \end{bmatrix}$
10	$^{3}\gamma_{4,10} = \begin{bmatrix} -533266.43907 \\ -176476.76010 \\ -80796.58896 \end{bmatrix}$	$^{2}f_{10,2} = \begin{bmatrix} -132507.03303 \\ -273670.14728 \\ 307659.88244 \end{bmatrix}$	$^{2}t_{10,2} = \begin{bmatrix} -1136597.27774 \\ -336027.50808 \\ 0.0 \end{bmatrix}$
11	$^{1}\gamma_{12,11} = \begin{bmatrix} -10648.75775 \\ -3875.83085 \\ 0.0 \end{bmatrix}$	$^{1}f_{11,1} = \begin{bmatrix} -10648.75775 \\ -3875.83085 \\ 0.0 \end{bmatrix}$	$^{1}t_{11,1} = \begin{bmatrix} 2461.15260 \\ -6761.96117 \\ -13563.74068 \end{bmatrix}$
12	$^{1}\gamma_{13,12} = \begin{bmatrix} 37027.72415 \\ -13476.98943 \\ 0.0 \end{bmatrix}$	$^{1}f_{12,1} = \begin{bmatrix} 47676.48191 \\ -9601.15860 \\ 0.0 \end{bmatrix}$	$^{1}t_{12,1} = \begin{bmatrix} 11019.04088 \\ 16750.64366 \\ 0.0 \end{bmatrix}$
13	$^{2}\gamma_{14,13} = \begin{bmatrix} -39284.71585 \\ 5781.60182 \\ 13077.43268 \end{bmatrix}$	$^{1}f_{13,1} = \begin{bmatrix} -76312.44001 \\ 399.55675 \\ 5781.60182 \end{bmatrix}$	$^{1}t_{13,1} = \begin{bmatrix} 79415.53652 \\ -7569.03327 \\ 0.0 \end{bmatrix}$
14	$^{3}\gamma_{4,14} = \begin{bmatrix} -33395.18476 \\ 11051.64994 \\ -5059.79154 \end{bmatrix}$	$^{2}f_{14,2} = \begin{bmatrix} 26998.15716 \\ -19312.29497 \\ -24595.61118 \end{bmatrix}$	$^{2}t_{14,2} = \begin{bmatrix} 91859.47344 \\ 52591.42970 \\ 0.0 \end{bmatrix}$

Table 7-20 Reaction Forces Associated with Carried Links .

Link	$f_{i,j}$ (10^{-5}N)	$t_{i,j}$ (10^{-7} N - m)
4	${}^{4}f_{4,3} = \begin{bmatrix} 778730.61034 \\ 46024.26472 \\ 51698.68250 \end{bmatrix}$	${}^{4}t_{4,3} = \begin{bmatrix} 1641337.75327 \\ -4390421.76780 \\ -6.98492\ E\ -10 \end{bmatrix}$
3	${}^{3}f_{3,2} = \begin{bmatrix} 825707.81105 \\ 19574.77027 \\ 44132.12097 \end{bmatrix}$	${}^{3}t_{3,2} = \begin{bmatrix} 1676781.75054 \\ -2.28465\ E\ -9 \\ -2208167.18735 \end{bmatrix}$
2	${}^{2}f_{2,1} = \begin{bmatrix} 1138682.25671 \\ -36645.17965 \\ 96776.25957 \end{bmatrix}$	${}^{2}t_{2,1} = \begin{bmatrix} 1579337.69536 \\ 2.32831\ E\ -10 \\ -3272815.81260 \end{bmatrix}$

Table 7-21 Reaction Forces Associated with Major Links.

$f_{i,j}$ (10^{-5}N)	$t_{i,j}$ (10^{-7} N - m)
${}^{2}f_{9,2} = \begin{bmatrix} 1138682.25671 \\ -36645.17965 \\ 96776.25957 \end{bmatrix}$	${}^{2}t_{9,2} = \begin{bmatrix} 1579337.69536 \\ 2.32831\ E\ -10 \\ -3272815.81260 \end{bmatrix}$
${}^{1}f_{9,13} = \begin{bmatrix} -2002230.33233 \\ 55488.10434 \\ 94252.30443 \end{bmatrix}$	${}^{1}t_{9,13} = \begin{bmatrix} -2141304.23375 \\ -4385696.138836 \\ -2.32831\ E\ -10 \end{bmatrix}$
${}^{1}f_{13,1} = \begin{bmatrix} 1925917.89232 \\ -55088.54759 \\ -88470.70261 \end{bmatrix}$	${}^{1}t_{13,1} = \begin{bmatrix} 2246044.88790 \\ 5291957.54318 \\ 2.32831\ E\ -10 \end{bmatrix}$

Table 7-22 Actual Reaction Forces.

CHAPTER 8

Conclusions and Future Works

8.1 Conclusions

This dissertation is aimed to develop systematic and efficient methodologies for dynamic analysis and synthesis of geared robotic mechanisms. The research has been concentrated on two aspects of geared robotic mechanisms: (1) dynamic analysis including the formulation of equations of motion and the reaction forces analysis, and (2) the selection of gearing configuration and the determination of gear ratios for geared robotic mechanisms. The major results are as follows:

1. Formulation of dynamic equations of motion.

Based on the motion separation of the carried links from the major links, the contribution to the generalized inertia forces of the dynamic equations are divided into two parts. The first part is due to the motion of the major links, and the second part is due to the relative motion of the carried links with respect to their carriers. The generalized active forces can be obtained by inspection. Then, equations of motion can be formulated and rearranged into various forms according to the purpose of application.

2. Reaction force analysis

Canonic graph representation is used to guide the evaluation process. It is found that this evaluation sequence can be carried out systematically in two steps. The first step is a link-by-link forward evaluation of the reaction forces acting on the revolute joints and gear teeth contact points associated with the carried links, starting from the input link along each transmission line. The second step is a link-by-link backward evaluation of the reaction forces acting on the revolute joints of the major links, starting from the output link of the equivalent open-loop chain. The actual reaction forces are then evaluated through the equivalent force system of coaxial links.

3. Performance indices establishment

Several performance indices, such as generalized velocity ratio, acceleration capacity, kinematic and dynamic condition numbers are established especially for geared robotic mechanisms. These performance indices can be used as design criteria or performance comparison in design or evaluation of such mechanisms.

4. Gearing configuration and gear ratio determination.

A methodology for the determination of gear ratios is first explored based on kinematic isotropy and maximum acceleration capacity conditions (KIMAC). It is shown that individual-joint drive manipulators cannot possess a kinematic isotropy property while certain gear-coupled manipulators can be designed to possess a kinematic isotropy property at a given end-effector position, through proper choice of gear ratios. The train values of these gear-coupled manipulators can be thought of as a product of two-stage gear reductions. The second-stage gear reduction provides the kinematic isotropic condition while the first-stage gear reduction provides the desired overall reduction. Since gear ratios of geared robotic mechanisms can not all be determined based on KIMAC, a more general methodology for the gearing configuration determination is then explored based on maximum acceleration capacity condition (MAC) alone. The principle of inertia match is extended from one D.O.F. system to multi-D.O.F. systems. It is shown that at the optimum design, the mass inertia of the input links reflected at the joint-space is equal to that of the major links, and the acceleration capacity is independent of the gearing configuration.

In conclusion, the methods developed for the dynamic analysis can greatly expand the designer's understanding of such mechanisms and lead to a more accurate model of system dynamics and improved system reliability. The methods developed for the dynamic synthesis provide rational procedures for the selection of gearing configuration and gear ratios in designing such complex mechanical systems. These developed methodologies can be the basis for a computer program which provides automated analysis and synthesis of a general class of geared robotic mechanisms. It is hoped that, the analysis and synthesis methodologies introduced herein will provide the impetus for future efforts towards manipulator design and performance assessment.

8.2 Future Works

The following research directions are suggested to extend the understanding of geared robotic mechanisms:

- Friction on the gear transmission can be modeled and added to the dynamic equations of motion. The inclusion of friction in the dynamic analysis provides better understanding of transmission efficiency and more accurate control of such devices.

- Nonlinear effects, such as Coriolis and centrifugal forces, can be included in the performance assessment, such that these performance indices can be used in a more general situation.

- Stress analysis in gear teeth can be modeled and evaluated through finite element method, using reaction forces computed from the force analysis.

- Research on mechanisms with rigid-elastic assemblies, such that the effect of compliance on the system dynamics can be assessed.

References

Angeles, J., 1985, "On the Numerical Solution of the Inverse Kinematic Problem", The International J. of Robotics Research, Vol. 4, No. 2, pp. 21-37.

Angeles, J. and Rojas, A. A., 1987, "Manipulator Inverse Kinematics Via Condition Number Minimization and Continuation", The International J. of Robotics and Automation, Vol. 2, No. 2, pp. 61-69.

Asada, H., 1983, "A Geometrical Representation of Manipulator Dynamics and Its Application to Arm Design", ASME J. of Dynamic Systems, Measurements, and Control, Vol. 105, pp. 131-135.

Asada, H. and Cro Granito, J. A., 1985, "Kinematic and Static Characterization of Wrist Joints and Their Optimal Design," Proc. IEEE Int. Conf. on Robotics and Automation, St. Louis, MO, pp. 244-250.

Beckenbach, E. and Bellman R., 1965, "Inequalities", 2nd revised printing, Springer-Verlag, New York, pp. 70.

Bejczy, A. K., 1974, "Robot Arm Dynamics and Controls", NASA Technical Memorandum 33-609, JPL, CIT, Pasadena, CA.

Bodley, C. S., Devers, A.D., Park, A. C. and Friseh, H.P., 1978, "A Digital Computer Program for the Dynamic Interaction Simulation of Controls and Structure(DISCOS)", NASA Technical Paper 1219, Vol. 1.

CADSI, "DADs User's Manual", 1988, Computer Aided Design Software, Inc., Rev. 5.0, Oakland, Iowa.

Chang, S. L. and Tsai, L. W., 1990, "Topological Synthesis of Articulated Gear Mechanisms," IEEE Int. J. of Robotics and Automation, Vol. 6, No. 1, pp. 97-103.

Chen, D. Z. and Tsai, L. W., 1991, "The Generalized Principle of Match for Geared Robotic Mechanisms", Submitted for publication in the IEEE J. of Robotics and Automation, also appears at the IEEE Int. Conf. on Robotics and Automation, April 9-11, Sacramento, CA, Vol. 2, pp. 1282-1287.

Chen, D. Z. and Tsai, L. W., 1990, "Kinematic and Dynamic Synthesis of Geared Robotic Mechanisms", Accepted for publication in ASME J. of Mechanical Design, also appears at ASME DE-Vol. 26, Cams, Gears, Robot and Mechanism Design, pp. 397-404.

Chen, J., Chen, D.Z. and Tsai. L.W., 1990, "A Systematic Methodology for the Dynamic Analysis of Articulated Gear Mechanisms", Proc. of 1990 Japan-U.S.A. Symposium on Flexible Automation, Kyoto, Japan, July 9-11, Vol. 1, pp. 273-278.

Chen J., 1989, "The Effects of Gear Reduction on Robot Dynamics", NASA Conference on Space Telerobotics, Pasadena, CA, Jan. 31- Feb. 2, Vol. 4, pp. 297-308.

Chiu, S. L., 1988, "Kinematic Characterization of Manipulators: An Approach to Defining Optimality", Proc. IEEE International Conf. on Robotics and Automation, St. Louis, MO, pp. 828-833.

Denavit, J. and Hartenberg, R. S., 1955, "A Kinematic Notation for Lower Pair Mechanisms Based on Matrices", ASME J. of Applied Mechanics, Vol. 77, pp. 215-221.

Doughty, S., 1988, "Mechanics of Machines", John Wiley & Sons Inc. New York.

Dubey, R. and Luh, J. Y. S., 1986, "Performance Measures and Their Improvement for Redundant Robots," Proc. ASME Winter Annual Meeting, DSC-Vol. 3, Anaheim, CA, pp.143-151.

Freudenstein, F., Longman, R. W. and Chen, C. K., 1984, "Kinematic Analysis of Robotic Bevel-Gear Trains", ASME J. of Mechanisms, Transmissions, and Automation in Design, Vol. 106, pp. 371-376.

Goldstein, H., 1981, Classical Mechanics, 2nd. ed., Addison-Wesley Pub. Co., Reading, MA.

Gosselin, C. and Angeles, J., 1988, "A New Performance Index For the Kinematic Optimization of Robotic Manipulators," ASME Trends and Developments in Mechanisms, Machines and Robotics, DE-Vol. 15-3, pp. 441-447.

Greenwood, D. T., 1965, "Principles of Dynamics", Prentice-Hall Inc., Englewood Cliffs, N.J..

Gupta, K. C., 1986, "On the Nature of Robot Workspace", The International J. of Robotics Research, Vol. 5, No. 2, pp. 112-121.

Hollerbach, J. M., 1980, "A Recursive Lagrangian Formulation of Manipulator Dynamics and a Comparative Study of Dynamic Formulation Complexity", IEEE Tran. of System, Man, and Cybernetics, Vol. SMC-10, No. 11, Nov., pp. 730-735.

Hooker, W. and Margulies, G., 1965, "The Dynamical Attitude Equations of an n-body Satellite", J. of Astronautical Sciences, Vol. 12.

Jeffreys, H., 1956, "Method of Mathematical Physics", 3rd. ed., The Syndics of the Cambridge University Press, Cambridge, U.K.

Kane, T. R. and Levinson, D.A., 1985, "Dynamics, Theory and Application", McGraw-Hill, New York, NY.

Khan, M. E., 1969, "The Near Minimum-Time Control of Open-Loop Articulated Kinematic Chain", Ph.D. Dissertation, Stanford University, Standford, CA.

Klafter, R. D., Chmielewski, T. A. and Negin, M., 1989, "Robotic Engineering, An Integrated Approach," Prentice-Hall, Inc, Englewood Cliffs, NJ.

Kohli, D. and Spanos, J., 1985, "Workspace Analysis of Mechanical Manipulators Using Polynomial Discriminants", ASME J. of Mechanisms, Transmissions, and Automation in Design, Vol. 107, No. 2, pp. 209-215

Kumar, A. and Patel, M. S., 1986, "Mapping the Manipulator Workspace Using Interactive Computer Graphics", The International J. of Robotics Research, Vol. 5, No. 2, pp. 122-130.

Lee, C. S. G, Lee, B. H., and Nigam, R., 1983, "Development of the Generalized D'alembert Equations of Motion for Mechanical Manipulators", IEEE Proc. 22nd Conf. on Decision and Control, pp. 1205-1210.

Litvin, F. L. and Zhang, Y., 1986, "Robotic Bevel-Gear Differential Trains", The International J. of Robotics Research. Vol. 5, No. 2, pp.75-81.

Luh, J. Y. S. and Walker, M. W. and Paul, R. P. C., 1980, "On-Line Computational Scheme for Mechanical Manipulators," ASME J. of Dynamic System, Measurement and Control, Vol. 102, pp. 69-76.

MDI, 1981, "User's Guide to ADAMS", Mechanical Dynamics, Inc., 5th Ed., Ann Arbor, MI.

Raibert, M. H., 1977, "Mechanical Arm Control Using a State-Space Memory", Society of Manufacturing Engineers Technical Paper, MS-77-742.

Salisbury, J. K. and Craig, J. J. , 1982," Articulated Hands: Force control and Kinematic Issues", The International J. of Robotics Research, Vol. 1, No. 1, pp. 4-7.

SDI, 1988, "SD/FAST User's Manual", Symbolic Dynamics, Inc., Mountain View, CA.

Shigley, J. E. and Mitchell, L. D., 1983, "Mechanical Engineering Design", 4th Ed., McGraw-Hill Book Inc., New York.

Silver, W. N., 1982, "On the Equivalence of Lagrangian and Newton-Euler Dynamics for Manipulators", The International J. of Robotics Research, Vol. 1 No. 2, pp. 60-70.

Spotts, M. F., 1985, "Design of Machine Elements", 6th Ed., Prentice-Hall Inc., Englewood Cliffs, NJ.

Stockdale, L. A., 1968, "Servomechanisms", Pitman Pub. Co., New York, NY.

Strang, G., 1980, "Linear Algebra and Its Applications", 2nd ed., Academic Press, New York.

Thomas, M. and Tesar, D., 1982, "Dynamic Modeling of Serial Manipulator Arms", ASME J. of Mechanisms, Transmissions, and Automation in Design, Vol. 104, pp.218-228.

Tsai, L. W., 1987, "An Application of Linkage Characteristic Polynomial to the Topological Synthesis of Epicyclic Gear Trains", ASME J. of Mechanisms, Transmissions, and Automation in Design, Vol. 109, No.3, pp.329-336.

Tsai, L. W., 1988, "The Kinematics of Spatial Robotic Bevel-Gear Trains," IEEE J. of Robotics and Automation, Vol. 4, No. 2, pp. 150-155.

Tsai, L. W. and Morgan, A. P., 1985, "Solving the Kinematics of the Most General Six- and Five-D.O.F. Manipulators by Continuation Methods", ASME J. of Mechanisms, Transmissions, and Automation in Design, Vol. 107, pp. 189-200.

Uicker, J. J., 1965, "On the Dynamic Analysis of Spatial Linkages Using 4X4 Matrices," Ph.D. dissertation, Northwestern University, Evanston, IL.

Vijaykumar, R., Waldron, K. J. and Tsai. M. J., 1986, " Geometric Optimization of Serial Chain Manipulator Structures for Working Volume and Dexterity", International J. of Robotics Research, Vol. 5, No. 2, pp. 91-103.

Walker, M. W., and Orin, D. E., 1982, "Efficient Dynamic Computer Simulation of Robotic Mechanisms", ASME J. of Dynamic System, Measurement, and Control, Vol. 104, No. 3, pp. 205-211.

Whitney, D. E., 1969, "State-Space Models of Remote Manipulation Tasks", IEEE J. of Automatic Control, Vol. 14, pp. 617.

Yang, D. C. H., Tseng, S. W., 1986, "Simplification and Linearization of Manipulator Dynamics by the Design of Inertia Distribution", The International J. of Robotics Research, Vol. 5, No. 3, pp. 120-128.

Yoshikawa, T. 1985a, "Manipulability and Redundancy Control of Robotic Mechanisms," Proc. IEEE International Conf. on Robotics and Automation, St. Louis, MO, pp. 1004-1009.

Yoshikawa, T. 1985b, "Dynamic Manipulability of Robot Manipulators," Proc. IEEE International Conf. on Robotics and Automation, St. Louis, MO, pp. 1033-1038.